Dissertation zur Erlangung des Doktorgrades
der Fakultät für Chemie und Pharmazie
der Ludwig-Maximilians-Universität München

Defined nanocarriers for improved and targeted gene delivery

Petra Kos

aus

Celje, Slowenien

2014

Erklärung

Diese Dissertation wurde im Sinne von § 7 der Promotionsordnung vom 28. November 2011 von Herrn Prof. Dr. Ernst Wagner betreut.

Eidesstattliche Versicherung

Diese Dissertation wurde eigenständig und ohne unerlaubte Hilfe erarbeitet.

München, 10.06.2014

.....

Petra Kos

Dissertation eingereicht am: 26.06.2014

1. Gutachter: Prof. Dr. Ernst Wagner

2. Gutachter: Prof. Dr. Stefan Zahler

Mündliche Prüfung am: 24.07.2014

TABLE OF CONTENTS

1 INTRODUCTION

1.1 Nucleic acids as therapeutic agents

A mind-boggling progress has been made in the identification of genes responsible for diverse cell processes. The completion of a Human Genome Project has provided myriad information on the target genes and thus vast advancement has been done in creation of tools that allow manipulating specific lethal genes and their functions. Numerous human diseases are now known to be of genetic origin, like Huntington's chorea [1], mucoviscidosis [2], hemophilia [3] etc. Hence, nucleic acid therapy presents a great prospect for the treatment of such genetic disorders in humans by modifying their cells genetically and being able to act only on the target responsible for the disease. In spite of their promises in healthcare, the role of nucleic acids as therapeutics is still in its infancy and their involvement in clinics modest. One reason lays in the complexity of genetic diseases (as for example cancer) which are usually caused by multiple gene mutations. Thus, there is no surprise that the first gene therapy human clinical trial protocol approved by the US RAC / Food and Drug Administration (FDA) was aimed at a monogenetic disorder, named severe combined immune deficiency (SCID) caused by a mutation of adenosine deaminase (ADA) gene only [4]. Patients' T cells were obtained from their blood, induced to proliferate in cell culture, transduced with the ADA retroviral vector to express the normal gene for adenosine deaminase and reinfused into patients [5]. In this and other similar trials [6] therapeutic DNA was applied to be delivered in the nucleus of the target cells to replace the defective or missing genes. With increasing knowledge and progress in genetics and genomics, additional approaches have been established where delivered nucleic acids can turn off genes by targeting the RNA which codes for the protein instead of coding for the protein product itself. The fundamental principle of oligonucleotide-mediated gene silencing is the binding of a target RNA through Watson-Crick base pairing. Single-stranded antisense oligonucleotides (ASOs) are capable to act as a single strand, whereas the small RNA duplex needs to be first incorporated into the RNA-induced silencing complex (RISC), followed by the separation of the strands. The passenger strand is lost, and the remaining guide strand guides RISC to the complementary or near-complementary region of target mRNA, suppressing the gene expression either by degrading mRNA or blocking

mRNA translation [7]. Unmodified single-stranded RNA oligonucleotides lack the stability and different modifications have been done to increase their resistance to nucleases. Chemical modifications like 2´-fluoro, or 2-O-methyl RNA or the introduction of phosphorothioate linkages can not only increase stability but have also shown an improved binding affinity of oligonucleotides for their complementary sequences. An ever higher affinity was obtained with the locked nucleic acid (LNA) having a bridge between the 2' and 4' position of the ribose locking it in the conformation ideal for binding to complementary sequences [8, 9]. Unmodified double-stranded short interfering RNA (siRNA) is much more stable, though rapidly cleared and thus chemical modifications are needed for improved *in vivo* results [9, 10]. As the nucleic acids are rapidly cleared from the body, local injection at the site of pathology has been inclined as administration route. The first RNAi-associated nucleotide reaching the market was antisense oligonucleotide for the local intraocular treatment of cytomegalovirus retinitis in patients with AIDS (Fomivirsen) [11], though it has been withdrawn from the European market based on the commercial reasons. The anti-vascular endothelial growth factor (anti-VEGF) RNA aptamer Pegaptanib [12] is another drug that has entered the market being utilized in the local treatment of acute macular degeneration. In spite of the abundance of clinical trials with antisense oligonucleotides to combat cancer, none of them has hit the clinics. Nevertheless, great hope has been laid in the siRNA therapy with the currently ongoing clinical studies showing encouraging results obtained with concomitant treatment in cancer [13]. In addition, over the past decades much effort has been done on improving the delivery systems that can reimburse for demanding biopharmaceutical characteristics of nucleic acids and help overcome the barriers of nucleic acid delivery.

1.2 Challenges for nucleic acid-based therapies

The nucleic acids applied systemically either naked or enclosed within a carrier encounter many challenges on their way towards the target cell compartment. The already mentioned stability of nucleic acids against the enzymatic degradation by nucleases in the physiological fluids is the first challenge to be faced [14]. Upon reaching the target tissue, the therapeutic oligonucleotides need to cross the cell

membrane being internalized into the endosomes. The endocytosis pathways can be divided in clathrin-mediated endocytosis, caveolae-mediated endocytosis, macropinocytosis, and clathrin- and caveolae-independent endocytosis [15]. The cellular uptake can be improved by attachment of targeting ligands inducing the receptor-mediated endocytosis. The endosomal pathway begins with the early endosomes which mature into late endosomes, thereby becoming progressively acidic [16]. Therefore, after their entry into the cell by endocytosis, nucleic acids need to escape from the endosomes as these later convert into lysosomes causing nucleic acid digestion. The proton pump vacuolar ATPase generates acidification by accumulating protons in the endocytic vesicles. For the nucleic acids complexed within the cationic carriers, the capability of the polymer to mediate endosomal escape can mainly be attributed to their strong buffering capacity in the pH range from 5 to7 [16]. This proton sponge hypothesis was proposed by Boussif *et al*. It suggests that the protonation of the basic polymer triggers an influx of Cl^- finally causing swelling and rupture of the endosomes [17]. Whereas siRNA only needs to reach the cytoplasm to interfere with translation, the plasmid needs to translocate to the nucleus to mediate gene expression. The cellular actin cytoskeleton hampers the migration of the plasmid to the perinuclear region [18]. Translocation into the nucleus presents another important challenge of gene delivery. The nuclear envelope contains nuclear pores allowing a passive transport with a limit of 70 kDa or 10 nm which is much less than the size of the naked pDNA or its polyplex [19]. Hence, nuclear entry by degradation of the nuclear membrane during mitotic cell division is believed to be a predominant factor. In slowly or non-dividing cells, the efficient nuclear translocation during mitosis is hampered and thus an active nuclear import through nuclear pore complex (NPC) can be exploited [20]. Recently, Gagnon *et al.* have identified RNAi factors within the cell nuclei that may broaden the investigation of RNAi-based therapeutics beyond the traditional targets in the cytoplasm to targets in the nucleus [21].

1.3 Non-viral carriers conquering barriers and promoting nucleic acid delivery

Synthetic non-viral carriers have attracted a great deal of attention over the past decades as the generally more potent viral vectors have been associated with a number of safety concerns. Non-viral vectors can circumvent some of the problems related to the viral vectors such as limited size and type of the payload, endogenous virus recombination and recognition by the host immune system [22]. Moreover, the chemical mimics of viruses have an advantage in terms of simplicity and straightforwardness of the large-scale production. Especially cationic lipids and cationic polymers have emerged as promising gene vectors as they can form condensed complexes with the negatively-charged nucleic acids through electrostatic interactions. Polyelectrolyte complexes formed with nucleic acid and cationic lipids are called lipoplexes, whereas the complexes with polymers are designated as polyplexes [23]. Felgner *et al.* reported the first use of a cationic lipid for gene transfer in 1987 employing N-[1-(2,3-dioleyloxy)propyl]-N,N,N-trimethylammonium chloride (DOTMA) which resulted in high transfection efficiency *in vitro* [24]. Apart from DOTMA, N-[1-(2,3-dioleoyloxy)propyl]-N,N,N-trimethylammoniumethyl sulfate (DOTAP) and dioleoylphosphatidylethanolamine (DOPE) represents the most commonly used cationic lipids [25]. The DOPE is usually used as a co-lipid due to its endosomolytic properties [26]. Among cationic polymers, several natural polymers such as chitosan [27], dendrimers such as polyamidoamines (PAMAM) and polypropylenimine (PPI) [28], polypeptides like polylysine (PLL) [29] or polyethylenimine (PEI) [30, 31] have attracted much attention with the letter emerging as a gold standard in gene delivery due to its high transfection potency based on its strong plasmid condensation and good buffering capacity promoting the endosomal escape.

1.3.1 Nucleic acid compaction facilitating domains

The non-viral carriers need to be able to stably compact nucleic acids in order to protect them from the enzymatic degradation. Thus, sufficient nucleic acid compaction is the first prerequisite for efficient gene delivery. However, its

reversibility is crucial, as the delivered nucleic acid needs to be available for subsequent transcription. The oligonucleotide binding is predominantly based on the electrostatic interactions between the positively charged groups of the carrier and negatively charged phosphate backbone of the nucleic acid. The polyplex properties are greatly determined by the polymer characteristics such as its size, shape, charge density and flexibility, as well as by the formulation conditions. Different nucleic acids call for different transfection agents as short siRNA with 42 negative charges cannot provide such stabilization as a much larger pDNA molecule with approx. 3000-fold more charges. Apart from electrostatic interactions, hydrogen bonding [32] and hydrophobic interactions can enhance the polyplex stability. The hydrophobic modifications of PEI are known to increase transfection efficiency. Several research groups demonstrated improved efficacy and reduced toxicity of PEI by conjugation of various hydrophobic chains [33-35]. Teo *et al*. systematically attached hydrophobic chains of different lengths (ethyl, octyl, deodecyl) and aromatic hydrophobic groups (benzyl, phenylurea) to the low molecular weight PEI (1.8 kDa) showing that the condensation capability and stability of the polyplexes can be easily adjusted and improved by controlling the degree of functional carbonate conjugation. Random modification of PEI nitrogens with tyrosines provided increased extracellular stability and enhanced siRNA transfection efficiency [36]. The self-assembly of tyrosine containing polymers into nanocarriers has been explained to be promoted through the π-π interactions of the aromatic rings of the neighboring tyrosines [37, 38]. The conjugation of pyridines to branched PEI25 kDa *via* thiourea linkages as well led to an improved siRNA delivery *in vitro*, and also considerably low toxicological profile [39].

1.3.2 Targeting ligands

Efficient *in vivo* targeting to cancerous tissues still represents a considerable challenge for non-viral gene delivery systems. The upregulation of surface receptors in cancer tissues enables selective targeting to tumor cells using various targeting ligands. Above mentioned PLL was the first targeted cationic polymer conjugate ever applied for DNA packaging introduced in 1987 by Wu *et al*. [40, 41] with liver cell-specific asialoglycoprotein receptor-mediated endocytosis already exploited for gene delivery *in vitro* and *in vivo*. Wagner *et al.* developed PLL-based carriers with

transferrin (Tf) serving as a ligand calling the process “transferrinfection” [42]. Several other groups have also applied Tf as a targeting ligand for nucleic acid delivery [43-45]. The transferrin receptor (TfR) is ubiquitously expressed at low levels in most normal human tissues representing the main entry mechanism for the iron bound Tf, whereas its expression on malignant cells is several fold higher than on normal cells and highly dependent on the stage of the tumor [46]. To date, antibodies and antibody fragments [47, 48], aptamers [49], glycoproteins [50, 51], small molecules [52, 53] and peptides [54-57] are just a few of the targeting ligands classes that can recognize and bind to receptors over-expressed in tumors. Especially the latter have gained increasing attention based on the straight-forward identification of high-affinity and high-selectivity binding sequences by phage display, their low molecular weight, efficient tumor penetration and minimal immune response [58]. In this regard, peptides containing the arginine-glycine-aspartic acid sequence (RGD) binding to the integrin receptors [55, 57] have been widely investigated. Integrins are playing a key role in the adhesion, migration, invasion and proliferation of tumor cells and are usually expressed at low or undetectable values in normal tissues, but can be highly upregulated in tumor tissues [59]. Harbottle *et al.* synthesized in 1998 an oligolysine peptide having a RGD targeting domain attached showing efficient binding to the fibronectin and vitronection integrin receptors and efficient gene transfer upon addition a lysosomotropic agent [55]. Moreover, the members of receptor tyrosine kinases family have a crucial role in tumorigenesis and various therapeutics targeting these receptors have been investigated and approved for the cancer treatment [60, 61]. Among them short peptides directed towards the growth factor receptors (EGFR, VEGFR) [62-65] have shown vast promise. Using a phage display library Li *et al.* identified a GE11 targeting peptide amino acid sequence YHWYGYTPQNVI that specifically and efficiently bound to EGFR [66]. Small ligand size and convenient synthesis, absence of EGFR signaling activation, increased surface levels of the EGFR during treatment with GE11-PEG-PEI poylpexes are the advantages of this phage display-derived ligand over its natural ligand EGF [63].

To enhance the selectivity and transfection efficacy of the single peptide ligand-based nucleic acid carriers, dual-targeted carriers have been investigated which simultaneously address two different surface receptors over-expressed in tumor tissues. With this dual-ligand approach, non-viral carriers attempt to mimic more potent natural viral carriers like adenoviruses which concurrently target coxsackie–

adenovirus receptor (CAR) and integrins $a_v\beta_3$ or $a_v\beta_5$ [67, 68]. Nie *et al.* have combined the short peptide B6 derived from a phage display as a substitute for natural Tf and RGD in PEGylated PEI-based carriers showing a clear synergy of dual-targeted over the single-targeted polyplexes [68]. Also PEI-based, a combination of YC25 peptide against fibroblast growth factor receptor (FGFR) and CP9 peptide binding to the integrins resulted in a significantly enhanced gene transfer in tumors with positive expression of FGF receptors and integrins [69].

1.3.3 Shielding domains

Gene delivery systems need to circulate in the blood long enough to reach their target site, thereby avoiding recognition by the immune system. Plasma proteins (opsonins) can bind the polyplexes rapidly removing them from the circulation through the reticulo-endothelial system (RES) [70]. Hydrophilic polymers have been demonstrated as essential for nanoparticle surface shielding against unintended interactions with biological surfaces and for prolonging the circulation half-life. Among them, polyethylene glycol (PEG) has been the most widely used. It reduces the tendency of the particles to self-aggregate by providing sterical stabilization. Moreover, the incorporation of targeting ligands *via* PEG spacer arm has emerged as a platform for active targeting providing accessibility of the ligand to the target tissue. The PEG shielding moiety can be either covalently attached to the polymeric carrier [57, 71, 72] or the nanocarriers can be postPEGylated after polyplex formation [73, 74]. Apart from PEG, other hydrophilic molecules have been exploited for reducing the surface charge such as N-(2-hydroxypropyl)methacrylamide (HPMA) [75, 76], dextran [77, 78], hyaluronan [79] or hydroxyethyl starch (HES) [80]. To develop carriers that could sense their environment and alter their behavior accordingly, various reversible shielding strategies were applied.

Environmentally programmed chemical linkages sensing *e.g.* changes in the redox potential, pH or the concentration of different enzymes have been have proven to increase the transfection efficiency. Disulfide linkages are most commonly exploited in the gene delivery as they remain stable in the blood circulation but are cleaved in the reducing intracellular environment [81, 82]. The enzymatic activity of matrix metalloproteinases (MMPs) for site-specific cleavage of PEG/MMP-substrate peptide

was exploited by Hatakeyama *et al.*, as MMPs are highly expressed in tumor cells and secreted into the extracellular space [83]. Furthermore, pH-sensitive systems have especially gained attention taking an advantage of lower pH values of the late endosomes and lysosomes (pH 4.5-6.5) as opposed to the higher extracellular pH values (pH 7.5). Miscellaneous acid-cleavable bonds were introduced ranging from ortho esters [84, 85], hydrazones [86], acetals [87, 88] etc.

1.3.4 Endosomal escape facilitating domains

The endosomal escape and efficient release of the payload in the cytosol represents a major bottleneck for the nucleic acid delivery. The incorporation of the lytic lipid domains into the polymeric carriers can be a way to overcome it. As lipids are the main component of the cell membrane, the modification of the polymeric carriers with the hydrophobic domains results in additional hydrophobic interactions between the membrane and the polyplexes, facilitating the cargo delivery in the cytosol. Several hydrophobic modifications have been exploited to date, *e.g.* oleic acid [89, 90], stearic acid [91-93], cholesterol [94, 95] etc. Moreover, the endosomolytic peptides derived from influenza virus haemagglutinin HA2 or melittin were introduced [96, 97]. Boeckle *et al.* demonstrated an enhanced endosomal escape and gene transfer efficiency by attaching the melittin sequence modified with glutamic acid residues to the PEI [98]. On the other hand the gold standard PEI has demonstrated high transfection efficiency due to the so called “proton sponge” effect. The ability of the PEI and many other polymeric carriers to mediate efficient nucleic acid delivery is predominantly attributed to their strong buffering capacity in the lower endosomal pH range. Amino acid histidine containing the imidazole ring (pK_a 6.03) is known to increase buffering capacity in endosomes and can be therefore used as a functional group to improve the endosomal escape of the nanocarriers [99, 100]. The low transfection efficiency of chitosan related to its low endosomal escape was for example improved by implementation of the histidine *via* disulfide linkage [101].

1.4 On the way towards precise carrier systems

1.4.1 Dendrimers

Although PEI exhibits good buffering capacity and high transfection efficiency, its inherent heterogeneity presents a limitation to its usage. Dendrimers represent an approach towards defined polymeric structures. They consist of a central core molecule that acts like a root from which a number of tree-like, highly branched arms originate in a symmetric manner. They are synthesized by covalent coupling of the branches and for each additional layer (generation) that is being added the reaction sequence is repeated. These hyper-branched molecules have distinctive characteristics with a well defined size and structure and low polydispersity index based on their stepwise synthesis being especially relevant [102]. Polyamidoamine (PAMAM) and polypropylenimine (PPI) dendrimers of different generations have been most investigated in terms of nucleic acid delivery. As both these commercially available dendrimers still leave room for improvement in transfection efficiency and cytotoxicity, several modifications of dendrimers have been performed addressing different challenges in nucleic acid delivery. For example, dendrimers were equipped with different targeting ligands. Sideratou *et al.* synthesized a folate functionalized PEGylated PPI with a high specificity towards the folate receptor and low toxicity [103]. Koppu *et al.* attached transferrin (Tf) as a targeting ligand to PPI by using dimethylsuberimidate (DMSI) as a crosslinking agent which resulted in rapid and sustained tumor regression in mice [104]. Apart from numerous other targeting ligands (*e.g.* EGF [105], LHRH [106], RGD [107]), several alternative dendrimer surface modifications efficiently enhanced different steps in pDNA or siRNA gene delivery like cellular binding, internalization or endosomal escape. In particular, several hydrophobic modifications, such as conjugation with different fatty acids (12-16 carbons) [108, 109] or aromatic amino acid phenylalanine [110] have been proven as beneficial for gene delivery leading to increased interactions with biological membranes and transmembrane activity as well as to improved endosomal escape by endosome fusion or destabilization. Moreover, simple modifications with arginine as additional cationic domain efficiently enhanced nucleic acid compaction and cellular uptake [111, 112]. Conjugation of proton sponge effect facilitating polyhistidines to the PAMAM surface resulted in an improved endosomal escape and high transfection efficiencies [113]. Surface acetylation of PAMAM dendrimers

furthermore reduced cytotoxicity whilst maintaining appreciable permeability [114]. Not only reduced cytotoxicity, but also temperature-sensitive surface property-induced active targeting with local hyperthermia was achieved with the oxyethylene unit surface modification [115]. Apart from surface modifications, other strategies have been applied to enhance transfection efficiency of dendrimers. Nuclear packaging as one of the basic prerequisites for successful gene delivery was substantially improved for the low generation PPI by dendrimer anchorage onto the gold nanoparticles. The latter were not included in the formed polyplexes which eliminated any potential toxicity issues [116].

1.4.2 Sequence-defined carriers synthesized via solid-phase synthesis

Another approach to synthesize defined monodisperse polymeric carriers offers the solid-phase synthesis (SPPS) introduced by Merrifield in 1963. The method enabled a stepwise addition of protected amino acids to a growing peptide chain that was by covalently bound to a solid resin particle. Due to fixing of the peptide on the resin, excess reagents and side-products can easily be washed away. The simplicity and quickness of the method was demonstrated by the synthesis of a model tetrapeptide [117]. A modification of this classical method was proposed by Hartmann *et al.* as a straightforward strategy for the synthesis of well-defined linear poly(amidoamines) (PAA)-polypeptides and PAA-PEG conjugates. This made possible to precisely position the functional moieties within the polymer chain to design user-defined multifunctional polymers with tailor-made properties [118]. Further modification of the method by Schaffert *et al.* enabled introduction of novel building blocks comprising diaminoethane motifs, essential for nucleic acid binding and endosomal buffering [119]. Therewith a library of >600 potent oligomers of different topologies (U-shape, T-shape, i-shape, combs) with various functional moieties (fatty acids, cysteines, histidines, targeting domains) was designed for efficient pDNA and siRNA delivery [120-124].

1.5 Aims of the thesis

Gene therapy carries a great potential of correcting genetic defects, yet its success is largely dependent on the suitable gene delivery vector. Different chemical approaches have been applied to develop polymeric carriers trying to surmount the extracellular and intracellular challenges of the nucleic acids delivery. However, the cytotoxicity of such potent cationic polymeric carriers related to polydispersity and lack of precise conjugation sites has limited their use. Thus, in the current thesis the focus was on the evolvement of novel precise polymeric nucleic acid carriers which allowed systematic determination of structure-activity relationships and revealed high gene transfer efficiency and good biocompatibility.

The first aim of the thesis was to evaluate defined biodegradable oligomers for gene delivery of a higher molecular weight (Mw) as high Mw is generally associated with higher gene transfer efficiency. Due to the fact that high Mw often correlates with increased cytotoxicity, the structurally-precise non-toxic lower Mw dendrimer PPI should serve as a core to which sequence-defined oligo (ethane amino) amides comprising terminal cysteines were to be attached *via* disulfide linkages. In the reducing cytosol environment these disulfide bonds should be cleaved and the assembled high molecular weight carrier dissociated into non-toxic low molecular weight compounds. Thus, not only high transfection efficiency but also low toxicity profile of these novel carriers should be achieved and possibly correlated with the length of the attached oligo (ethane amino) amides.

The second aim was to evaluate a small library of oligomers with increasing Mw comprising only the diaminoethane containing building blocks as another approach to increase the carrier efficacy by increasing its Mw but maintaining the cytotoxicity profile low. Again the correlation between the increasing Mw and the biophysical and biological properties should be performed in order to find an optimal minimal length of the carrier that would allow efficient gene transfer already in the absence of additional functional moieties. The study should provide a better fundamental understanding to the diaminoethanes consisting oligomers prior to the succeeding steps of carrier functionalization.

The third aim of the thesis was to test targeted receptor-specific carriers based on the highly functionalized oligo ethane (amino amide) oligomers. Therefore, a precise

conjugation technique was to be utilized for easy conversion of existing non-targeted oligomers from our library into FolA-targeted and shielded oligomers. The suitability of the method for gene delivery carriers should be verified. Moreover, the significance of such high-throughput method in a search for an optimal target-specific carrier should be demonstrated.

The fourth aim was to investigate the potential to enhance the specificity and efficacy of targeted carriers by a dual-ligand approach. For this purpose, defined oligo (ethane amino) amides containing a PEG chain with a peptidic targeting ligand at its distal end prepared *via* all-in-one solid-phase synthesis were to be assessed. Integrin receptor-directed cyclic peptide cRGDfk, transferrin receptor-addressing peptide B6, and epidermal growth factor receptor-targeting peptide GE11 should serve as targeting ligands. Dual-receptor targeted pDNA polyplexes should be designed by combining two of the above peptides at various ratios, in order to find an optimal ligand combination.

The final aim of the thesis was to optimize the oligomers towards potent, defined, targeted and shielded carriers. As a targeting moiety novel HGFR/c-Met receptor-binding ligands were to be evaluated. Receptor-specific cell binding, cellular internalization and gene transfer of the novel targeted carriers should be demonstrated. The influence of increased shielding and enhanced polycationic part of the carrier should be investigated *in vitro* and *in vivo*. Furthermore, the impact of the co-addition of a non-shielded oligomer on the compaction of the particles and resulting gene expression *in vivo* should be elucidated.

2 Materials and methods

2.1 Chemicals and reagents

Cell culture media, antibiotics and fetal calf serum (FCS) were purchased from Invitrogen (Karlsruhe, Germany), HEPES from Biomol GmbH (Hamburg, Germany) and glucose from Merck (Darmstadt, Germany). Plasmid pCMVLuc (encoding a Photinus pyralis luciferase under control of the CMV promoter) for *in vitro* experiments was produced with the Qiagen Plasmid Giga Kit (Qiagen, Hilden, Germany) according to the manufacturer specifications, pCMVLuc for *in vivo* experiments was purchased by Plasmid Factory (Bielefeld, Germany). Cy5-labeling kit was obtained from Mirus Bio (Madison, WI, USA). Luciferase cell culture lysis buffer and D-luciferin sodium salt were obtained from Promega (Mannheim, Germany). LPEI was synthesized by Wolfgang Rödl, LMU Biotechnology as described in [125]. Sequence-defined oligomers were synthesized by Dongsheng He, Ulrich Lächelt, Irene Martin, Edith Salcher, Claudia Scholz and Christina Troiber, all from LMU Pharmaceutical Biotechnology.

2.2 Biophysical characterization

2.2.1 Polyplex formation

pCMVLuc (200 ng) and oligomers at indicated nitrogen/phosphate (N/P) ratios were diluted in separate tubes in 10 µL of 20 mM HEPES buffered 5% glucose pH 7.4 (HBG) each. Only protonatable nitrogens were considered in the N/P calculations. The polycation solution was added to the nucleic acid, mixed vigorously up to 20 times and incubated for 30 min at room temperature.

2.2.2 Agarose gel shift assay for pDNA binding

For pDNA gel-shift assay, a 1% agarose gel was prepared by dissolving agarose in TBE buffer (trizma base 10.8 g, boric acid 5.5 g, disodium EDTA 0.75 g, in 1 L of water) and boiling it up to 100 °C. After addition of GelRed for the detection of the

nucleic acid, the agarose solution was casted in the electrophoresis unit and left to form a gel. Polyplexes were prepared as described above containing 200 ng of pDNA in 20 µL HBG. Next, 4µL of loading buffer (prepared from 6 mL of glycerine, 1.2 mL of 0.5 M EDTA, 2.8 mL of H_2O, 0.02 g of bromphenol blue) were added to each sample before they were placed into the sample pockets. Electrophoresis was performed at 120 V for 80 min.

2.2.3 Ethidium bromide assay for pDNA condensation

Oligomer solution was added at increasing N/P ratios to 10 µg pDNA in 1 mL HBG containing 0.4 µg EtBr. After each addition the EtBr fluorescence was measured at the excitation wavelength λ_{ex} = 510 nm and emission wavelength λ_{em} = 590 nm using a Cary Eclipse spectrophotometer (Varian, Germany). 0.4 µg EtBr in 1ml HBG presented blank value. Maximal fluorescence intensity was set 100% for the EtBr solution containing free nucleic acid (10 µg) and decrease in fluorescence was measured after stepwise addition of oligomer solution.

2.2.4 Particle size and zeta potential measurement

Particle size and zeta potential of formulations were measured by laser-light scattering using a Zetasizer Nano ZS (Malvern Instruments, Worcestershire, U.K.). 10 µg pDNA were vigorously mixed with oligomers at N/P 12 in 100 µl HBG and incubated for 30 min. Just before dynamic light scattering (DLS) measurement polyplex samples were diluted to 1 mL in 20 mM HEPES pH 7.4 and transferred in a folded capillary cell (DTS1060). Zetasizer Nano ZS with backscatter detection (Malvern Instruments, Worcestershire, UK) was utilized, the equilibration time was set to 0 min, the temperature was 25 °C and an automatic attenuator was applied. The refractive index of the solvent, in our case water, was 1.330 and the viscosity 0.8872, the refractive index of polystyrene latex (1.590) was fixed. Each sample was measured 3 times with 10 subruns.

2.2.5 pH titrations for determination of buffer capacity

The oligomer sample, containing 15 µmol protonatable amines, was diluted in a total volume of 3.5 mL NaCl solution (50 mM) and the pH was adjusted to 2.1 by addition of 0.1 M HCl. Afterwards, a back titration with 0.05 M NaOH solution was performed with an automatic titration system (Titrando 905 from Metrohm, Germany) until pH of 11 was reached. Furthermore a titration with 50 mM NaCl was performed and the consumption of NaOH in this control titration was substracted from the consumption in the oligomer titrations at the corresponding pH values. Percentage of buffer capacity C in a certain pH range (x – y), where ΔV stands for the volume consumption of NaOH in the considered pH range, was calculated according to equation (1). The pH titrations were performed by Claudia Scholz (PhD 2014, LMU Munich).

$$C_{pHx\text{-}y} = \frac{[\Delta V(Sample)_{pHx-y} - \Delta V(NaCl)_{pHx-y}] \times 50\ \text{mM}}{15\mu moles} \times 100\%$$

2.2.6 Transmission electron microscopy

A carbon coated 200 mesh copper grid (Plano GmbH, Wetzlar, Germany) was activated by mild plasma cleaning. Afterwards, one drop (10 µL) of the polyplex solution at N/P 12 prepared as described above was placed on the grid. Excess liquid was blotted off using filter paper until the grid was almost dry. Subsequently, the copper grid was incubated with 10 µL of a 1% phosphotungstic acid solution (PTA) (Science Services, Germany), air-dried as before and analyzed immediately by Dr. Markus Döblinger (LMU Munich) using a FEI Titan 80 - 300 operated at 80 kV.

2.3 Biological characterization *in vitro*

2.3.1 Cell culture

Mouse neuroblastoma cells (N2A) were grown in Dulbecco's modified Eagle's medium (DMEM), human prostate cancer cells (PC3 and DU145) were cultured in RPMI-1640 medium, human cervix carcinoma KB cells were grown in folate free RPMI-1640 medium and hepatocellular carcinoma cells (Huh7) were grown in a

50:50 mixture of Dulbecco's modified Eagle's medium (DMEM) and Ham's F12 medium, at 37 °C in humidified atmosphere containing 5 % CO_2. All media were supplemented with 10% fetal calf serum (FCS), 4 mM stable glutamine, 100 U/mL penicillin, and 100 µg/mL streptomycin.

2.3.2 Receptor levels estimation

The surface receptor levels were determined on cells either in suspension or attached as in cell binding/internalization studies. In the first case, 800 000 cells were incubated in 100 µL buffer (10% FCS in PBS) containing monoclonal mouse anti-human EGFR or HGFR/c-Met antibody (1:100 dilution) or IgG control for mouse primary antibodies (1:100 dilution) for 1 h on ice and subsequently washed twice with buffer (10% FCS in PBS). The cells were then stained with Alexa 488-labeled goat anti-mouse (1:400 dilution) secondary antibody for 1 h on ice, washed and counterstained with DAPI (1 µg/mL). In the second case, the cells were seeded into 24-well plates coated with collagen at a density of 50 000 cells/well. After 24 h, cells were treated were incubated on ice with the monoclonal mouse anti-human EGFR antibody (1:500 and 1:5000 dilution) or IgG control in 500 µL medium for 30 min on ice and subsequently washed three times with PBS buffer. The cells were then stained with Alexa 488-labeled goat anti-mouse secondary antibody for 30 min on ice with the same dilutions (1:500 and 1:5000 dilution), washed again three times with PBS, detached with trypsin/EDTA and taken up in PBS with 10% FCS. The samples were then counterstained with DAPI (1 µg/mL) and analyzed on a Cyan™ ADP flow Cytometer (Dako, Hamburg, Germany) using Summit™ acquisition software (Summit, Jamesville, NY, USA). DAPI fluorescence was excited at 405 nm and detected with a 450/50 bandpass filter, Alexa-488 fluorescence was excited at 488 nm and detected with a 530/40 nm bandpass filter. The percentage of EGFR positive cells was determined as compared to control IgG stained cells. The mean fluorescence intensity (MFI) corresponds to the arithmetic mean of the living cell population.

2.3.3 Cellular association

The cells were seeded into 24-well plates coated with collagen at a density of 50 000 cells/well. After 24 h, culture medium was replaced with 400 µL fresh growth medium. pDNA polyplexes (N/P 12) in 100 µL HBG, containing 1 µg pDNA (20% of the nucleic acid was Cy5-labeled) were added to each well and incubated on ice for 30 min. Subsequently, cells were washed twice with 500 µL PBS. Cells were detached with trypsin/EDTA and taken up in PBS with 10% FCS. Cellular association was assayed by excitation of Cy5 at 635 nm and detection of emission at 665 nm. Cells were appropriately gated by forward/sideward scatter and pulse width for exclusion of doublets. DAPI (4',6-diamidino-2-phenylindole) was used to discriminate between viable and dead cells. Data were recorded by Cyan™ ADP flow Cytometer (Dako, Hamburg, Germany) using Summit™ acquisition software (Summit, Jamesville, NY, USA).

2.3.4 Cellular internalization

The appropriate cells were seeded into 24-well plates coated with collagen at a density of 50 000 cells/well. After 24 h, culture medium was replaced with 400 µL fresh growth medium. pDNA polyplexes (N/P 12) in 100 µL HBG, containing 1 µg pDNA (20% of the nucleic acid was Cy5-labeled) were added to each well and incubated at 37°C for either 30-45 min (in case of targeted oligomers) or 4 h (for untargeted oligomers). Subsequently, cells were washed twice with 500 µL PBS, containing 1000 I.U. of heparin, for 15 min to remove any polyplexes sticking to the cell surface. Cells were detached with trypsin-EDTA and taken up in PBS with 10% FCS. Cellular uptake was assayed by excitation of Cy5 at 635 nm and detection of emission at 665 nm. Cells were appropriately gated by forward/sideward scatter and pulse width for exclusion of doublets. DAPI (4',6-diamidino-2-phenylindole) was used to discriminate between viable and dead cells. Data were recorded by Cyan™ ADP flow Cytometer (Dako, Hamburg, Germany) using Summit™ acquisition software (Summit, Jamesville, NY, USA) and analyzed by FlowJo® 7.6.5 flow cytometric analysis software.

2.3.5 Nuclear association

N2A cells were plated into 24-well plates coated with collagen at a density of 50 000 cells/well. After 24 h, the culture medium was replaced with 400 µL fresh medium. pDNA polyplexes (N/P 12) in 100 µL HBG, containing 1 µg pDNA (20% of the nucleic acids were Cy5-labeled) were added to each well and incubated at 37°C. After 24h isolation of cell nuclei was performed as described by Grandinetti *et al.* [126]. N2a cells were pelleted by centrifugation using tabletop centrifuge (Heraeus Biofuge Fresco, DJB Labcare, UK) at 2000 rpmi at 4 °C for 10 min and resuspended in 2 mL of ice-cold PBS (phosphate-buffered saline) buffer containing 2 mM DTT, 1 µg/mL protease inhibitor cocktail, and 40 µg/mL digitonin. The cells were incubated on ice for 5 min in order to permeabilize them. Nuclei from the permeabilized cells were then pelleted at 5000 g at 4°C for 10min and resuspended in 2 mL of ice-cold PBS containing 2 mM DTT and 1 µg/mL protease inhibitor cocktail and incubated again on ice for 5 min. Nuclei were then centrifuged at 5000 rpmi at 4°C for 10 min and resuspended in 500 µL PBS containing 10% FCS prior to flow cytometry analysis. Cellular association was assayed by flow cytometry as described above.

2.3.6 Luciferase gene transfer

Cells were seeded 24 h prior to pDNA delivery using 10 000 cells per well in 96-well plates. Transfection efficiency of the oligomers was evaluated using 200 ng pCMVLuc per well. All experiments were performed in quintuplicates. Before transfection, medium was replaced with 80 µL fresh medium containing 10% FCS. Polyplexes formed in 20 µL HBG in sterile Eppendorf caps at 25 °C were added to each well. In the case of experiments performed with the non-targeted oligomers, the polyplexes were incubated on cells for 24 h at 37 °C. LPEI at nontoxic optimum N/P 6 with 24 h polyplex incubation on cells was used as positive control. In the case of targeted oligomers, a shorter 30-45 min polyplexes incubation with cells was used, followed by incubation with fresh medium containing endosomolytic agent chloroquine at concentration of 100 µM (for control experiments without chloroquine only fresh medium was added). After 4 h medium was again replaced by fresh medium and cells were further incubated for 20 h. LPEI at nontoxic optimum N/P 6 with 4 h polyplex incubation on cells was used as positive control. HBG buffer was used as negative control. For all experiments 24 h after transfection, cells were

treated with 100 µL cell lysis buffer (25 mM Tris, pH 7.8, 2 mM EDTA, 2 mM DTT, 10% glycerol, 1% Triton X-100). Luciferase activity in the cell lysate was measured using a luciferase assay kit (100 µL Luciferase Assay buffer, Promega, Germany) and a Centro LB 960 plate reader luminometer (Berthold Technologies, Germany).

2.3.7 Cell viability assay (MTT assay)

The cells were transfected in 96-well plates as described above. 24 h post transfection, 10 µL of MTT (3-(4,5-dimethylthiazol-2-yl)-2,5-diphenyltetrazolium bromide; 5 mg/mL) were added to each well reaching a final concentration of 0.5 mg/mL. After an incubation time of 2 h, unreacted dye and medium were removed and the 96-well plates were stored at -80°C for at least one hour. The purple formazan product was then dissolved in 100 µL DMSO (dimethyl sulfoxide) per well and quantified measuring absorbance using microplate reader (Tecan Spectrafluor Plus, Tecan, Switzerland) at 530 nm with background correction at 630 nm. All studies were performed in quintuplicates. The relative cell viability (%) related to control wells treated only with 20 µL HBG was calculated as ([A] test/[A] control) × 100%.

2.3.8 Metabolic activity assay (CellTiter-Glo® assay)

N2A cells were plated in 96-well plates at 5 000 cells/well. After 24 h, medium was replaced by fresh medium containing increasing concentrations of oligomers (0.01; 0.1; 0.2; 0.4; 0.8 and 1mg/mL). After 48 h of incubation, half of the medium in the well (50 µL) was replaced by 50 µL of CellTiter-Glo® Reagent (Promega, USA). The relative metabolic activity was determined as the ratio of measured luminescent signal proportional to the amount of ATP present over the signal of untreated cells. For this purpose Lumat LB9507 luminometer (Berthold, Bad Wildbad, Germany) was used.

2.3.9 Fluorescence microscopy

The Huh7 cells were seeded into eight-well chamber slides coated with collagen at a density of 30 000 cells/well. After 24 h, culture medium was replaced with 240 µL fresh growth medium. pDNA polyplexes (N/P 12) in 60 µL HBG, containing 600 ng pDNA (20% of the nucleic acid was Cy5-labeled) were added to each well and incubated at 37°C. After 45 min, DAPI was added and pictures were obtained using Zeiss Axiovert 200 fluorescence microscope (Carl Zeiss AG, Germany).

2.3.10 Western blotting

Huh7 cells (200 000 /well) were seeded in 4 ml medium using six-well plates. After 24 h, medium was replaced with 2 ml fresh medium. The transfection polyplexes were performed as described above using 5 µg pDNA. After 45 min of incubation, the cells were lysed and total protein concentration was determined using a BCA assay. 30 µg of protein in loading buffer were applied per lane and were separated by SDS-PAGE under reducing conditions, blotted on nitrocellulose membrane and blocked with NET gelatine for 1 h at room temperature. Immunostaining was performed using Met (Santa Cruz Biotechnology, USA), phospho-Met (Cell Signalling, USA), Akt and phospho Akt antibodies (Cell Signaling, Germany) overnight at 4 °C. After the incubation with the applicable primary antibodies, membranes were washed three times for 15 min with NET gelatine before incubating with the adequate secondary peroxidase antibody for 1 h. When necessary the membranes were stripped in 2% SDS (w/v) with 0.8% (v/v) ß-mercaptoethanol in 0,07 M Tris/HCl solution for 1 h at 50 °C. After another three washing cycles, the membranes were cut accordingly and the proteins were then visualized using Lumi-Light Western blotting substrate (Roche, Germany).

2.3.11 Serum stability assay

1 µg pDNA and the polymer at N/P 12 were diluted in separate tubes in HBG to a total volume of 12.5 µL. The polyplexes were formed and incubated for 30 min at room temperature. 112.5 µL of fetal bovine serum (FCS) were added to the samples to reach a final concentration of 90% FCS. The samples were then incubated with

FCS for 1, 10, 30 or 90 min at 37 °C. Where indicated, 100 I.U. heparin was added to the polyplexes incubated in serum. Agarose gel (1%) was prepared by dissolving agarose in TBE buffer. After addition of GelRed, the agarose solution was casted into an electrophoresis unit to form a gel. 4 µL loading buffer were added to the samples before they were placed into the sample pockets. Electrophoresis was performed at 120 V for 80 min.

2.3.12 Erythrocyte leakage assay

Fresh, citrate buffered murine blood was washed several times with PBS. Washed murine erythrocyte suspension was centrifuged and the pellet was diluted to 5×10^7 erythrocytes/mL with two different PBS buffers (pH 7.4, and 5.5). A volume of 75 µL of erythrocyte suspension and 75 µL of oligomer solution were added to each well of a V-bottom 96-well plate (NUNC, Denmark) resulting in final concentration of 5 µM oligomer per well. 1% Triton X-100 served as the positive control, addition of only PBS buffer of each pH to the erythrocyte suspension as the negative control. The plates were then incubated at 37 °C under constant shaking for 1 h. After centrifugation, 100 µL of the supernatant were analyzed for hemoglobin release measuring its absorbance at 405 nm with the microplate reader (Tecan Spectrafluor Plus, Tecan, Switzerland).

2.4 Biological evaluation *in vivo*

2.4.1 Luciferase gene transfer

Animal experiments were carried out in female Rj:NMRI-nu (nu/nu) (Janvier, Le Genest-St-Isle, France). $5x10^6$ Huh7 cells were inoculated subcutaneously into the left flank and experiments started approximately 12 days after tumor cell injection when the tumors reached the adequate size. For intratumoral administration, polyplexes containing 50 µg pCMVLuc (around 2.5 µg/g body weight) at N/P 12 in HBG in total volume of 60 µL were applied and mice were sacrificed after 24 h. Systemic gene transfer in tumor bearing mice was conducted using polyplexes containing 80 µg pCMVLuc (around 4 µg/g body weight) at N/P 12 in HBG in total volume of 200 µL. Polyplexes were injected into the tail vein and animals were

sacrificed 48 h after application. Tumors and/or organs were dissected and homogenized in cell culture lysis reagent using a tissue and cell homogenizer (FastPrep®-24, MP Biomedicals, USA). The samples were then centrifuged at 3000 g at 4 °C for 10 min to separate insoluble cell components. Luciferase activity was determined in the supernatant using a Centro LB 960 luminometer (Berthold, Germany). The animal experiments were performed together with Annika Herrmann (veterinary MD study, LMU). All animal procedures were approved and controlled by animal experiments ethical committee of Regierung von Oberbayern, District Government of Upper Bavaria, Germany, and carried out according to the guidelines of the German law of protection of animal life.

2.4.2 Quantitative real time polymerase chain reaction

For pDNA quantification by real-time PCR (RT-PCR) in tumors, polyplexes were administered as described above. Total DNA was isolated according to manufacturer's instructions using peqGOLD guanidinisothiocynate/phenol method (Peqlab, Germany). Quantitative RT-PCR was then performed on a LightCycler 480 system (Roche) using UPL Probe #84 (Roche) and Probes Master (Roche). The following primer sequences were used: reverse primer 5'-CCC CGT AGA AAA GAT CAA AGG-3' and forward primer 5'-GCT GGT AGC GGT GGT TTT T-3'. The pDNA dilution series were run in parallel to allow the absolute quantification.

2.5 Statistical analysis

All values are stated as mean ± SD unless otherwise indicated. The number of replicates is indicated in the corresponding methods section. For statistical analysis, student’s t-tests were performed (*$p<0.05$; **$p<0.01$; ***$p<0.001$).

3 RESULTS

3.1 Polypropylenimine dendrimers bioreducibly tailored with sequence-defined oligo (ethane amino) amides as gene delivery systems

Efficient pDNA delivery with cationic polymers is known to be dependent also on the polymer size. For instance, a relatively high molecular weight (Mw) of linear PEI (LPEI) of 22 kDa is required for high transfection efficiency. However, its high Mw is also strongly associated with carrier toxicity [127, 128]. Due to its static structure, accumulation in cells or organs of living systems can occur, causing undesired toxic effects. Low Mw cationic gene carriers, on the other hand, may not provide sufficient polyplex stability *in vivo* during blood circulation [129-131]. Therefore, a connection of non-toxic small Mw compounds by biodegradable linkages into larger polymeric structures presents a possible solution [129, 130, 132-136]. Previously, in our lab Russ *et al.* [137] presented a method for assembly of so-called “pseudodendrimers” by connecting low Mw oligoethylenimine (OEI) units with the biodegradable linker hexanedioldiacrylate (HD) resulting in efficient and biocompatible gene carriers. In a subsequent work, the structurally better defined dendrimers G2 or G3 polypropylenimine (PPI) were used as core structures and connected with the same HD linker to either PPI or oligoethylenimine surface units [138]. Nevertheless, uncertainty of the resulting structures still remained due to their polydisperse nature and absence of precise connection sites between core and surface units. For the current evaluation, we chose PPI as a core of our carriers with a focus on generating more defined biodegradable gene vectors with higher Mw and biocompatibility (Edith Salcher, PhD thesis LMU 2013). PPI and other dendrimers have already previously gained much attention in gene delivery [139, 140] due to a well defined size and structure, monodispersity and especially high ratio of multivalent surface moieties to molecular volume which offers multiple attachment sites for various domains such as shielding and targeting domains. In order to overcome the main limitations of PEI, polydispersity and cytotoxicity, analogs have recently been designed based on the artificial amino acid succinoyl-tetraethylene pentamine (Stp) [119]. Stp contains the

1,2-diaminoethane motif also present in PEI and responsible for nucleic acid complexation and endosomal buffering [120, 121]. In the current study such small, sequence-defined linear oligomers consisting of increasing number of Stp units were used attached as octamers to a PPI core.

3.1.1 Design of oligo(ethanamino)amides-equipped polypropylenimines

Small Stp oligomers [141] mediate efficient gene transfer only upon cysteine incorporation and disulfide-based oligomerization into larger structures. These sequence-defined linear oligomers consisting of increasing number of Stp units [119] were used for modification of the PPI core (Edith Salcher, PhD thesis, LMU 2013).

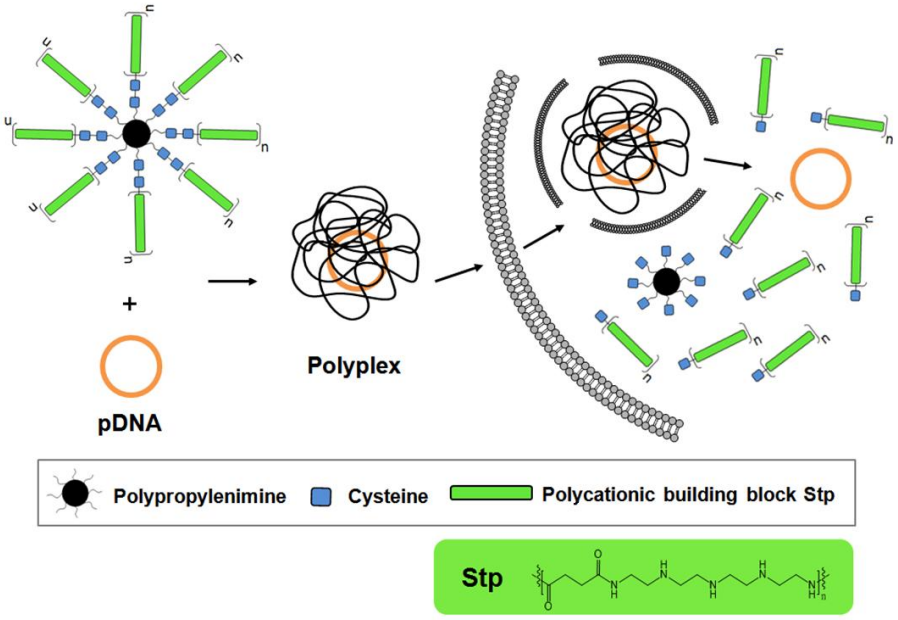

Scheme 1. Schematic presentation of defined dendritic structures consisting of PPI G2 core linked *via* disulfide linkages to sequence-defined Stp oligomers and their biodegradation in the reducing cytosol environment [142].

Low generation 2 (G2) PPI [143] was chosen due to its lower cytotoxicity and moderate efficiency concerning pDNA gene transfer. Disulfide bonds were introduced as a biodegradable linkage between the PPI core and linear Stp oligomers, as these can be generated in a controlled manner and are rather stable in the extracellular environment, not leading to polymer degradation until reaching the reducing cytosolic environment. In order to enable efficient reaction of PPI with cysteine-containing linear Stp oligomers (Scheme 1), the eight primary amines on the surface of PPI G2

were amidated with an activated cysteine derivative and then reacted with cysteine-containing linear oligomers (separately synthesized by solid-phase supported synthesis) containing one C-terminal cysteine and 1 to 5 Stp units). The library of resulting synthesized PPI conjugates (synthesis by Edith Salcher and Claudia Scholz, LMU Pharmaceutical Biotechnology, see [142]) is presented in Table 1.

Table 1. Identification numbers, sequences, abbreviations and number of Stp units and protonatable amines of the synthesized conjugates.

Conjugate (Polymer Id)	Sequence	Abbreviation	n (Stp units)	Protonatable Amines
418	PPI-(C-C-Stp)8	**PPI-Stp1**	1	46
427	PPI-(C-C-Stp2)8	**PPI-Stp2**	2	70
428	PPI-(C-C-Stp3)8	**PPI-Stp3**	3	94
430	PPI-(C-C-Stp4)8	**PPI-Stp4**	4	118
536	PPI-(C-C-Stp5)8	**PPI-Stp5**	5	142
PPI G2			0	14

3.1.2 Biophysical characterization of polypropylenimines

The ability of synthetic gene carriers to condense pDNA to nanosized particles is a crucial requirement for successful gene delivery. Therefore, the pDNA binding ability of synthesized PPI conjugates was first evaluated by EtBr exclusion assay (Figure 1A). LPEI was used as a “positive control” displaying the fastest and the greatest decrease in the intercalator fluorescence and therewith the highest compaction ability already at low N/P ratios. For unmodified PPI G2 with increasing N/P ratios the fluorescence decreased at a slightly slower rate than for LPEI, though at N/P ratios above around 8 PPI G2 was able to extinguish fluorescence to the same extent as LPEI. Of the novel Stp conjugates, the PPI conjugate with the highest number of Stp units, PPI-Stp5, also exhibited good pDNA compaction ability. With conjugates comprising 2-4 Stp units per branch, moderate reductions in EtBr fluorescence were obtained. The lowest binding capacity was observed for the conjugate with only 1 Stp unit per branch. The gel-shift assays for pDNA binding (Figure 1B) were in accordance with the findings above showing the best binding for PPI-Stp5 conjugate.

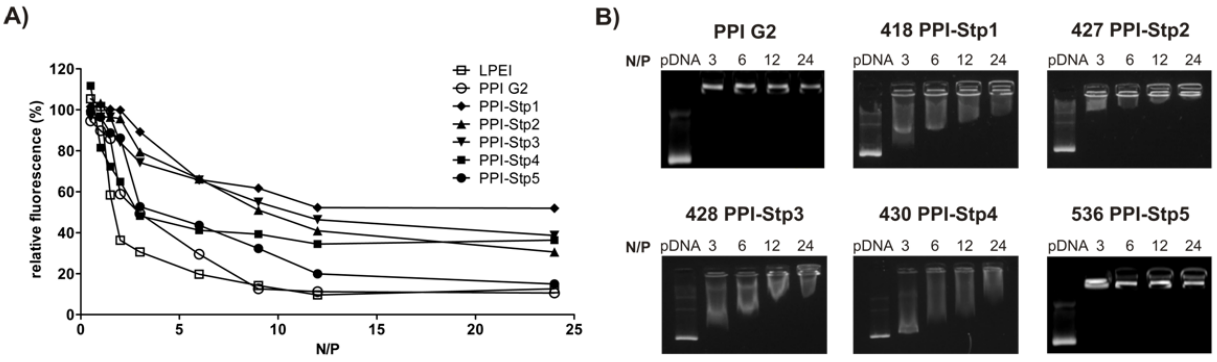

Figure 1. pDNA compaction ability of PPI G2 and its analogues with Stp units attached to a dendritic core. A) EtBr exclusion assay. Oligomer solution was added at increasing N/P ratios to 10 µg pDNA containing 0.4 µg EtBr. Reduction of EtBr fluorescence was calculated as percentage of maximal fluorescence of EtBr containing pDNA solution. B) pDNA binding assay by electrophoresis. The gel retardation of polyplexes at increasing N/P ratios was compared to the shift of plain pDNA.

This was the only PPI conjugate, apart from unmodified PPI G2, that exhibited a complete cargo binding at all N/P ratios. Size measurements of polyplexes at N/P 12 (Table 2) revealed that all Stp modified PPI conjugates form nanoparticles with pDNA of around 150-400 nm, acceptable for potential *in vivo* experiments [144]. The size of the particles increased with the number of Stp units up to 4 Stp units per conjugate branch. The PPI-Stp5/pDNA nanoparticles had a somewhat smaller (~270 nm) size. Their polydispersity index as an indicator of heterogeneity of sizes of the analyzed particles, calculated from a Cumulants analysis of the dynamic light scattering (DLS)-measured intensity autocorrelation function was also somewhat lower which was in line with good compaction ability of PPI-Stp5 as described above. However, all polydispersity indices were below 0.7, the value above which the samples are (due to their broad size distribution) unsuitable for the DLS technique. The unmodified PPI G2 on the other hand formed very large particles of around 1.2 µm with high polydispersity pointing out to the necessity of its surface modification. All polyplexes displayed similar positive surface charge with zeta potentials of around 20-30 mV (Table 2).

Table 2. Particle size, polydispersity index and zeta potential of PPI conjugate/pDNA polyplexes formed at N/P 12. The measurements were performed by Edith Salcher (PhD 2013, LMU).

Conjugate	Mean Size (nm)	Mean Polydispersity Index (PI)	Mean Zeta Potential (mV)
PPI-Stp1	155.3 ± 60.6	0.140 ± 0.04	21.7 ± 0.3
PPI-Stp2	272.8 ± 94.8	0.245 ± 0.01	25.6 ± 1.3
PPI-Stp3	321.5 ± 32.9	0.320 ± 0.01	32.1 ± 1.3
PPI-Stp4	369.6 ± 90.9	0.349 ± 0.01	20.3 ± 0.5
PPI-Stp5	266.7 ± 29.5	0.278 ± 0.03	29.5 ± 0.6
PPI G2	1198 ± 636	0.496 ± 0.02	27.1 ± 1.6

3.1.3 Biological in vitro characterization

Cellular internalization studies were performed on two different cell lines, mouse neuroblastoma (N2a) and humane prostate cancer (PC3) cells, to investigate any cell line dependent behavior of PPI conjugate/pDNA polyplexes. For this purpose fluorescently labeled (Cy5) pDNA was used. After pDNA transfection the cellularly bound but not internalized polyplexes were removed by polysaccharide heparin, taking advantage of its negative charge density. The flow cytometry results are displayed as histograms plotting the Cy5 fluorescence intensity against the number of events.

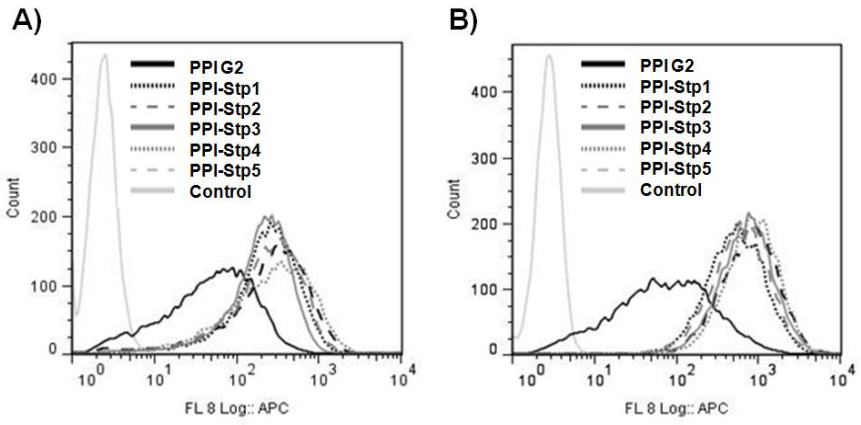

Figure 2. Cellular internalization of PPI conjugate/Cy5-pDNA polyplexes formed at N/P 12 assayed 4h after transfection. Flow cytometry experiments were performed on A) N2a and B) PC3 cells. DAPI was used to discriminate between viable and dead cells.

They showed that all Stp modified PPI conjugates were taken up by the cells to a similar extent. Unmodified PPI G2 on the other hand, in spite of the presence of bigger polyplex aggregates, showed much lower cellular internalization of polyplexes than the Stp modified conjugates. Almost no difference was observed between cellular internalization on N2a (Figure 2A) and PC3 cells (Figure 2B).

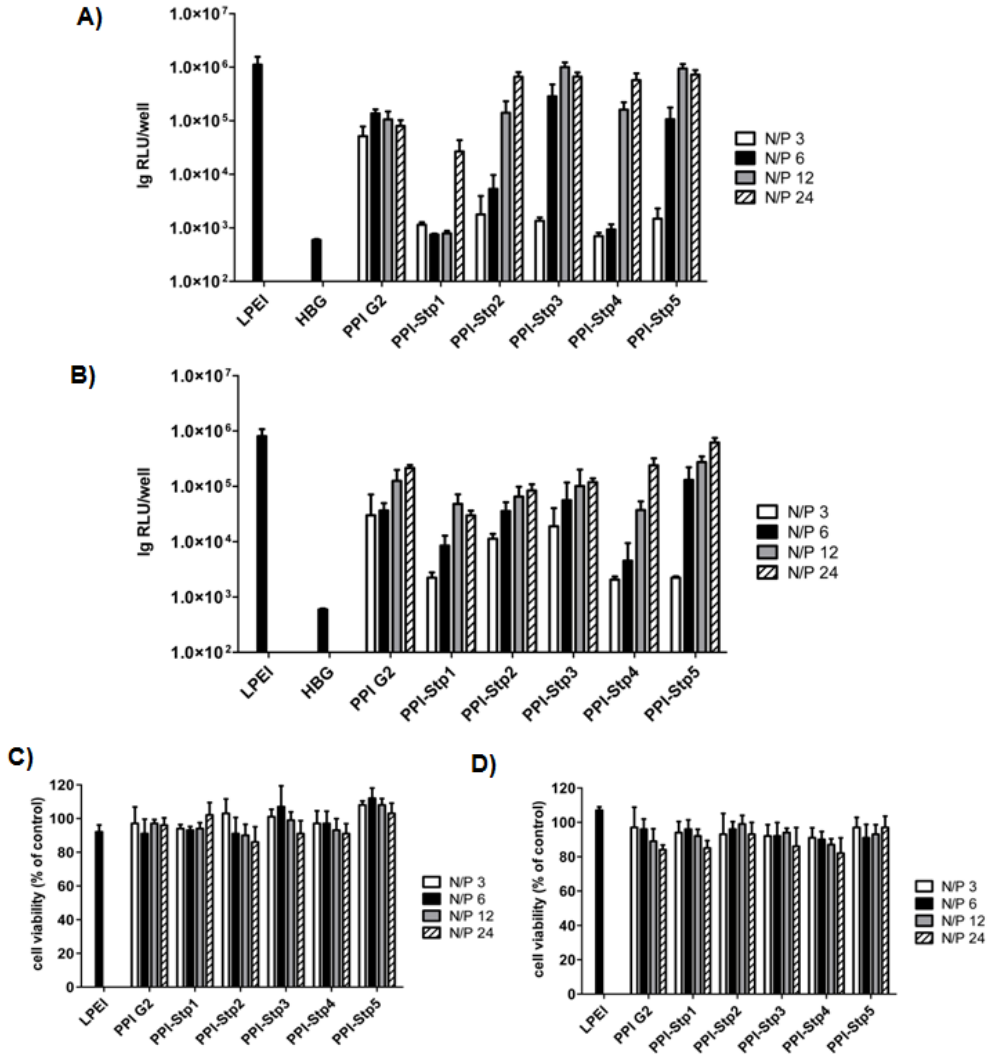

Figure 3. Luciferase gene transfer on A) N2a and B) PC3 cells and corresponding cell viabilities (MTT assay) on C) N2a and D) PC3 cells. The luciferase activity in the cell lysates was analyzed 24h after transfection. LPEI was used as a positive control, HBG buffer treated cells served as a background. Cell viability was related to control wells treated only with HBG. Data are presented as mean values (±SD) out of quintuplicate.

Next, gene transfer studies (Figure 3) were performed evaluating polyplexes at different N/P ratios and luciferase gene expression in both cell lines. Results in the two cell lines were similar with the exception of a higher N/P dependence with N2a

(Figure 3A) as compared to PC3 (Figure 3B) cells. With the increasing number of Stp units per dendrimer branch the transfection efficiency generally increased, reaching its optimum again for the PPI-Stp5 conjugate, at a similar level as the “gold standard” LPEI. PPI G2 showed only moderate efficacy (around 1 log unit below LPEI). None of the synthesized polyplexes affected the cell viability (Figure 3C, D) as determined with MTT assay, thus displaying high biocompatibility at applied conjugate amounts.

Favorable transfection results depend not only on sufficient polyplex stability (Figure 1) and cellular uptake (Figure 2), but also on subsequent steps, including escape from the endocytic vesicles and transport to and into the nucleus. To further elucidate the delivery process, we tested the proton sponge activity of polyplexes (considered as important for endosomal escape). pH titrations of PPI G2 and the two most potent PPI-Stp conjugates, PPI-Stp4 and PPI-Stp5, were performed. Consistent with the higher transfection efficiency, both PPI-Stp conjugates exhibited a higher total buffering capacity (approximately 30%, Figure 4A) in the endolysosomal pH range from pH 7.4 to pH 5.0, as compared to PPI G2 (22% buffering capacity). Evaluation of the relative buffer capacities more in detail at different pH ranges within the endolysosomal pH range for the two conjugates displayed an increase in buffer capacity with an increasing pH, with a maximum around pH 7 (Figure 4B).

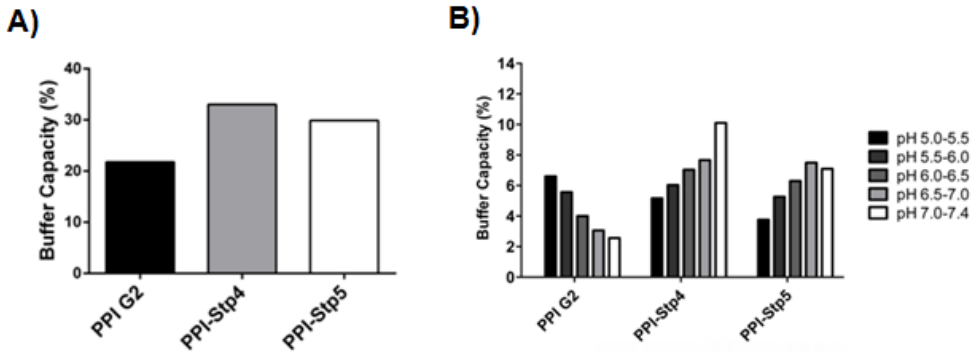

Figure 4. (A) Total buffer capacity in the endolysosomal pH range (from pH 7.4 to pH 5.0) and (B) relative protonation distribution at different pH ranges within the endolysosomal pH range of PPI-Stp4 and PPI-Stp5 conjugates compared to PPI G2. The experiment was carried out by Claudia Scholz (PhD thesis 2014, LMU).

The opposite was observed for PPI G2, exhibiting the highest buffering capacity at the lowest pH 5. Furthermore, an erythrocyte leakage assay was performed (Figure 5) to evaluate the lytic activity of the conjugates and its possible contribution to endosomal escape. For this purpose hemoglobin release was measured at different

pH values (pH 7.4, 6.5, 5.5) at the conjugate concentration of 5 μM. PPI conjugates did not mediate any significant lytic activity, consistent with their low cytotoxicity.

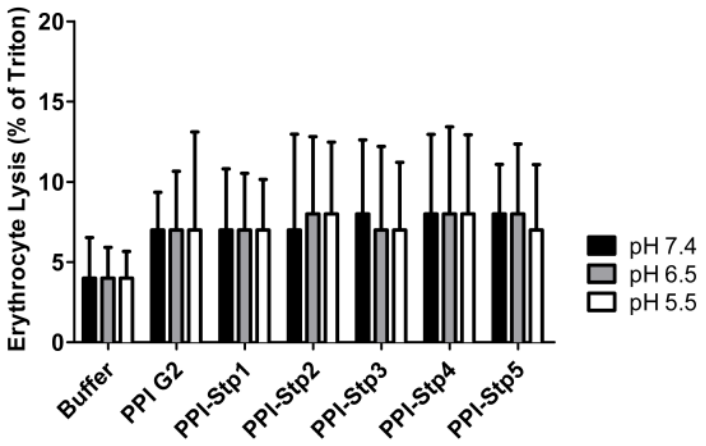

Figure 5. Erythrocyte leakage assay at different pH values: PPI conjugates were incubated on erythrocytes at the concentration of 5 μM at 37°C at indicated pH values. Hemoglobin release was measured after 1 h.

In the following, to determine the further intracellular delivery fate of the PPI conjugate/pDNA polyplexes towards the cell nucleus, N2a cells were transfected with the Cy5-pDNA polyplexes at N/P 12, analogously as in the case of cellular internalization studies. After 24h cell nuclei were isolated and analyzed by flow cytometry (Figure 6). It is important to emphasize that in these 'nuclear association' studies we cannot discriminate whether polyplexes are attached to the nuclei surface or whether the signals derives from pDNA already internalized by the nuclei. In any case, the resulting histograms were well in accordance with the luciferase reporter gene expressions in N2a cells. The PPI-Stp1/pDNA polyplexes showed the weakest nuclear association, whereas the PPI-Stp5/pDNA polyplexes the highest association with the nuclei (Figure 6).

In further assessment of the influence of PPI surface modifications on the cytotoxicity, an ATP assay was performed where the metabolic activity of cells after treatment with increasing concentrations of PPI conjugates was analyzed after 48h. Figure 7 presents the relative metabolic activity of N2a cells defined as a ratio of measured ATP content over the ATP content of untreated cells.

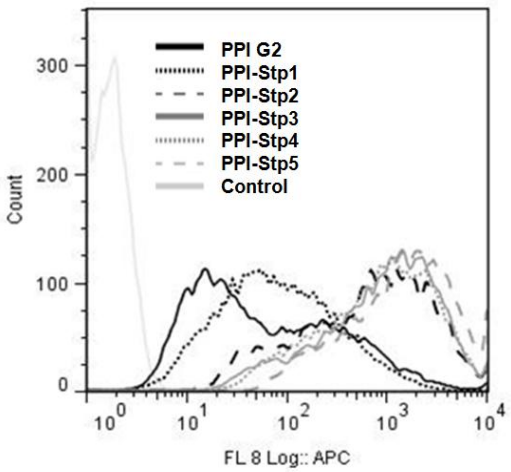

Figure 6. Nuclear association of PPI conjugate/Cy5-pDNA polyplexes formed at N/P 12 using N2a cells. Flow cytometry experiments with the isolated nuclei were performed 24h after transfection.

At lower dendrimer concentrations no reduction of metabolic activity was observed for all the applied conjugates, whereas above 0.2 mg/mL unmodified PPI G2, in contrast to all Stp modified conjugates, showed significant cytotoxicity; this highlights the importance of the surface modification of PPI G2.

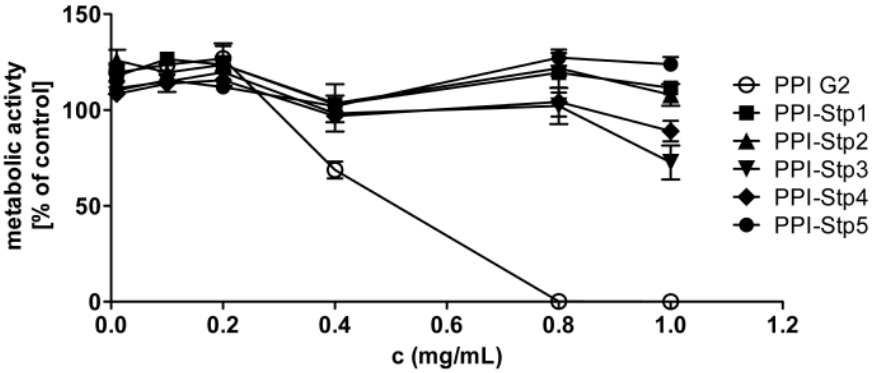

Figure 7. Relative metabolic activity of N2a cells after treatment with PPI conjugates for 48 h determined with CellTiter-Glo® and defined as the ratio of measured ATP content over the ATP content of untreated cells. The metabolic activity was determined as the ratio of measured luminescent signal over the signal of untreated cells.

3.1.4 Biological in vivo characterization

According to the above biophysical and biological studies the most promising Stp modified conjugate, PPI-Stp5, was further evaluated in studies *in vivo* and compared to PPI G2 dendrimer. Both dendrimers sufficiently bound their cargo in serum as shown by pDNA gel shift assay after incubation of polyplexes in 90% FCS for 1, 10, 30 or 90 min (Figure 8A).

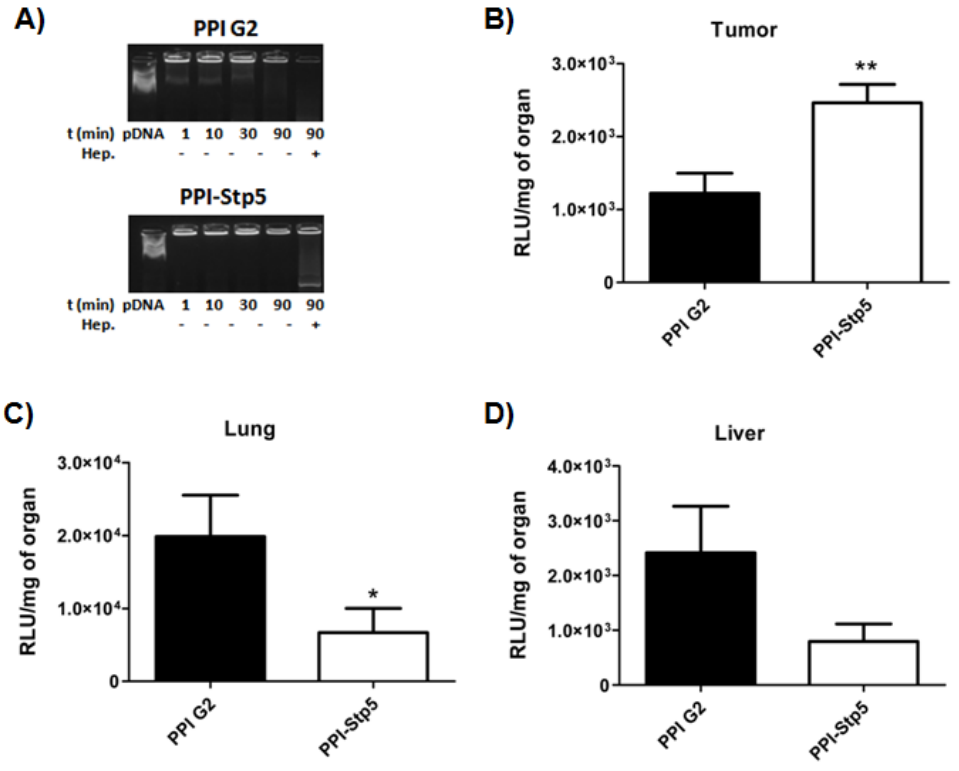

Figure 8. A) Polyplex stability in 90% FCS at 37 °C at different time points: Polyplexes of PPI G2/pDNA and PPI-Stp5/pDNA were incubated at room temperature for 30 min in order to allow polyplex formation. Subsequently, FCS was added followed by incubation for 1, 10, 30 or 90 min. Heparin (50 I.U.) was added to dissociate the polyplexes. Lane 1 shows the plain pDNA with added FCS, lanes 2-5 polyplexes at different FCS incubation times and lane 6 the polyplexes with the longest FCS incubation time (90 min) and heparin addition. B, C, D) Luciferase gene expression 48 h after i.v. administration of PPI G2/pDNA and PPI-Stp5/pDNA polyplexes at N/P 12 into N2a tumor bearing mice (N=4, mean±SEM) in B) tumor, C) lung and D) liver. Luciferase gene expression is presented as relative light units per organ or tumor weight (RLU/mg of organ). Lysis buffer RLU values were subtracted. Liver weight was around 1.5 g, lung weight around 190 mg and N2a tumor weight 433±134 mg. The animal experiments were performed together with Annika Herrmann (veterinary MD study, LMU).

Only upon heparin addition after 90 min of FCS incubation the polyplexes partially dissociated. *In vivo* experiments were performed in N2a tumor-bearing mice. When the tumors reached the necessary size, PPI-Stp5 and PPI G2 polyplexes at N/P 12 were injected into the tail vain of the mice. After 2 days mice were sacrificed, organs collected and homogenized in lysis buffer and subsequently centrifuged. Luciferase activity measurements of the supernatant resulted in significant gene expressions in tumor, lung and liver (Figure 8), whereas hardly any gene transfer could be observed in kidney, spleen and heart (data not shown). The gene expression of PPI G2 polyplexes in the lung and liver may be attributed to the lower colloidal polyplex stability and aggregate formation into micrometer-sized structures (see Table 2), consistent with accumulation in lung capillaries and rapid clearance. For PPI-Stp5 polyplexes, lower luciferase transgene expressions in the lung (Figure 8C) and in the liver (Figure 8D) were found than for PPI G2/pDNA polyplexes. Notably, PPI-Stp5 polyplexes enabled significantly higher gene transfer in N2a tumor as compared to PPI G2 (Figure 8B).

3.2 Sequence-defined linear oligo (ethane amino) amides of increasing length in gene delivery

As mentioned above, the cytotoxicity and polydispersity of PEI constitute main drawbacks for further clinical development and evidence has emerged indicating that the cytotoxicity of cationic polymers is often correlated with their molecular weight (Mw) [145-147]. Therefore, several studies have been performed replacing the effective PEI structures (approximately 25 kDa, linear or branched) with their analogs to decrease cytotoxicity while simultaneously maintaining or even increasing their efficiency. These include the oligomerization of low molecular weight (LMw) PEI *via* biodegradable linkages [148, 149], the attachment of LMw PEI to other polymer backbones [150] or the functionalization of the amine groups of PEI for the purpose of changing its chemical and thus biological properties [39, 151]. We previously demonstrated that the implementation of PEI-mimicking 1,2-diaminoethane motif containing artificial amino acids like succinoyl-tetraethylene pentamine (Stp) in nucleic acid carriers enables highly efficient gene transfer and contributes to nucleic acid binding, endosomal buffering and endosomal escape [120, 141]. A simple linear

sequence of 5 Stp units was found inactive in gene transfer [120]. This was not surprising as the number of only 16 protonatable nitrogens was much smaller than the approximately 500 (±200) protonatable nitrogens of standard LPEI. The small precise oligomer was not able to form stable polyplexes with nucleic acids. However, when these short 5 Stp units chains were bioreducibly attached to each of the eight branches of the PPI dendritic core (see chapter 3.1 above), a high transfection efficiency comparable to the gold standard linear PEI (LPEI) was achieved (Figure 3A, B). For the development of more effective transfection carriers without the need for a dendritic core, additional moieties such as cysteines [141, 152], which stabilize polyplexes by disulfide-formation between oligomers, tyrosine trimers [121] or fatty acids [120, 123], which provide hydrophobic stabilization of formed nanoparticles, had to be incorporated. Here, the fundamental question was whether the linear Stp oligomers alone, without any further functional modification, could serve as pDNA carriers above a certain oligomer size threshold, similar as LPEI does. For this purpose a series of linear oligomers was synthesized (synthesis by Claudia Scholz, PhD thesis 2014, LMU), in which the number of Stp repeats was consecutively increased from 5 to 40 units (comparable to the number of Stp units in PPI-Stp_x conjugates having from 8 to 40 Stp units; see Scheme 1), resulting in oligomers with a Mw of 1.5 to 11 kDa.

3.2.1 Design of carriers of increasing lengths

Previous studies have demonstrated the suitability of the diaminoethane motif containing artificial amino acid Stp to be applied for an assembly of the sequence-defined carriers for gene delivery *via* solid-phase assisted synthesis. Here, a small library of linear oligo (ethane amino) amides of increasing lengths without any additional functional domains was evaluated. The synthesized oligomers consisted of 5, 10, 15, 20, 30 and 40 Stp units (synthesis by Claudia Scholz, see [153]). As the two primary amino groups of the tetraethylene pentamine (tp) are bound in amide bonds of the oligomers backbone, each Stp unit provides three protonatable secondary amino nitrogens available for electrostatic interactions with the oppositely charged nucleic acid (Scheme 2). A C-terminal terminal tryptophane was included for a better analytical characterization.

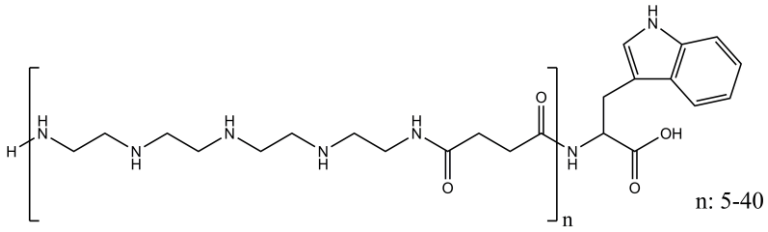

Scheme 2. Chemical structure of the oligomers Stp_n-W.

Table 3. Sequences of oligomer structures written from N- to C-terminus and the corresponding molecular weights [Da].

Compound	Sequence	Calculated molecular weight (Da)
681	Stp**5**-W	1561,0
643	Stp**10**-W	2917,8
644	Stp**15**-W	4274,6
645	Stp**20**-W	5650,6
554	Stp**30**-W	8345,0
555	Stp**40**-W	11058,6

3.2.2 Biophysical characterization of the carriers

First, the pDNA binding characteristics of the synthesized oligomers were examined by means of agarose gel electrophoresis. The shifts in the gel revealed that with an increasing number of Stp units in the carrier the polyplex stability improved. Stp5-W was not able to form stable polyplexes even at the highest tested N/P ratio of 24, Stp10-W showed a partial pDNA binding from N/P 12 to 24. Stp15-W displayed a complete binding at N/P 18 and higher, whereas all polymers with 20 or more Stp units exhibited complete pDNA binding already at N/P 12 and partial binding at N/P 6 and 3 (Figure 9).

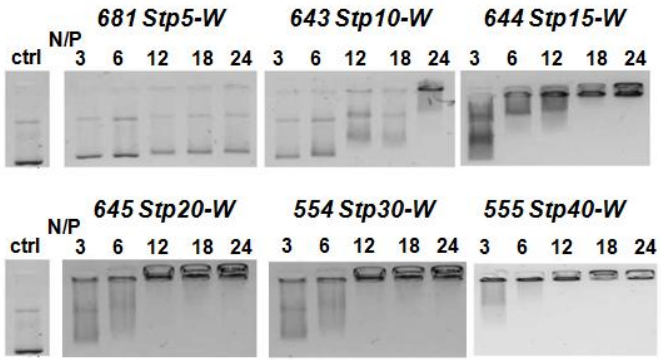

Figure 9. pDNA binding capability determined by gel shift assay at increasing N/P ratios. The experiment was performed by Claudia Scholz (PhD thesis 2014, LMU).

The improvement in pDNA condensation ability through oligomer elongation was confirmed in the EtBr exclusion assay were the decrease in fluorescence, resulting from higher EtBr exclusion by polyplex formation after oligomer addition, increased with increasing Mw of the oligomers (Figure 10). LPEI still displayed a higher pDNA condensation ability compared to the best-performing Stp oligomer.

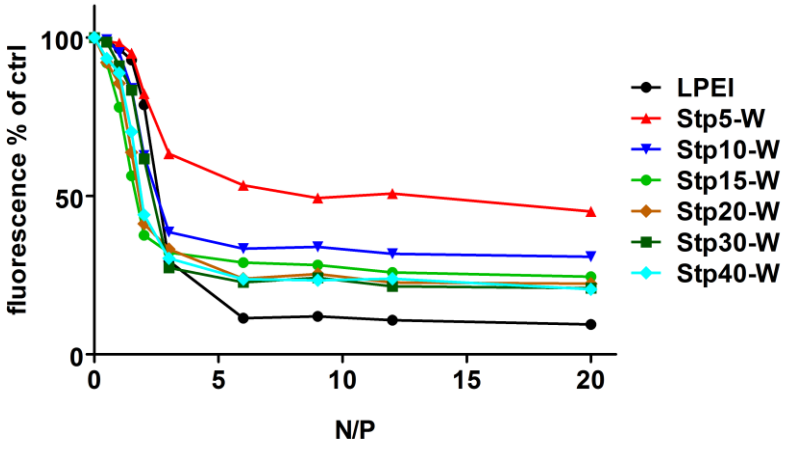

Figure 10. pDNA binding capacity of LPEI and linear Stp oligomers. EtBr exclusion assays with increasing N/P ratios obtained by stepwise addition of the oligomer to pDNA solution at pH 7.4. 100 % value displays fluorescence intensity of pDNA and EtBr before the addition of the polymer. The experiment was performed by Claudia Scholz (PhD thesis 2014, LMU).

Next, the influence of the carrier length on the cellular uptake was investigated in order to define the minimum length of the oligomer necessary for successful cellular internalization of the polyplexes (Figure 11). In accordance with the pDNA binding

studies, the polyplexes formed with Stp5-W showed only a weak uptake in N2a cells, which was then already remarkably enhanced for the Stp10-W polyplexes and further improved for Stp15-W polyplexes (Figure 11A). Nanoparticles formed with oligomers containing more Stp units (20, 30 or 40) all showed similarly high cellular internalization properties (Figure 11B).

The influence of the oligomer Mw on transfection efficiency was examined by luciferase reporter gene expression in N2a cells (Figure 12). Whereas the smallest Stp oligomer Stp5-W was completely inactive, increasing the number of Stp units led to a continuously improving gene transfer. Stp15-W at its highest N/P ratio 24 already exceeded the activity of LPEI at its optimum, non-toxic N/P ratio of 6. Stp30-W displayed the highest transfection efficiency of all tested oligomers, outnumbering LPEI 6-fold. An additional elongation to 40 Stp units could not further improve pDNA delivery. Altogether the results nicely demonstrated a positive impact of increasing Mw on transfection efficiency.

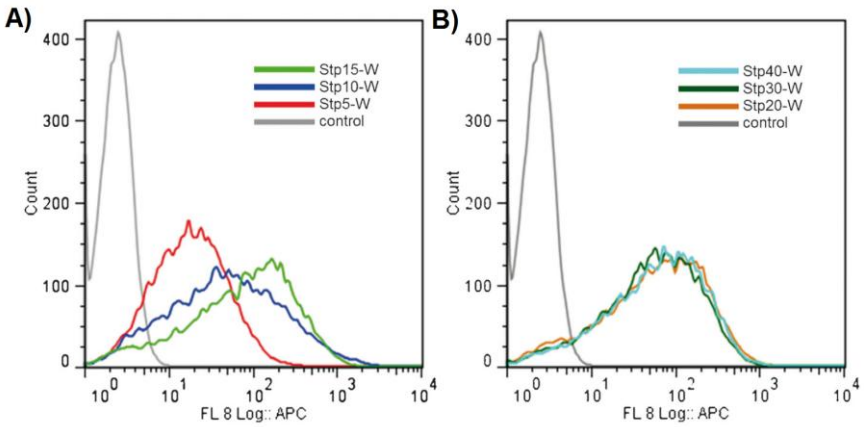

Figure 11. Cellular internalization of Cy5-labeled DNA/oligomer complexes at N/P 12 determined by flow cytometry in N2A cells after 4 h at 37 °C. a) Stp5-W = red, Stp10-W = dark blue, Stp15-W = light green; b) Stp20-W = orange, Stp30-W = dark green, Stp40-W = light blue. X-axis represents the intensity of the Cy5 signal and "Count" the number of cell counts with according fluorescence signal after appropriate gating. All incubations were performed in standard serum-supplemented culture medium. In the internalization studies, cells were washed for 15 min with heparin to remove polyplexes on the cell surface.

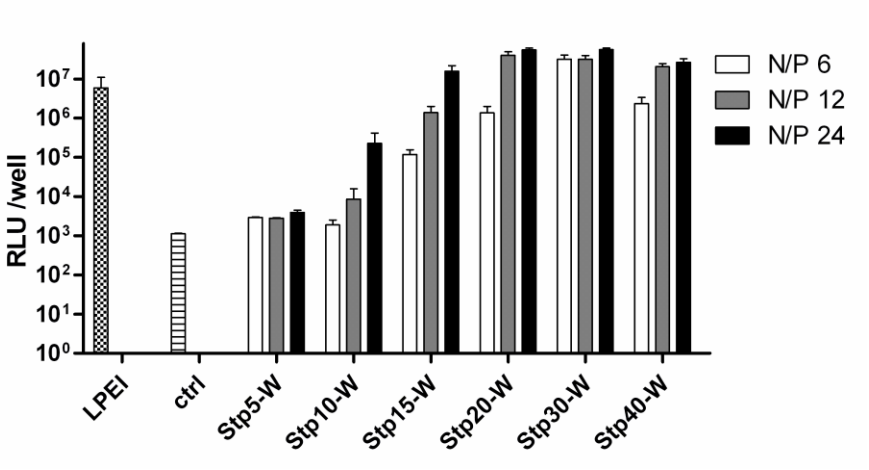

Figure 12. Luciferase gene transfer by LPEI and linear Stp oligomers in N2A cells at N/P ratios 6, 12 and 24.

3.2.3 Cytotoxicity

As important biological characteristics we next determined the cytotoxicities of the synthesized carriers by two different methods: MTT and CellTiter-Glo® assay. Regardless of their length, the polyplexes formed with the synthesized oligomers did not exhibit any significant cytotoxicity with the MTT assay which measures the mitochondrial redox state as a quantification of cell viability. Also LPEI at the optimum N/P 6 caused no noteworthy reduction in cell viability detectable by the MTT assay Figure 13). When the oligomers were tested as free oligomers at increasing concentrations with the CellTiter-Glo® assay which measures intracellular ATP levels, considerable differences in cytotoxicity were observed between them (Figure 14). For cells treated with LPEI already at a concentration of 0.2 mg/ mL metabolic activity was lost, whereas for Stp40-W, the most toxic of the linear Stp oligomers, still 90 % residual metabolic activity was observed at a concentration of 0.4 mg/ml. For the Stp oligomers, toxicity levels were very low; nevertheless a clear increase of toxicity was detected with increasing Mw. While Stp5-W did not show any toxicity at any examined concentration, all oligomers with 15 or more Stp units displayed a reduced metabolic activity (below 20 %) at the highest tested concentration of 1.0 mg/ mL. It has to be emphasized that oligomer concentrations as used in optimum transfection experiments are around 10 µg/ mL.

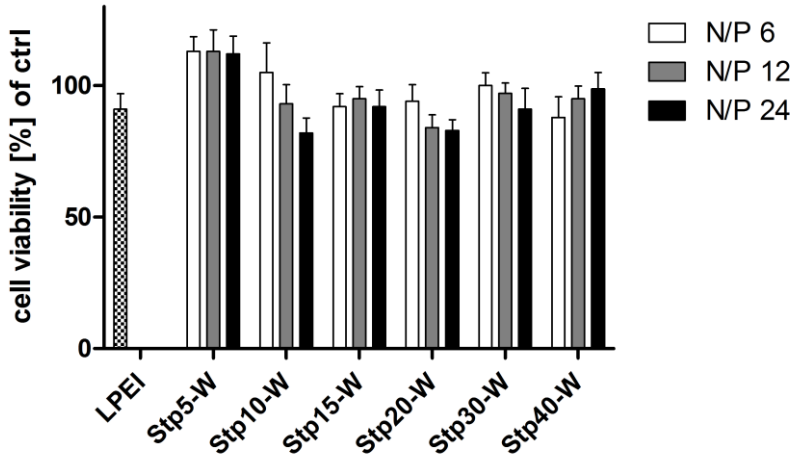

Figure 13. Metabolic activity after treatment of N2a cells with polyplexes as determined with MTT assay. Cell viability was related to control wells treated only with HBG.

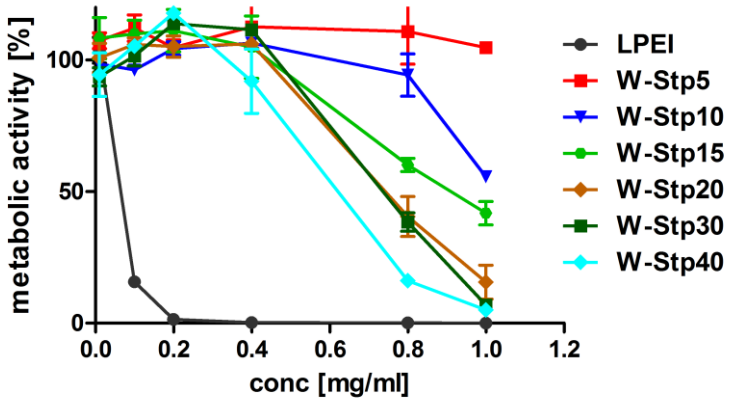

Figure 14. Metabolic activity of N2A cells treated with increasing LPEI or oligomer concentrations determined by CellTiter-Glo® assay. A metabolic acitivity of 100% was defined for untreated cells and all other values refer to this value.

3.3 Native chemical ligation as a screening tool for easy conversion of sequence-defined oligomers into targeted pDNA carriers

Native chemical ligation (NCL) is a chemoselective conjugation reaction [154, 155] that forms an amide bond by transthioesterification followed by intramolecular nucleophilic rearrangement between a thioester and N-terminal cysteine. Blanco-

Canosa *et al*. published a variation compatible with SPPS [156]. Two prerequisites are necessary for the successful ligation: i) an oligomer with an *N*-terminal cysteine, and ii) a ligation partner with a *C*-terminal, aromatic *N*-acylurea moiety (such as *N*-acyl-benzimidazolinone, Nbz). This simple reaction can occur under mild conditions in aqueous solution, and gives almost quantitative yields. NCL has been largely applied on the total synthesis of proteins and larger peptides, but not for nucleic acid carriers. In our lab, Christina Troiber (LMU thesis 2013) and Can Yang Zhang (visiting PhD student in 2013) applied NCL for converting sequence-defined oligomers into targeted oligomers.

3.3.1 Design of targeted and shielded oligomers of different topologies via native chemical ligation

The two applied NCL ligation substrates **500** and **501** (Table 4) contain a precise bifunctionalized PEG of 24 monomer units and either folate as targeting ligand (Nbz-G-PEG_{24}-FolA, **500**) or alanine as a control (Nbz-G-PEG_{24}-A, **501**). For modification by NCL, six succinoyl-tetraethylene pentamine (Stp) or succinoyl-pentaethylene hexamine (Sph) containing cationic oligomers of different topologies and modifications [121, 122] were selected as core oligomers. They can be divided in 2-arm oligomers, three 3-arm oligomers and one 4-arm oligomer (see Scheme 3). These structures were previously identified as active pDNA transfection agents [120-122]. Each oligomer arm is terminated by a cysteine (*C* or *N*-terminal) which stabilizes polyplexes by intermolecular disulfide bond formation.

Table 4. Activated control and FolA-targeted substrates for NCL.

Id	Sequence
501	Nbz-G-PEG_{24}-A
500	Nbz-G-PEG_{24}-FolA

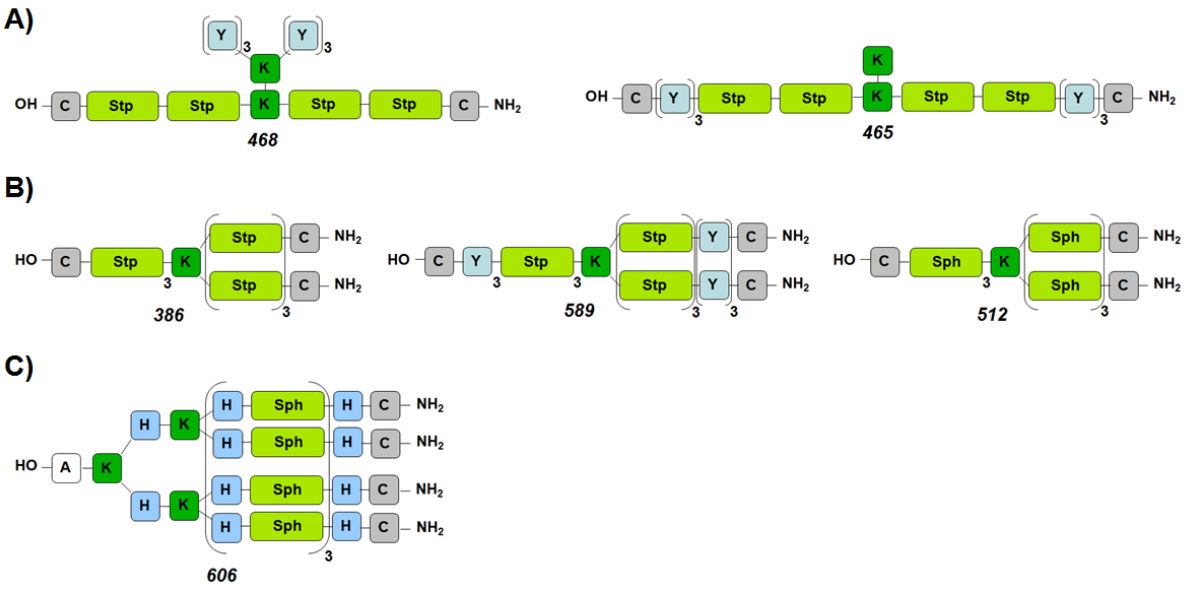

Scheme 3. Oligomer library for the NCL reaction.

Table 5. Oligomers synthesized *via* NCL reaction (Sequences from left: *C*- to *N*-terminus). Syntheses performed by Can Yang Zhang, Visiting PhD student , LMU 2013)

Id	Sequence	Topology
659	C-Y_3-STP_2-K(K)-STP_2-Y_3-C-G-PEG_{24}-**A**	2-arm
660	C-Y_3-STP_2-K(K)-STP_2-Y_3-C-G-PEG_{24}-**FolA**	
661	C-STP_2-K(K-$(Y_3)_2$)-STP_2-C-G-PEG_{24}-**A**	
662	C-STP_2-K(K-$(Y_3)_2$)-STP_2-C-G-PEG_{24}-**FolA**	
663	C-SPH_3-K(SPH_3-C)-SPH_3-C-G-PEG_{24}-**A**	3-arm
664	C-SPH_3-K(SPH_3-C)-SPH_3-C-G-PEG_{24}-**FolA**	
665	C-STP_3-K(STP_3-C)-STP_3-C-G-PEG_{24}-**A**	
666	C-STP_3-K(STP_3-C)-STP_3-C-G-PEG_{24}-**FolA**	
667	C-Y_3-STP_3-K(STP_3-Y_3-C)-STP_3-Y_3-C-G-PEG_{24}-**A**	
668	C-Y_3-STP_3-K(STP_3-Y_3-C)-STP_3-Y_3-C-G-PEG_{24}-**FolA**	
669	A-K-(H-K-(H-SPH)$_3$-H-C)$_2$)-H-K-(H-(SPH-H)$_3$-C)-(H-SPH)$_3$-H-C-G-PEG_{24}-**A**	4-arm
670	A-K-(H-K-(H-SPH)$_3$-H-C)$_2$)-H-K-(H-(SPH-H)$_3$-C)-(H-SPH)$_3$-H-C-G-PEG_{24}- **FolA**	

Therefore the number of arms/number of cysteines is beneficial for transfection. Only the *N*-terminal cysteines are substrates for NCL, but sulfhydryl groups are regenerated. Incorporated tyrosine trimers (in **465**, **468**, **589**) are supposed to stabilize polyplexes by aromatic ring interactions [121, 157]. Histidines and Sph building blocks were incorporated into the selected 4-arm structure **606**, for an improved proton-sponge effect recently shown to facilitate endosomal escape [122]. Regardless of the number of polycationic arms and *N*-terminal cysteines, for all oligomers a 1: 1 molar ratio of cationic oligomer and ligation agent Nbz-G-PEG_{24}-FolA or Nbz-G-PEG_{24}-A, respectively, was used, in order to preferentially obtain only one polycationic arm coupled with the shielding and targeting domain. Thus, by NCL a small library of twelve PEG-shielded oligomers (**659**-**670**; Table 5) with or without FolA-targeting was synthesized by Can Yang Zhang (visiting PhD student, LMU 2013).

3.3.2 Biophysical characterization

Agarose gel shift assays (Figure 15) demonstrated efficient pDNA binding for all NCL conjugates already at lower N/P ratios. The lowest binding was observed with the 2-arm structures having the lowest number of polycationic arms. Particle size measurements were determined with DLS (Table 6). The pDNA polyplexes formed with the PEGylated oligomers were between 100 nm and 300 nm. The zeta potential measurements of polyplexes formed with the NCL modified conjugates and pDNA are presented in Figure 16. As expected, the highest zeta potential was observed for the unmodified oligomers (depending on the structure, +15 to +30 mV), the lowest for folate-PEG polyplexes (+1 to +5 mV). The alanine-PEG negative controls showed a medium-low zeta potential (+1 to +10 mV), always slightly higher than the folate-PEG analogs, most probably because of the protonatable amine of the terminal alanine.

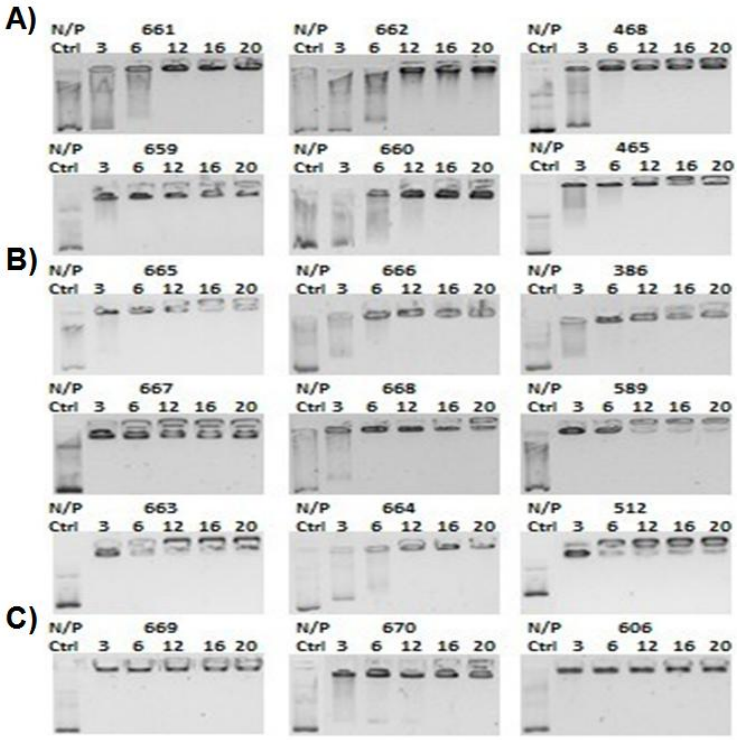

Figure 15. pDNA binding (agarose gel shift) assays of linear 2-arm (A), 3-arm (B) and 4-arm structures (C). The experiment was performed by Can Yang Zhang (visiting PhD student at LMU).

Table 6. Particle sizes of polyplexes (N/P 12 for pDNA, N/P 16 for siRNA) formed in HEPES buffer determined with DLS. Variations refer to the median of three measurements of the same sample. The experiment was performed by Can Yang Zhang (visiting PhD student at LMU).

Id	Modification	Topology	Z-average (nm)
659	**A**-control	**2-arm**	270.5 ± 32
660	**FolA**-targeted		150.8 ± 17
661	**A**-control		217.6 ± 20
662	**FolA**-targeted		224.3 ± 12
665	**A**-control	**3-arm**	151.1 ± 13
666	**FolA**-targeted		253.4 ± 9
667	**A**-control		326 ± 11
668	**FolA**-targeted		233.8 ± 15
663	**A**-control		126.2 ± 14
664	**FolA**-targeted		190 ± 12
669	**A**-control	**4-arm**	183.3 ± 9
670	**FolA**-targeted		247.3 ± 16

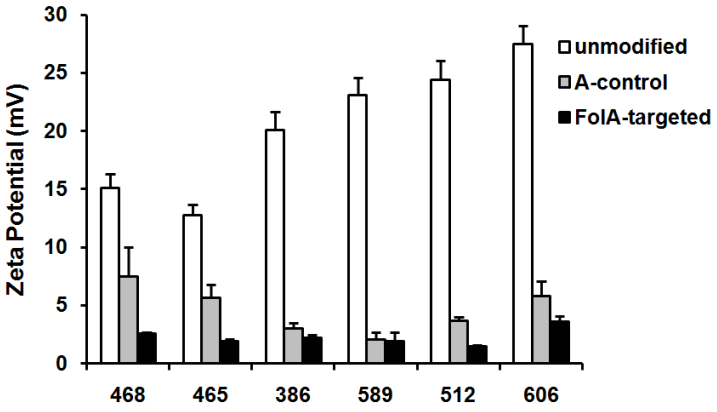

Figure 16. Zeta potential of pDNA polyplexes at N/P 12, formed in HEPES buffer. Each data value represents mean±SD of 3 experiments. The experiment was performed by Can Yang Zhang (visiting PhD student at LMU).

To simulate *in vivo* conditions, the stability of the FolA-modified pDNA polyplexes was additionally evaluated in serum. The pDNA polyplexes were incubated in fetal calf serum (FCS) for 1, 10, 30 or 90 min and subsequently subjected to gel electrophoresis. The retardation in gel revealed a partial instability of 2-arm oligomers, whereas the other oligomers remained stable even after the addition of highly negatively charged heparin (Figure 17).

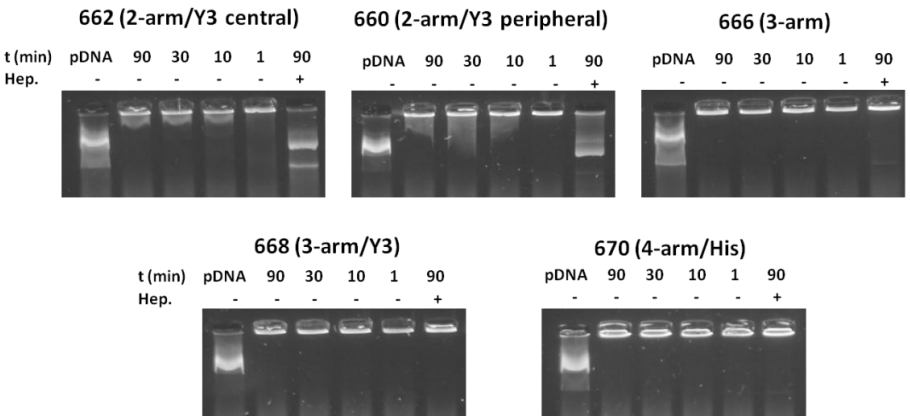

Figure 17. Stability of pDNA polyplexes (N/P 12) in serum. pDNA complexation of FolA-PEG-modified oligomers **662**, **660**, **666**, **668** and **670** in the presence of 90% fetal bovine serum as detected by agarose gel shift. Where indicated (last lanes), heparin was added to the polyplexes after incubation in FCS for 90 min to evaluate the influence of this highly negatively charged biological molecule on polyplex stability.

3.3.3 Biological evaluation

The cellular internalization of polyplexes formed with Cy5-labeled pDNA using folate receptor-rich KB cells is presented in Figure 18. For 2-arm structures with peripheral tyrosines, polyplexes formed with unmodified oligomer **465** or alanine-PEG **659** displayed almost no pDNA uptake after 45 min incubation (Figure 18-upper row). The folate-targeted **660** polyplexes showed the amplest shift to the right compared to control, demonstrating the highest pDNA cellular uptake. Also in the case of 3-arm structures, the unmodified oligomer **386** did not mediate any cellular internalization, the alanine-PEG **665** interestingly displayed an increased cellular internalization and the folate-modified oligomer **666** again showed the highest uptake. The similar results were obtained with other oligomers with increased number of polycationic arms regardless of tyrosine or histidine modification.

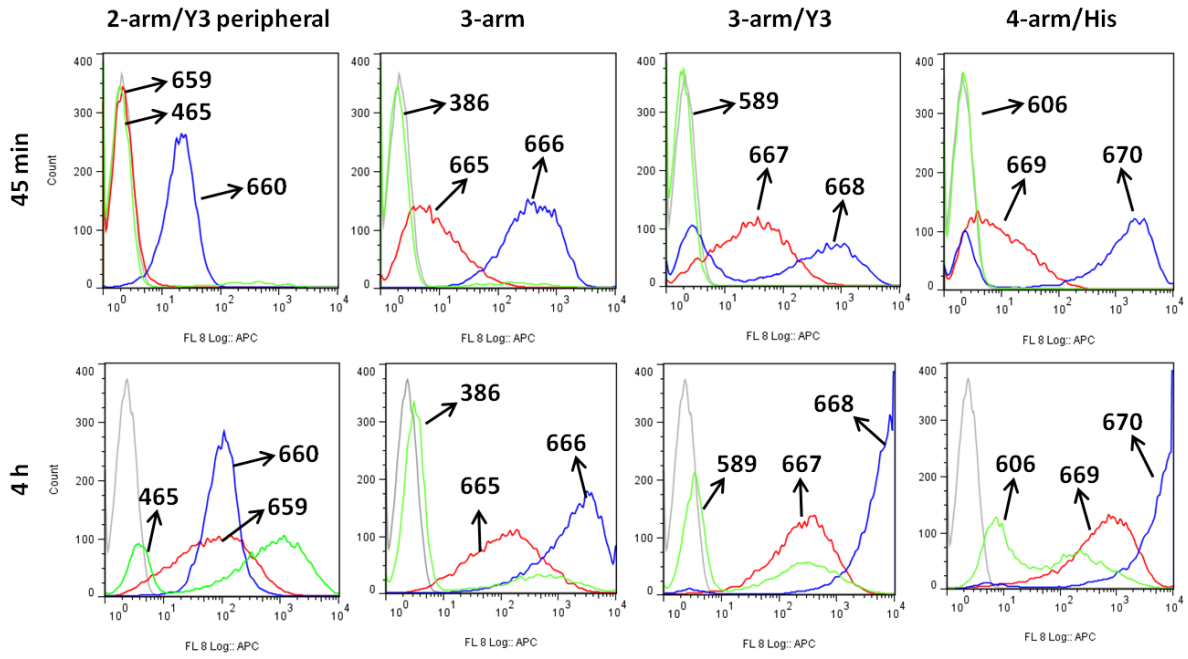

Figure 18. Cellular internalization of Cy5-labeled pDNA (N/P 12) polyplexes after 45 min (above) and 4 h (below) determined by flow cytometry. The intensity of the Cy5 signal resembles the amount of polyplexes binding with KB cells. “Count” represents cumulative counts of cells with indicated Cy5 fluorescence after appropriate gating by forward/sideward scatter and pulse width. Dead cells (DAPI positive, less than 2%) were excluded from analysis. Unmodified oligomers are presented in green, FolA-modified in blue, alanine controls in red and HBG buffer only treated cells in grey.

With increased polyplex incubation time (4 h) for all oligomers (Figure 18-lower row), modified or not, an increased cellular internalization was observed leading to partial unspecific uptake of initial unmodified oligomers and very high uptake of FolA-targeted polyplexes. Furthermore, pDNA cell binding studies were performed showing similar results to the uptake studies (Figure 19), though with a higher binding of the unshielded oligomers polyplexes as compared to the cellular internalization. Two of the oligomer triplets (468, 512) displayed untypical cell binding profiles with hardly any differences between unmodified, A-PEG and Fol-PEG (Figure 20).

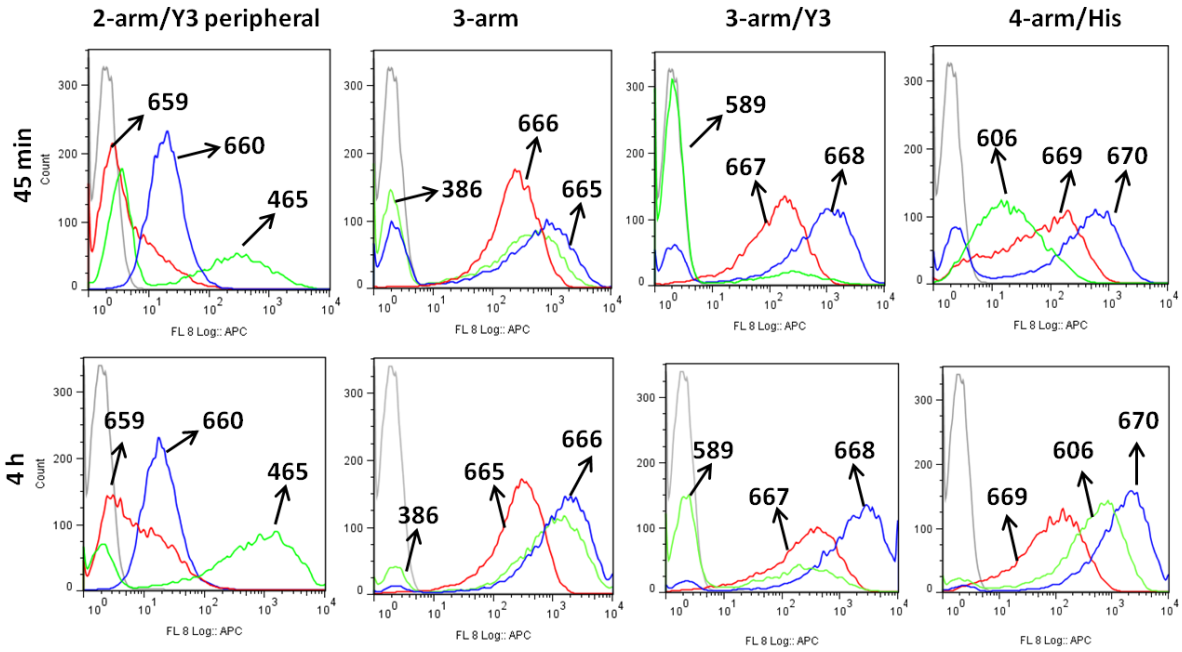

Figure 19. Cellular association of Cy5-labeled pDNA (N/P 12) polyplexes after 45 min and 4 h analyzed by flow cytometry. Dead cells (DAPI positive, less than 2%) were excluded from analysis. Unmodified oligomers are presented in green, FolA-PEG oligomers in blue, alanine-PEG controls in red and HBG buffer only treated cells in grey.

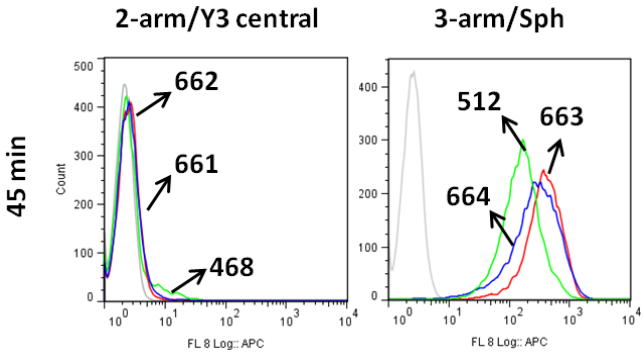

Figure 20. Cellular association study using flow cytometry. Two-arm oligomers with central tyrosine trimers modified (A); 3-arm oligomers with Sph block (B).

3.3.4 Folate receptor-targeted pDNA transfection

Transfection efficacies of control alanine-PEG, targeted folate-PEG, and non-modified cationic oligomers were assessed (Figure 21). Folate receptor-rich KB cells were incubated with polyplexes for a relatively short incubation time (45 minutes at 37 °C) in order to monitor active, specific cell interactions. Optionally chloroquine was added to investigate to which extent endosomal escape presents a bottleneck in gene transfer. The PEGylated 2-arm oligomers with central oligotyrosines (**661** and **662)** displayed no increase in luciferase expression (Figure 21A) compared to their unmodified precursor (**468**). This is well consistent with the cell association data (Figure 20). Modification of oligomer **465** with peripheral oligotyrosines (Figure 21B) resulted in decreased transfection efficiency for the alanine-PEG control **659**, but an increased luciferase activity for the PEGylated targeted folate-PEG conjugate **660**. The chloroquine-dependent expression was more than 3 log units higher as compared to the alanine control. Thus, the oligomers with peripherally positioned tyrosines turned out to be beneficial over the oligomers with centrally positioned tyrosines as observed also with the cellular association studies (Figure 18). Three-arm oligomers comprising Stp building block (Figure 21C) showed moderate activity only upon chloroquine addition and for the folate-targeted polymer **666** mainly at the lowest N/P ratio. Replacing the Stp backbones of 3-arm oligomers by Sph building blocks (**663**, **664**) gave similar moderate results (Figure 21E). After modification of 3-arm oligomers with tyrosine trimers pDNA transfection efficacy was greatly improved (Figure 21D). Compared to 3-arm conjugate without tyrosines (**666**), the tyrosine containing folate-targeted oligomer (**668**) showed up to 40-fold higher transfection

activity. The highest activity was obtained in the presence of chloroquine, whereas the alanine-PEG control **667** was ineffective. Finally, the 4-arm oligomers derived from the histidine-rich oligomer **606** were analyzed (Figure 21F).

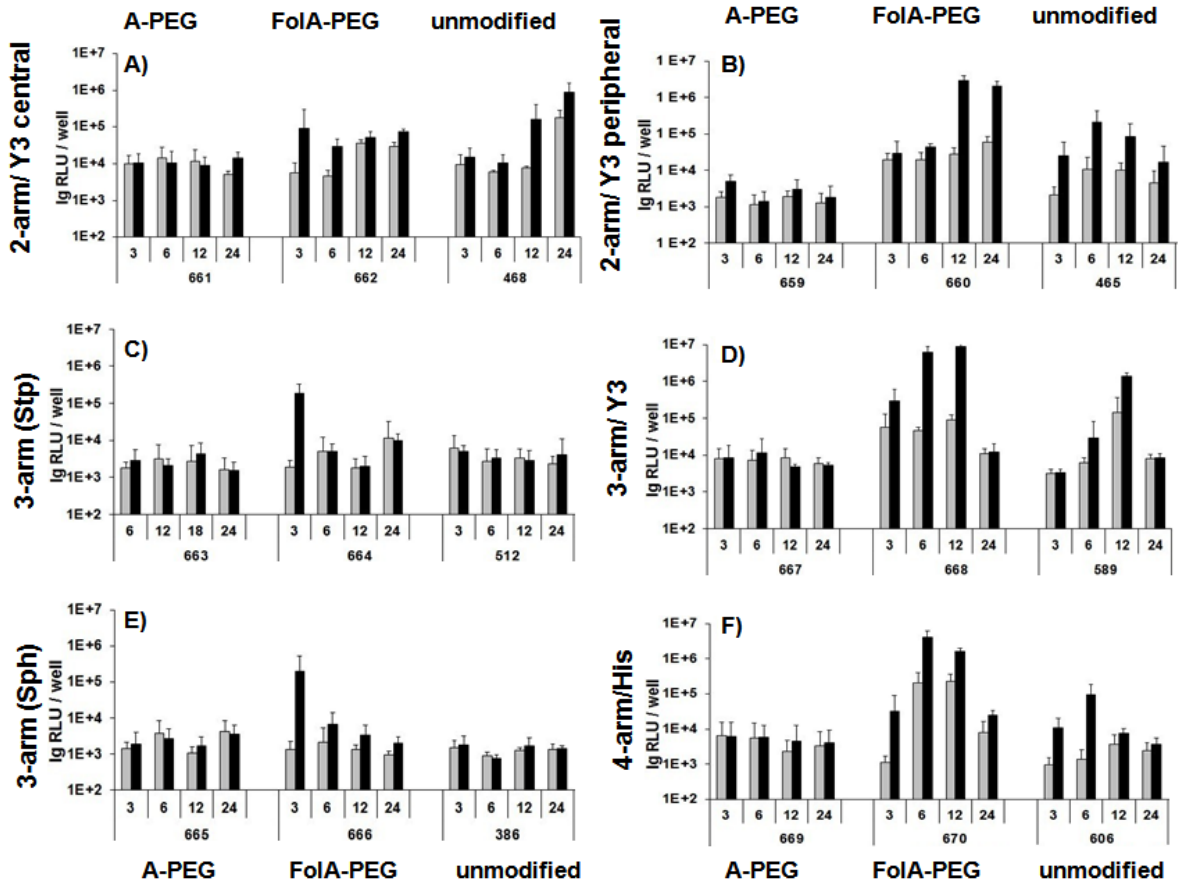

Figure 21. Folate receptor-targeted pDNA transfection. Luciferase gene transfer by pDNA polyplexes in KB cells without (gray bars) or with chloroquine incubation (black bars). Polyplexes were formed at indicated N/P ratios with 2-arm oligomers with central (A) or peripheral (B) oligotyrosines; 3-arm Stp oligomers without (C) or with oligotyrosines (D); 3-arm oligomers comprising Sph building block (E) and 4-arm Sph containing oligomer with histidines (E). Each row compares A-PEG, FolA-PEG or unligated oligomers.

The control A-PEG polymer **669** mediated no significant pDNA transfection with or without chloroquine addition. Targeted folate-PEG **670** polyplexes displayed a high efficiency being superior to that of unmodified oligomer **606** and far less dependent on chloroquine addition than in the case of other oligomers. The number of polycationic arms of carriers played a superior role as compared to the influence of different (Stp or Sph) cationic building blocks, providing increased gene transfer with

increasing number of polycationic arms. In summary, for all NCL modified oligomers, the incorporation of alanine-PEG oligomer led to decreased gene transfer, whereas the targeted folate-PEG oligomers generally showed the highest transfection efficiency reaching the transfection efficiencies comparable to those of FolA-targeted PEGylated **356** structure [158] synthesized *via* all-in one solid phase synthesis (Figure 22). The peripheral tyrosine trimer modification was more efficient than the central modification.

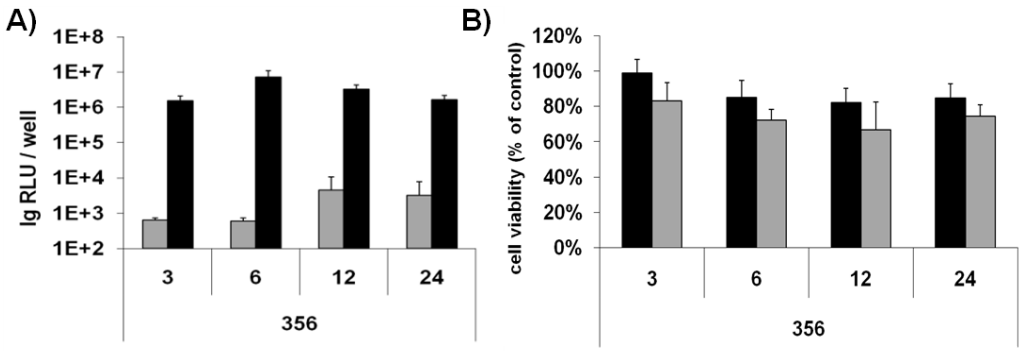

Figure 22. Folate receptor-directed pDNA transfection of KB cells with an adequate control. Two-arm FolA-targeted PEGylated oligomers **356** as synthesized *via* all-in one solid phase synthesis as published [52] presents a folate receptor targeted positive control oligomer for pDNA transfection. A) pCMVLuc luciferace reporter gene transfections with pDNA polyplexes without (gray bars) or with (black bars) chloroquine incubation and B) corresponding cell viabilities determined with MTT assay.

In parallel to gene transfer studies, MTT assays were performed to evaluate the cell viabilities of transfected cells. Importantly, no significant cytotoxicity was observed for all tested pDNA polyplexes. Only chloroquine addition led to a slight reduction in cell viability (Figure 23). The improved gene transfer (Figure 21) of PEG-folate oligomers with increased complexity (tyrosine modification, increased number of arms) and convenience of using an existing oligomer library highlights the great utility of NCL for this purpose.

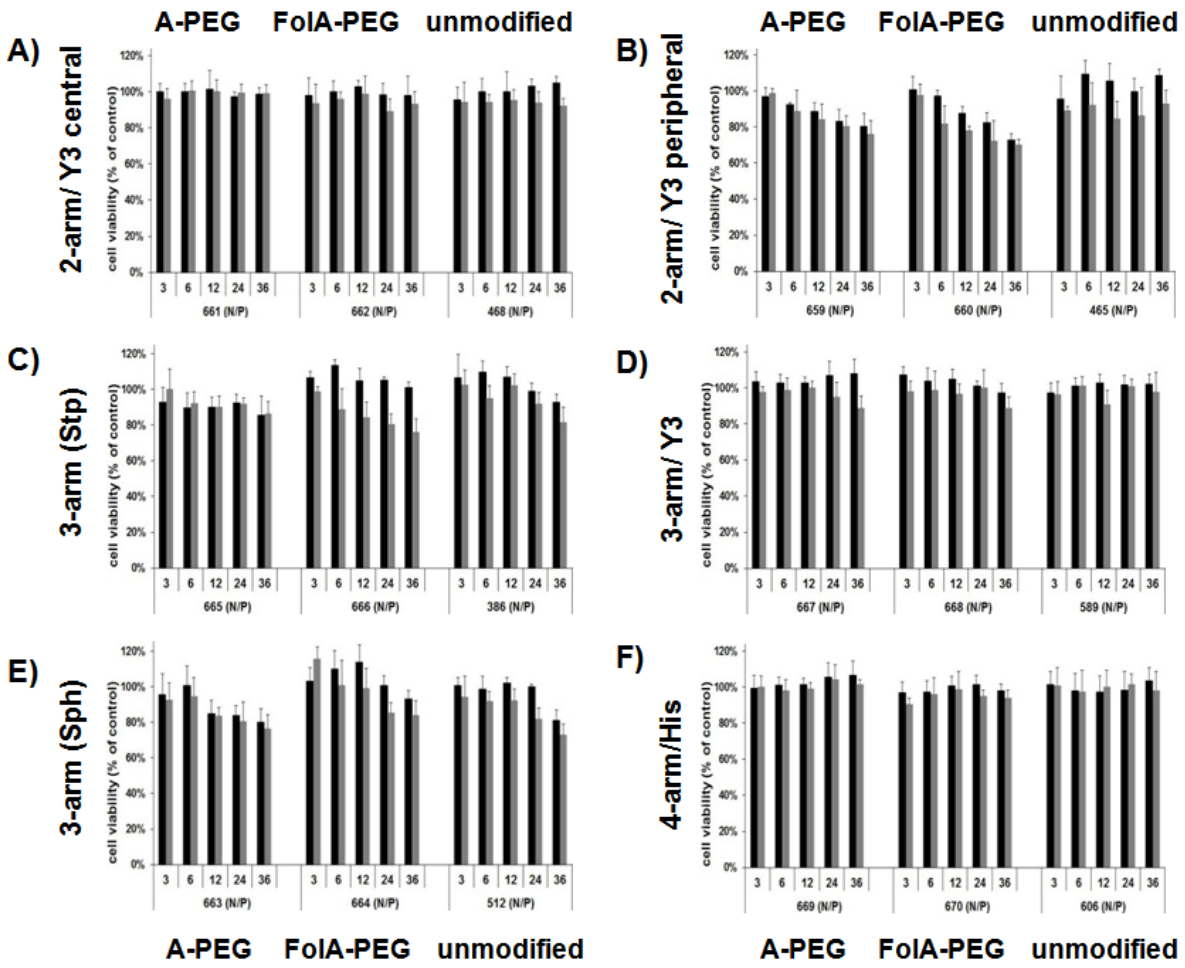

Figure 23. Cell viability of KB cells after transfection with pDNA polyplexes determined by MTT assay at different N/P ratios. Black indicates without chloroquine, gray with chloroquine incubation.

3.4 Dual-targeted polyplexes based on sequence-defined peptide-PEG-oligoaminoamides

Apart from the above mentioned small molecule folic acid [52, 159, 160], short peptides and their mimetics derived from phage-display screens have gained increasing attention as targeting ligands for receptors over-expressed on the surface of miscellaneous tumor cells [58, 161]. Receptor targeting may serve at least two purposes: specific cell attachment, and enhanced cellular uptake. As the single peptide ligand-based nucleic acid carriers often remain unsatisfactory with regard to either selectivity or their transfection efficacy, dual-targeted carriers simultaneously

addressing two different surface receptors over-expressed in tumor tissues have been investigated. With this dual-ligand approach, non-viral carriers should mimic the entry of potent natural viruses like adenoviruses which concurrently target coxsackie–adenovirus receptor and integrin $a_v\beta_3$ or $a_v\beta_5$ receptors [67, 68]. A combination of YC25 peptide against fibroblast growth factor receptor and CP9 peptide binding to the integrins was reported to mediate a significantly enhanced PEI-based gene transfer in tumors with positive expression of FGF receptors and integrins [69]. Previously, combined Tf- and RGD-containing PEGylated PEI-based carriers, showed a clear synergy of dual-targeted over single-targeted polyplexes [162].

In this thesis, the dual-targeting concept was applied for the first time in the context of novel sequence-defined oligo (ethane amino) amide oligomers [119, 120]. The following targeting ligands *via* a bridging polyethylene glycol (PEG) chain: short cyclic RGD peptide [57, 163-165] targeting the integrin receptor, B6 ligand [57, 122, 166] targeting the TfR, and GE11 peptide [63, 66, 167] targeting the epidermal growth factor receptor (EGFR). Thus, B6-PEG-STP and c(RGDfK)-PEG-STP conjugates were synthesized as described before [57]. Pairs of these targeted PEGylated sequence-defined carriers were combined at different oligomer ratios and used for pDNA polyplex formation at two different N/P ratios, in order to find optimal dual-targeted carriers being superior to the single-targeted carriers.

3.4.1 Design and biophysical characterization of single- and dual-targeted polyplexes

Three different peptidic ligands c(RGDfK), B6 (GHKAKGPRK) and GE11 (YHWYGYTPQNVI), were selected for pDNA polyplex targeting to three different surface receptors over-expressed in tumors. For this purpose, targeted PEGylated Stp oligomers (Table 7) comprising C-terminal targeting peptide, a monodisperse polyethylene glycol (PEG) moiety with 24 oxyethylene units, lysine as branching point, and two cationic arms each bearing four repeat units of the artificial amino acids succinoyl-tetraethylene pentamine (Stp), completed by an N-terminal cysteines, were utilized (Table 7). The oligomers were synthesized by Ulrich Lächelt and Dongsheng He, PhD students LMU. The PEG moiety had been introduced for

subsequent polyplex surface shielding, and the cysteines for subsequent polyplex stabilization by disulfide bond formation as described before [120].

Table 7. Oligomer ID numbers, sequences and abbreviations.

Oligomer Id	Sequence	Abbreviation
188	**A**-PEG_{24}-K[Stp_4-C]$_2$	A-PEG-STP
391	**c(RGDfK)**-PEG_{24}-K[Stp_4-C]$_2$	RGD-PEG-STP
203	**B6**-PEG_{24}-K[Stp_4-C]$_2$	B6-PEG-STP
186	**GE11**-PEG_{24}-K[Stp_4-C]$_2$	GE11-PEG-STP

The ability of polymeric carriers to complex nucleic acids is the first prerequisite for successful gene delivery. Thus, the pDNA binding capacity of the synthesized targeted oligomers was evaluated at the oligomer/pDNA mixing ratios N/P 6 and N/P 12 by means of agarose gel-shift assay. All targeted oligomers were able to bind their cargo as demonstrated by the electrophoretic gel retardation (Figure 24A). Each of the targeted conjugates was then co-formulated prior to pDNA polyplex formation with another targeted conjugate directed towards a different surface receptor, yielding dual-ligand polyplexes. These polyplexes were assembled using different ratios of the two oligomers. Again, polyplexes were formed at the total N/P 6 or N/P 12 and subjected to gel electrophoresis (Figure 24B, C). All dual-targeted polyplexes exhibited full pDNA binding without migration in the gel.

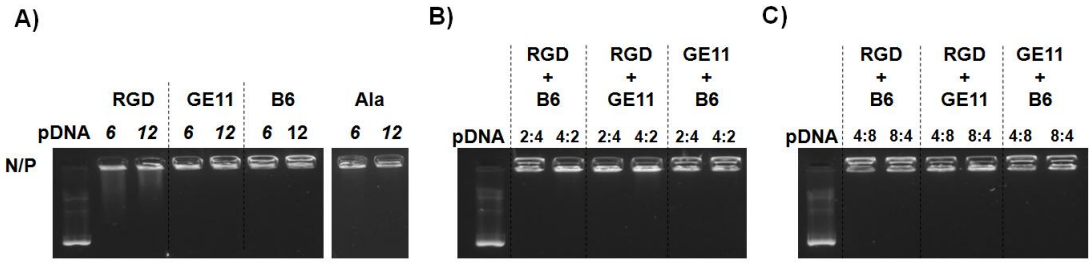

Figure 24. pDNA binding ability of A) single-targeted oligomers at N/P 6 and N/P 12, and dual-targeted formulations of oligomers at total B) N/P 6 or c) N/P 12. Numbers in B) and C) indicate the N/P ratio of each targeted oligomers in the dual-targeted polyplex.

The synthesized oligomers formed with pDNA nano-sized polyplex particles (< 400 nm, Table 8). The alanine control and RGD- or GE11-equipped single-ligand polyplexes revealed low surface charge with zeta potentials below 6 mV, whereas the

polyplexes formed with the B6-STP oligomer yielded higher zeta potentials of around 20 mV. With increased N/P ratio a minor increase in nanoparticles surface charge was observed (Table 8). Dual-targeted polyplexes were of similar sizes (Table 9). Their surface charges were in accordance with the values obtained with the single-targeted polyplexes. The zeta potential of all B6-containing dual-targeted polyplexes was between 10 and 20 mV that increased with increased amount of B6-STP oligomer in the polyplex. The influence of the mixing ratio on the zeta potential was more pronounced at the lower N/P 6, whereas at the higher N/P 12 less impact of the ratio between the oligomers was observed. The RGD- and GE11-containing dual-targeted polyplexes had a lower surface charge below 4 mV.

3.4.2 Biological evaluation of single-targeted polyplexes

Following the efficient formation of stable and adequately sized nanoparticles, the cell binding represents the next crucial step towards efficient gene transfer. Thus, the cellular association of targeted and fluorescently (Cy5) labeled pDNA polyplexes was assayed using the prostate cancer cell line DU145 over-expressing integrins [162], transferrin receptor [162] and epidermal growth factor receptor [168]. First, single-targeted polyplexes were investigated for their cell association. To highlight selective differences, all evaluations were performed after a short incubation time of only 30 min at 4 °C. Flow cytometry histograms plotting the Cy5 fluorescence intensity against the number of events are displayed for polyplexes at N/P 6 (Figure 25A) and N/P 12 (Figure 25B). Practically no cell binding was observed for alanine control polyplexes. The RGD- and B6-decorated polyplexes showed a clear targeting effect; a much higher cell binding at N/P 6 (Figure 25A) that even increased at higher N/P 12 (Figure 25A). The histograms obtained with the labeled EGFR-binding GE11-PEG-STP polyplexes revealed distinctly different, bimodal association property; a subpopulation of cells hardly binding the polyplexes and another cell subpopulation exhibiting a very high polyplex association was observed. EGFR expression on DU145 cells is unimodal (see Figure 26), when sufficient amount of anti-EGFR antibody is applied, ruling out heterogeneous receptor expression as reason for the bimodal polyplex binding. Nevertheless, the association data indicate that a certain targeting ligand threshold should be achieved in order to be able to target all the cells. Also here the cell binding increased with a higher N/P ratio. Following cell

surface binding, cellular uptake of the polyplexes represents the next gene delivery step. This process can be quite fast (within few minutes to less than an hour) or slower (over several hours). To obtain an impression on uptake kinetics, the cellular internalization studies were performed at an early time point after 30 min incubation at 37 °C using flow cytometry. Not internalized polyplexes were removed by a heparin wash. The Cy5 fluorescence and the corresponding histograms (Figure 27) revealed that at both analyzed N/P ratios the cellular uptake of RGD-, GE11-, or B6-equipped single-targeted polyplexes very much resembles their cell association.

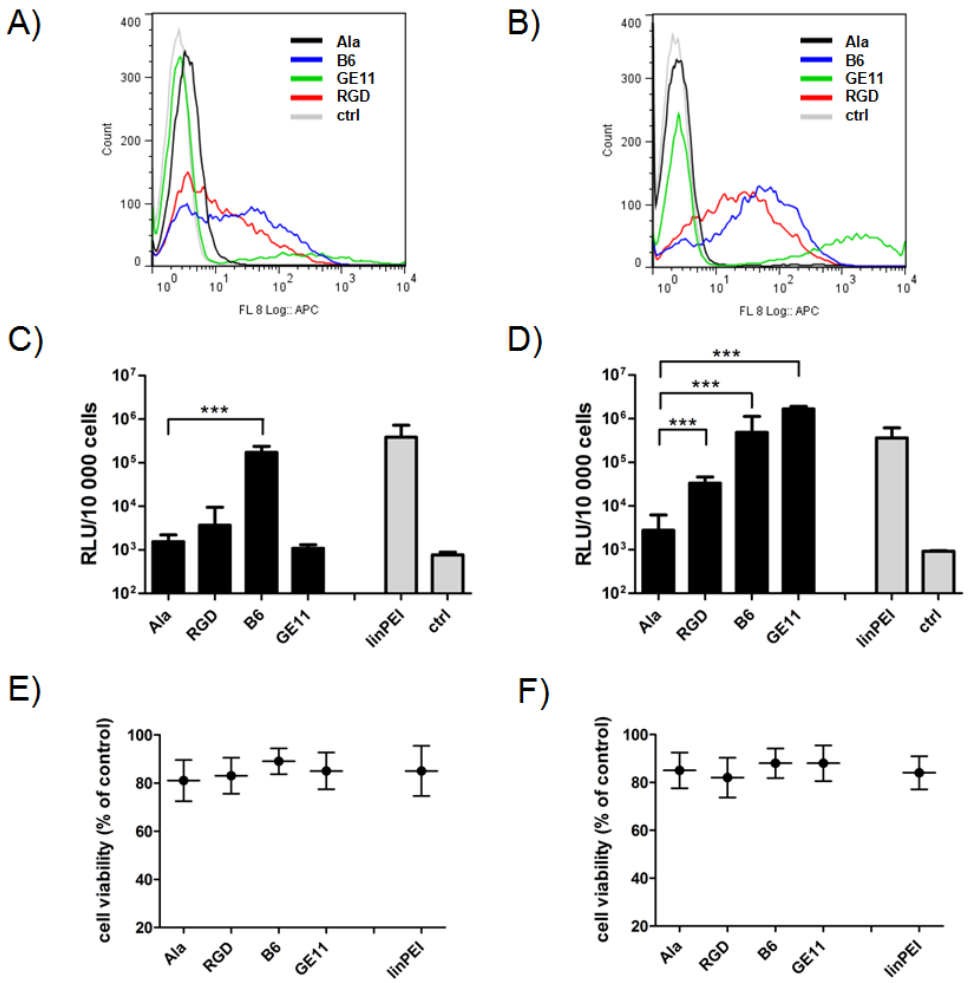

Figure 25. A, B) DU145 cell association of polyplexes formed with Cy5-labeled pDNA and each of the single-targeted oligomers (RGD-PEG-STP, B6-PEG-STP, GE11-PEG-STP) or alanine control as analyzed by flow cytometry. Logarithmic X-scale represents the Cy5 fluorescence of bound polyplexes. “Count” represents cumulative counts of cells with indicated fluorescence after appropriate gating by forward/sideward scatter and pulse width. Dead cells (DAPI positive, less than 2 %) were excluded from analysis. C, D) Luciferase reporter gene expression and E, F) cell viability (MTT) assays performed at 24 hours after transfection. linPEI was used a positive control, HBG treated cells served as background. Cell viability was calculated as percentage to cells treated with HBG. Data are presented as mean value (±SD) out of quintuplicate. The experiments were performed with polyplexes formed at N/P 6 (left) and N/P 12 (right).

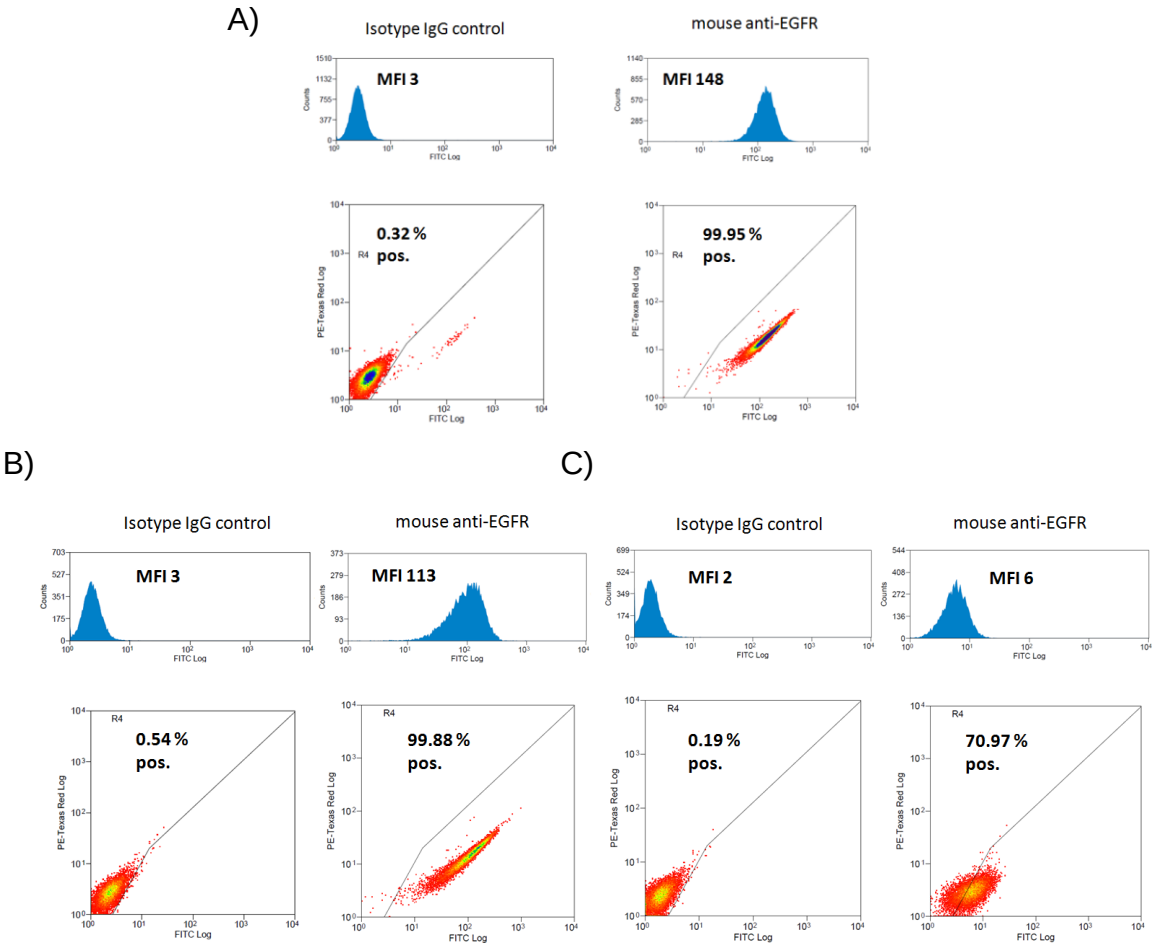

Figure 26. A) Estimated EGFR receptor expression levels on DU145 cells in suspension. B) Estimated EGFR receptor expression levels on attached DU145 cells at B) 1:500 and C) 1:5000 antibody dilution.

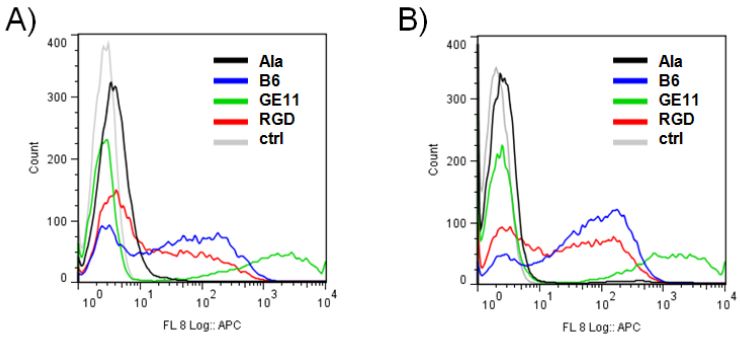

Figure 27. Cellular internalization of single-targeted polyplexes formed with RGD-PEG-STP, GE11-PEG STP or B6-PEG-STP, or alanine control polyplexes at A) N/P 6 and B) N/P 12. Flow cytometry experiments were performed on DU145 cells, extracellularly bound polyplexes were removed by heparin. DAPI was used to discriminate between viable and dead cells.

Next, luciferase pDNA transfections with single-targeted polyplexes were performed using only 30 min short incubations with DU145 cells. Gene expression levels (Figure 25C and D) and cell metabolic activities (Figure 25E and F) were determined after 24 hours. Escape of polyplexes from endosomes is a known bottleneck in gene transfer [169]. Therefore, to rule out a significant influence of the endosomal escape step, all transfections were performed in the presence of the lysosomotropic agent chloroquine [170]. At N/P 6 (Figure 25), the alanine control polyplexes yielded practically no gene transfer, whereas the B6-PEG-STP polyplexes led to the highest gene transfer, exceeding the alanine control 110-fold. Despite the 30 min short polyplex incubation with cells, gene expression was comparable to that of linear PEI (linPEI) with a much longer incubation time of 4 h. RGD-PEG-STP and GE11-PEG-STP polyplexes at N/P 6 mediated only low transfection levels. In accordance with the cell association studies, at N/P 12 all targeted polyplexes (RGD-PEG-STP, B6-PEG-STP and GE11-PEG-STP) revealed higher transfection efficiencies (Figure 25D) still showing a significant targeting effect over the alanine control. Interestingly, at N/P 12 the GE11-decorated polyplexes displayed the highest gene transfer of all targeted polyplexes. In all transfection studies, the cell viability assay (Figure 25E, F) did not reveal any significant cytotoxicity of the polyplexes. The only minor reduction in metabolic activity (<20 %) can be attributed to the addition of chloroquine as shown before [57, 122].

3.4.3 Biological evaluation of dual-targeted polyplexes

The dual-targeted polyplexes simultaneously addressing two different receptors over-expressed on the cell surface of DU145 cells were compared to the single-targeted polyplexes to find an optimal dual-ligand combination. Thus, the synthesized targeted carriers were co-formulated at different oligomer combinations and different ratios as described above in their biophysical characterization, in order to investigate any synergistic effects of either RGD and B6, RGD and GE11 or GE11 and B6 ligand combination.

Ligand Combination cRGD and B6

First, the dual-targeted combination of RGD and B6 targeting ligands was analyzed. Cell association studies of co-formulated RGD-PEG-STP and B6-PEG-STP oligomers at total N/P 6 (Figure 28) revealed a clear shift of the histogram curve towards the higher fluorescence as compared to each single-targeted polyplexes, demonstrating an obvious dual-targeting effect at both analyzed ratios (4:2 and 2:4) of targeting oligomers in the polyplex. The same was observed with the luciferase reporter gene expression assay (Figure 28).

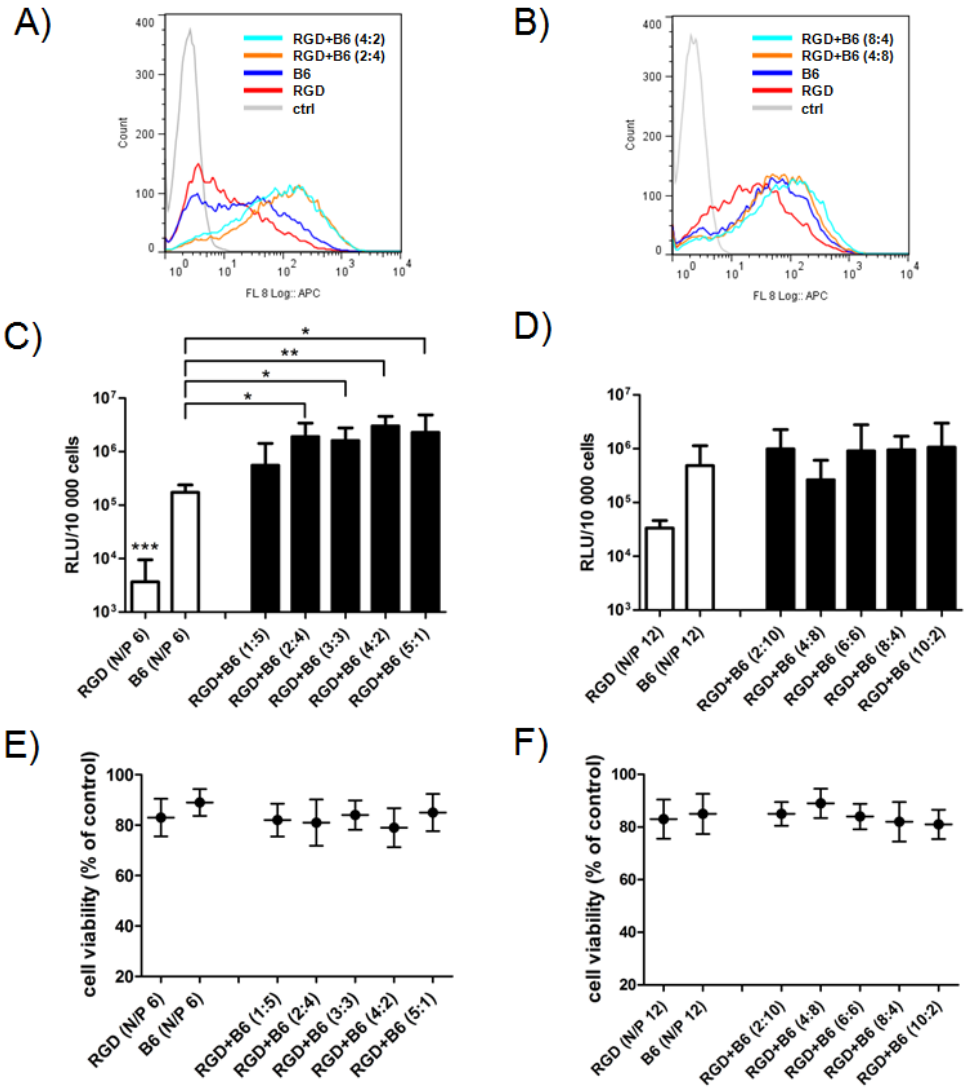

Figure 28. A, B) DU145 cell association of single-targeted polyplexes (RGD, B6) as compared to dual-targeted polyplexes at 2:4 and 4:2 ratios. C, D) Luciferase reporter gene expression obtained with dual-targeted polyplexes as compared to single-targeted polyplexes and E, F) cell viability (MTT) assays performed in parallel. Data are presented as mean value (±SD) out of quintuplicate. The experiments were performed using polyplexes with N/P 6 (left) and N/P 12 (right).

Up to 20-fold higher expression was obtained with dual-targeted polyplexes as compared to the single-targeted B6-STP polyplexes and up to 800-fold higher than for the single-targeted RGD-PEG-STP polyplexes. Interestingly, already a minor addition of the B6-PEG-STP conjugate to the RGD-PEG-STP conjugate (see the 5:1 ratio) led to a 13-fold higher reporter gene expression.

Increasing the total N/P ratio to 12, the cell association of dual-targeted polyplexes remained comparable to that at N/P 6 (Figure 28B). However, the cell binding of the single-targeted oligomers was higher and hence the dual-targeting effect at N/P 12 as compared to N/P 6 diminished. Consistently, in the pDNA transfections (Figure 28D) the RGD and B6-containing dual-targeted polyplexes at N/P 12 were superior to the single-targeted RGD polyplexes (up to 32-fold), though up to only 2.2-fold higher luciferase expression was obtained as compared to B6-PEG-STP polyplexes. The cell viability assay of pDNA transfections again did not show any significant cytotoxicity (Figure 28E, F). The similar lack of cytotoxicity was observed for both other dual-ligand combinations (see next two sections; Figure 30, 32E, F). Interestingly cellular uptake studies performed at the early 30 min time point of transfection (Figure 29A, B) showed a faster uptake for all B6-containing single or dual polyplexes at the lower N/P ratio of 6, consistent with analogous previous PEI polyplex studies [162].

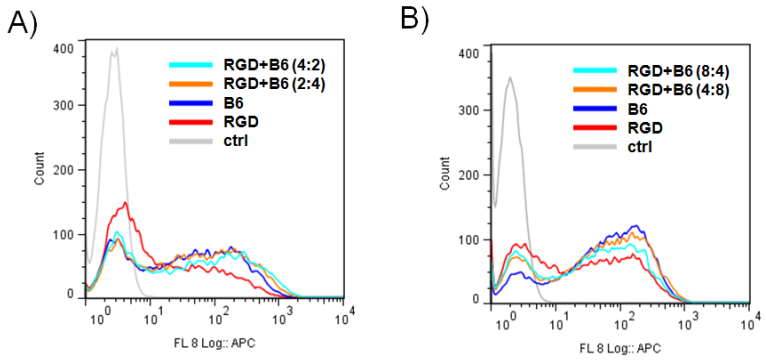

Figure 29. Cellular internalization of RGD- and B6-containing dual-targeted polyplexes at two different ratios as compared to the single-targeted polyplexes at a total A) N/P 6 and B) N/P 12. Flow cytometry experiments were performed on DU145 cells, extracellularly bound polyplexes were removed by heparin. DAPI was used to discriminate between viable and dead cells.

Ligand Combination cRGD and GE11

Next, the integrin targeting cRGD peptide was combined with the epidermal growth factor receptor targeting GE11 peptide ligand. Cell binding studies at the total N/P 6 (Figure 30A) displayed moderate cell attachment of dual-targeted polyplexes at RGD:GE11 ratio of 2:4, while a reverse ratio of 4:2 led to a greatly ameliorated cell attachment exceeding both single-targeted GE11-PEG-STP and B6-PEG-STP polyplexes.

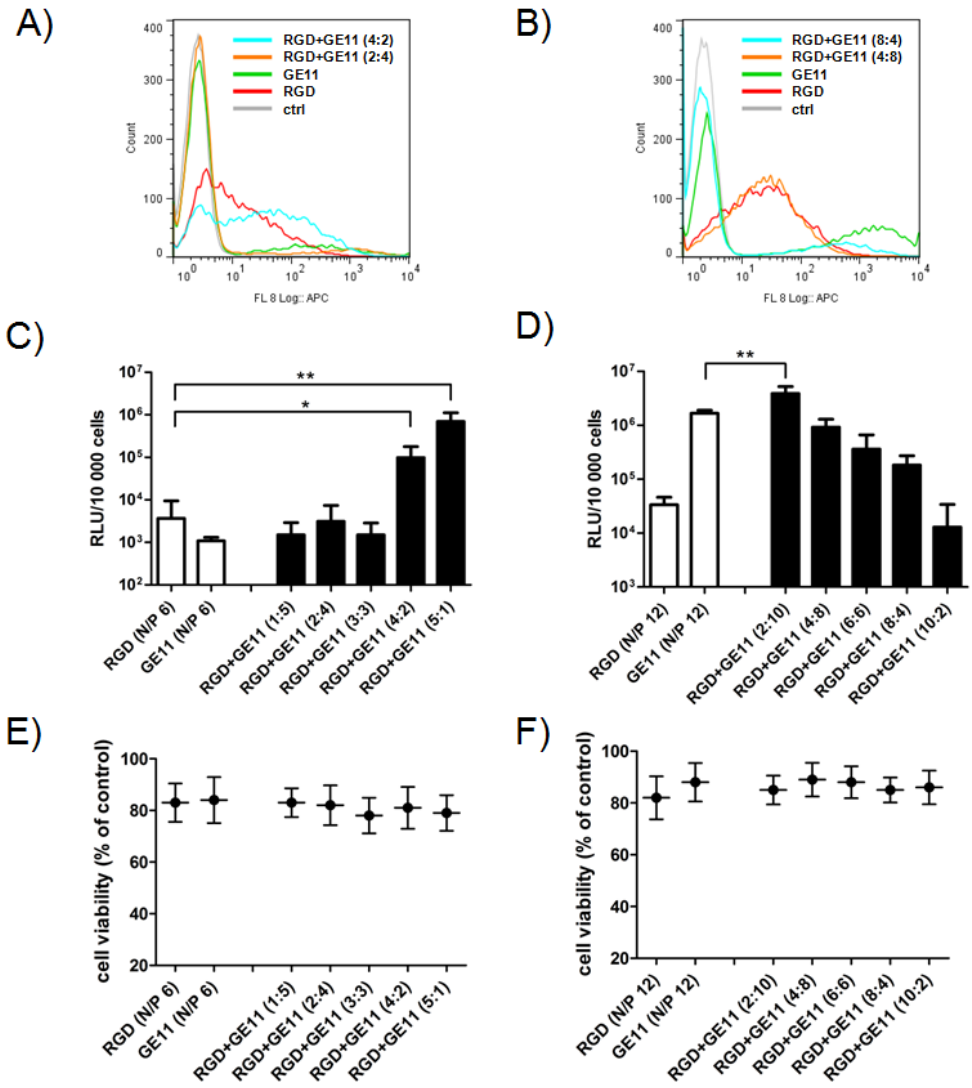

Figure 30. A, B) DU145 cell association of single-targeted polyplexes (RGD, GE11) as compared to dual-targeted polyplexes at 2:4 and 4:2 ratios. C, D) Luciferase reporter gene expression obtained with dual-targeted polyplexes as compared to single-targeted polyplexes and E, F) cell viability (MTT) assays performed in parallel. Data are presented as mean value (±SD) out of quintuplicate. The experiments were performed with polyplexes at N/P 6 (left) and N/P 12 (right).

In contrast to pure GE11-PEG-STP polyplexes which trigger bimodal cell binding, an increased uptake was found for the majority of cells. The cellular uptake studies yielded similar results (Figure 31). The findings were confirmed in luciferase gene transfer studies (Figure 30C). With increasing fraction of RGD as compared to GE11 (up to 5:1) an increased luminescence signal was achieved going greatly beyond (up to 190-fold) both single-targeted polyplexes. For polyplexes formed at total N/P 12 the situation was reversed (Figure 30B and D), due to the very high transfection potency of GE11-PEG-STP single polyplexes at this higher ratio. The highly bimodal cell attachment however shifts towards a unimodal cell binding as observed for the RGD-PEG-STP polyplexes.

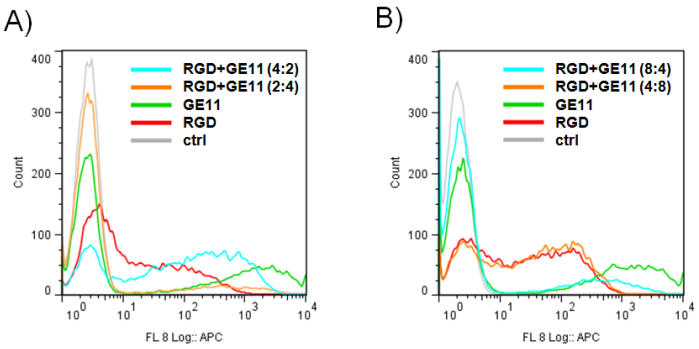

Figure 31. Cellular internalization of RGD- and GE11-containing dual-targeted polyplexes at two different ratios as compared to the single-targeted polyplexes at a total A) N/P 6 and B) N/P 12. Flow cytometry experiments were performed on DU145 cells, extracellularly bound polyplexes were removed by heparin. DAPI was used to discriminate between viable and dead cells.

Ligand Combination GE11 and B6

Also the third investigated combination GE11 and B6 demonstrated an evident dual-targeted effect at the N/P 6 ratio. GE11- and B6-equipped dual-targeted polyplexes at both tested oligomer mixing ratios displayed a homogenous very high cell binding being markedly superior to the cell attachment of both single-targeted polyplexes (Figure 32A). The cellular internalization of dual-targeted polyplexes was comparable to the cell association, however, was less evident as the uptake of single-targeted polyplexes at N/P 6 was shifted to higher Cy5 fluorescence values (Figure 33A). The pDNA transfections confirmed the synergistic effect of both targeting ligands at N/P 6 (Figure 32C). The highest transfection efficiency was obtained at the GE11:B6 ratio of 4:2 exceeding that of B6-containing single-targeted polyplexes 40-fold.

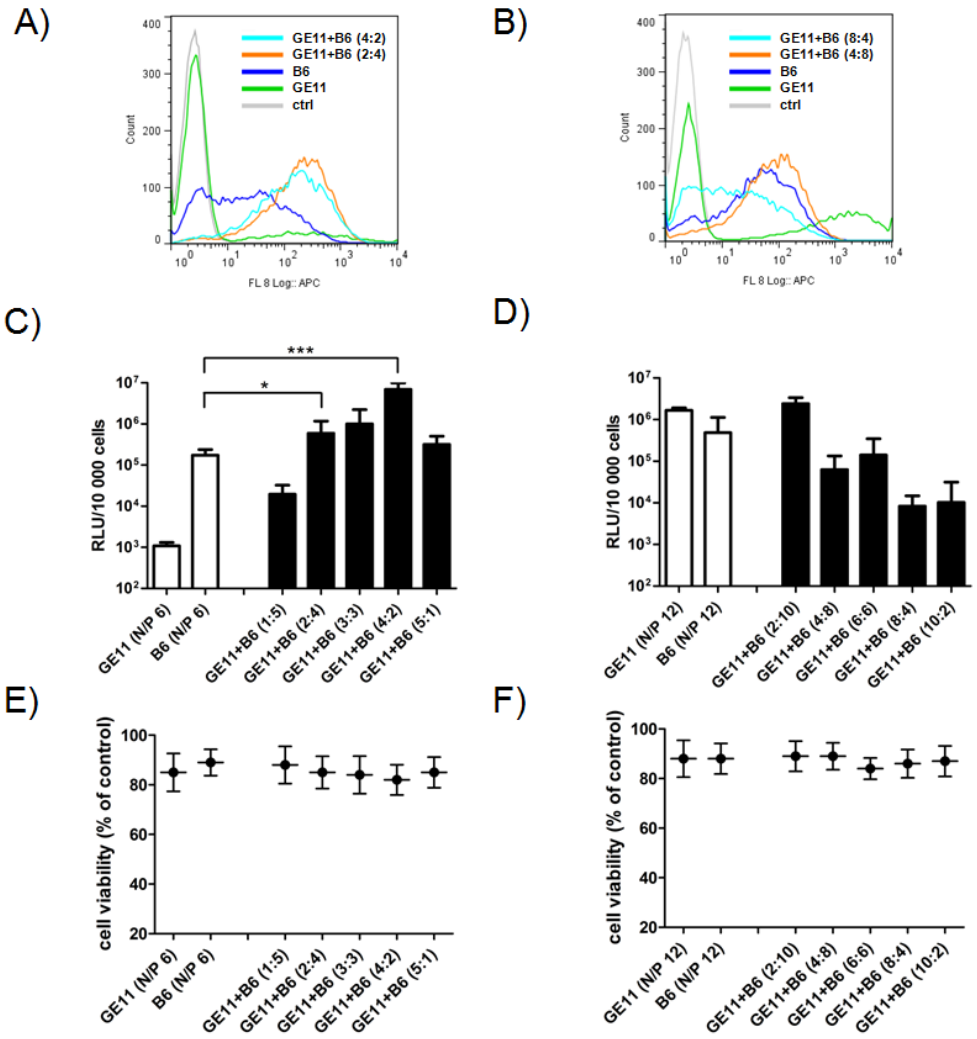

Figure 32. A, B) DU145 cell association of single-targeted polyplexes (GE11, B6) as compared to dual-targeted polyplexes at 2:4 and 4:2 ratios. C, D) Luciferase reporter gene expression obtained with dual-targeted polyplexes as compared to single-targeted polyplexes and E, F) cell viability (MTT) assays performed in parallel. Data are presented as mean value (±SD) out of quintuplicate. The experiments were performed with polyplexes formed at N/P 6 (left) and N/P 12 (right).

At higher total N/P ratio of 12, the polyplexes with the GE11:RGD ratio of 4:8 showed only a moderate dual-targeting effect according to cell binding studies (Figure 32B). In fact, the reporter gene expression of dual-targeted polyplexes at N/P 12 (Figure 32D) was, apart from GE11:B6 ratio of 2:10, lower than of the single-targeted polyplexes and also notably lower than of the dual-targeted polyplexes at total N/P 6. Interestingly, although the GE11- and B6-equipped dual-targeting polyplexes at 8:4 ratio exhibited only a moderate cell binding (Figure 32B), in the cellular internalization studies (Figure 33B) the same polyplexes displayed the highest shift of the curve to the right pointing at a dual-targeting effect.

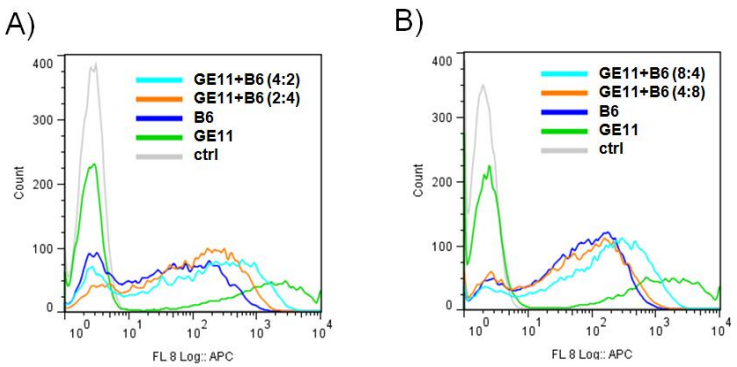

Figure 33. Cellular internalization of GE11- and B6-containing dual-targeted polyplexes at two different ratios as compared to the single-targeted polyplexes at a total A) N/P 6 and B) N/P 12. Flow cytometry experiments were performed on DU145 cells, extracellularly bound polyplexes were removed by heparin. DAPI was used to discriminate between viable and dead cells.

Table 8. Particle size and zeta potential of single-targeted polyplexes formed at N/P 6 and N/P 12.

Oligomer	Abbreviation	N/P	Mean Size (nm)	Zeta Potential (mV)
188	Ala-PEG-STP	6	185.9 ± 8.74	2.8 ± 0.35
		12	198.3 ± 21.0	4.7 ± 0.24
391	RGD-PEG-STP	6	375.4 ± 51.8	2.5 ± 0.24
		12	269.8 ± 39.4	5.5 ± 1.60
203	B6-PEG-STP	6	202.3 ± 54.3	20.4 ± 0.80
		12	186.4 ± 81.6	21.6 ± 0.95
186	GE11-PEG-STP	6	224.1 ± 96.5	2.0 ± 0.49
		12	233.5 ± 54.9	2.8 ± 0.61

Table 9. Particle size and zeta potential of dual-targeted polyplexes at different ratios formed at total N/P 6 and N/P 12.

Oligomer	N/P	Ratio	Mean size (nm)	Zeta potential (mV)
RGD and B6	6	2:4	125.8 ± 13.9	16.4 ± 1.19
	6	4:2	145.6 ± 28.5	11.4 ± 0.81
	12	4:8	200.4 ± 22.7	16.0 ± 0.90
	12	8:4	203.7 ± 42.5	15.2 ± 0.32
RGD and GE11	6	2:4	287.4 ± 38.3	2.4 ± 0.52
	6	4:2	295.2 ± 41.9	2.9 ± 0.39
	12	4:8	347.5 ± 46.2	3.9 ± 0.30
	12	8:4	397.2 ± 64.3	3.2 ± 0.23
GE11 and B6	6	2:4	216.9 ± 72.2	18.8 ± 0.12
	6	4:2	384.1 ± 77.5	13.7 ± 0.06
	12	4:8	175.4 ± 24.8	18.6 ± 0.75
	12	8:4	227.2 ± 10.9	17.6 ± 0.67

3.5 Targeted c-Met receptor-directed oligo(ethanamino) amides for efficient gene transfer *in vitro* and *in vivo*

The receptor tyrosine kinase HGFR/c-Met is over-expressed in epithelial-derived tumors as well as in stromal and interstitial cell-derived tumors such as sarcomas [171]. Binding of the natural ligand hepatocyte growth factor (HGF) to c-Met stimulates cell motility and migration, triggers mitogenesis and morphogenesis and thereby promotes oncogenesis and tumor progression. Therefore, different approaches based on c-Met signaling have been refined in cancer treatment: development of (1) antagonists preventing HGF receptor binding to cell surface c-Met, (2) cytosolic active tyrosine kinase inhibitors and (3) antagonists of the interactions between activated receptors and downstream effectors [172]. To date, targeting c-Met over-expressed in cancer tissues has been mostly limited to a variety of receptor binding antibodies intended primarily for *in vivo* imaging [173-175]. Conjugation of an anti-c-Met antibody fragment to the chemotherapeutic drug doxorubicin led to more effective antitumor activity [176]. Nguyen *et al.* demonstrated enhanced gene transfer selectivity to hepatocarcinoma cells using retrovirus displaying single-chain variable-fragment (scFv) directed against the c-Met receptor [177]. Surprisingly, despite the known oncological relevance of the c-Met proto-oncogene, up to now it has not been utilized for non-viral receptor-targeted gene delivery.

3.5.1 Suitability of c-Met binding ligands for targeted gene delivery with sequence-defined oligomers

For the first time we evaluated the two c-Met binding ligands cMBP1 and cMBP2 in terms of nucleic acid delivery. Solid-phase supported synthesis was utilized for the assembly of targeted and shielded oligomers (Scheme 4). By this method, the targeting ligand (cMBP1 or cMBP2) can be directly attached to the multifunctional oligomers within a single solid-phase synthesis, providing high-precision conjugates (synthesis by Ulrich Lächelt, PhD LMU, 2014). The first-generation targeted oligomers (Scheme 4-I) consist as the oligomers in previous chapter of a monodisperse polyethylene glycol (PEG) moiety with 24 oxyethylene units for the

reduction of unspecific interactions with blood components, lysine as a branching point, polycationic core comprising four repeating units of the novel artificial amino acids succinoyl-tetraethylene pentamine (Stp) for nucleic acid packaging, endosomal buffering and endosomal escape [120, 152], as well as an N-terminal cysteine residue at the end of each polycationic arm for redox-sensitive beneficial polyplex stabilization [120, 121, 153].

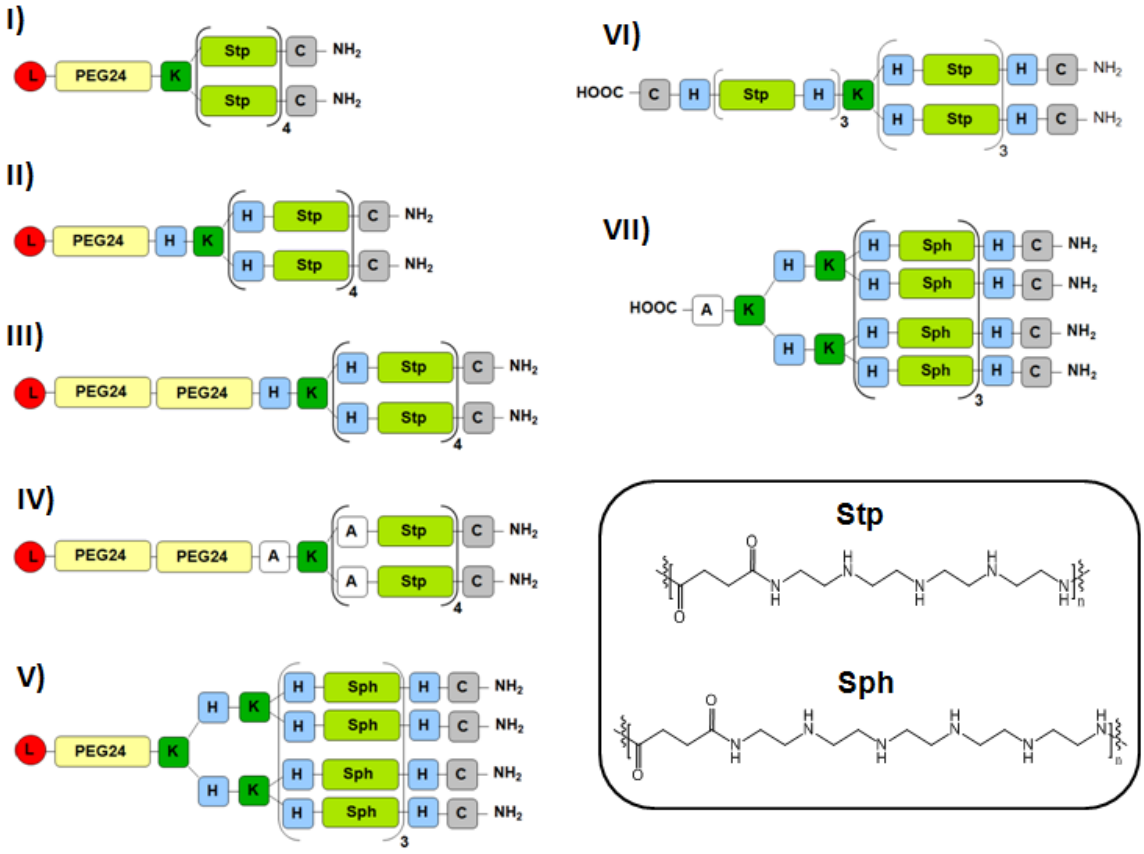

Scheme 4. Schematic overview of the synthesized oligomers. A, K, H and C represent the *α*-amino acids in a one-letter-code, L stands for the targeting ligand or the corresponding control. Syntheses were performed by Ulrich Lächelt and Dongsheng He, PhD students LMU.

The resulting cMBP1-targeted conjugate was denoted as oligomer #**1** and the cMBP2-containing conjugate as oligomer #**2**. A non-targeted alanine oligomer (#**3**) was constructed as a control. Sequences are displayed in Table 10.

Table 10. Synthesized oligomers with assigned numbers, topologies and structures in corresponding Scheme 4, sequences and identification numbers (compound ID).

No.	Structure in Scheme 4	Topology	Sequence (C to N Terminal)	ID
#1		2-arm; w/o His	K[dPEG$_{24}$-K(Stp$_4$-C]$_2$-cMBP1	***696***
#2		1 PEG	K[dPEG$_{24}$-K(Stp$_4$-C)$_2$]-cMBP2	***443***
#3			A-dPEG$_{24}$-K[Stp$_4$-C]$_2$	***188***
#4	**I)**		K[dPEG$_{24}$-K(Stp$_4$-C)$_2$]-cMBP2sc1	***697***
#5			K[dPEG$_{24}$-K(Stp$_4$-C)$_2$]-cMBP2sc2	***698***
#6			K[dPEG$_{24}$-K(Stp$_4$-C)$_2$]-cMBP2sc3	***699***
#7			K[dPEG$_{24}$-K(Stp$_4$-C)$_2$]-cMBP2sc4	***700***
#8		2-arm; with His	K[dPEG$_{24}$-HK[H-(Stp-H)$_4$-C]$_2$]-cMBP2	***442***
#9	**II)**	1 PEG	A-dPEG$_{24}$-HK[H-(Stp-H)$_4$-C]$_2$	***440***
#10		2-arm; with His/Ala	K[(dPEG$_{24}$)$_2$-HK[H-(Stp-H)$_4$-C]$_2$]-cMBP2	***694***
#11	**III)** and **IV)**	2 PEG	K[(dPEG$_{24}$)$_2$-AK[A-(Stp-A)$_4$-C]$_2$]-cMBP2	***695***
#12			A-(dPEG$_{24}$)$_2$-HK[H-(Stp-H)$_4$-C]$_2$	***616***
#13		4-arm; with His	K[dPEG$_{24}$-K(HK(H-(Sph-H)$_3$-C)$_2$)$_2$]-cMBP2	***677***
#14	**V)**	1 PEG	A-dPEG$_{24}$-K[HK(H-(Sph-H)$_3$-C)$_2$]$_2$	***678***
#15	**VI)**	3-arm; with His	C-H-(Stp-H)$_3$-K-[(H-Stp)$_3$-H-C]$_2$	***689***
#16	**VII)**	4-arm; with His	AK[HK(H-(Sph-H)$_3$-C)$_2$]$_2$	***606***

All three oligomers decorated with cMBP1, cMBP2 or alanine were able to fully complex pDNA already at the low N/P ratio of 6 as observed from the complete polyplex retention in gel (Figure 34A). Fulfilling this first prerequisite, cell association studies were performed using the hepatocellular carcinoma (Huh7) cell line. Flow cytometry with help of an anti-c-Met antibody confirmed high receptor expression in almost 100% Huh7 cells (Figure 35).

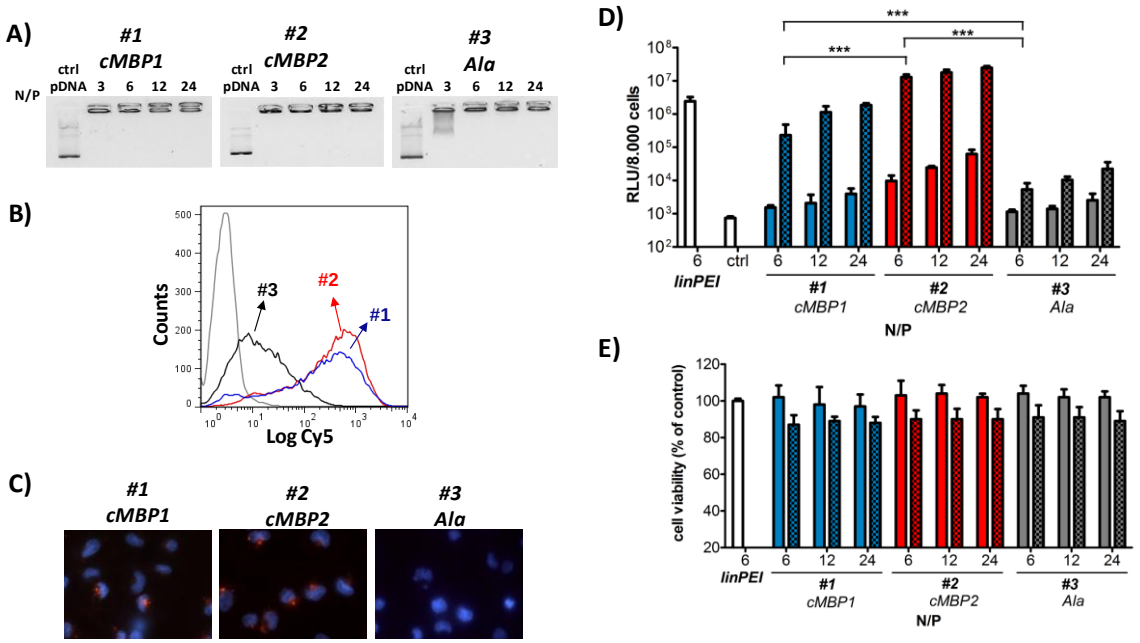

Figure 34. A) pDNA binding assay by electrophoresis. Gel retardations of cMBP1-, cMBP2-containing and alanine control polyplexes at increasing N/P ratios were compared to the mobility of the free pDNA. B) Cell association of oligomer/Cy5-pDNA polyplexes at N/P 12 to Huh7 cells after 30 min incubation at 4°C as determined by flow cytometry. Logarithmic X-scale represents Cy5 fluorescence of polyplexes bound to Huh7 cells. "Count" represents the cumulative counts of cells with indicated Cy5 fluorescence after appropriate gating by forward/sideward scatter and pulse width. C) Fluorescence microscopic images of the cellular uptake of the cMBP1-, cMBP2-containing and alanine control polyplexes formed with Cy5-labeled pDNA at N/P 12 (blue: DAPI staining, red: Cy5). D) Luciferase gene transfer in Huh7 cells without (no pattern) or with (pattern) the addition of endosomolytic chloroquine, as obtained with the cMBP1- and cMBP2-containing polyplexes in comparison to the alanine control polyplexes (45 min incubation). Linear PEI 22 kDa (linPEI) at optimal non-toxic ratio (N/P 6, w/w 0.8; 4 h incubation) was used a positive control, HBG treated cells served as a negative control. Data are presented as mean value (±SD) out of quintuplicate. E) Corresponding cell viability (MTT) assay. Cell viability was calculated as percentage to cells treated with HBG.

Using Cy5-labeled pDNA, the cMBP1-targeted polyplexes **(#1**) displayed efficient cell binding (>90% of cells) and the cMBP2-containing polyplexes **(#2**) an even more effective cell attachment of >95% (Figure 34B). The alanine control oligomer (**#3**) showed far lower cellular attachment. To exclude a cell line dependency for the ligand binding specificity, and to prove the usefulness of the novel ligands on different c-Met expressing cell lines, cell binding experiments were additionally performed on the prostate cancer cell line DU145 which also exhibited high c-Met receptor expression, though at a slightly lower intensity in comparison to the Huh7 cell line (Figure 35). The cell binding studies on DU145 cells resulted in a similarly

high binding for cMBP1- and cMBP2-equipped polyplexes, and insignificant cell association for the alanine control polyplexes (Figure 36).

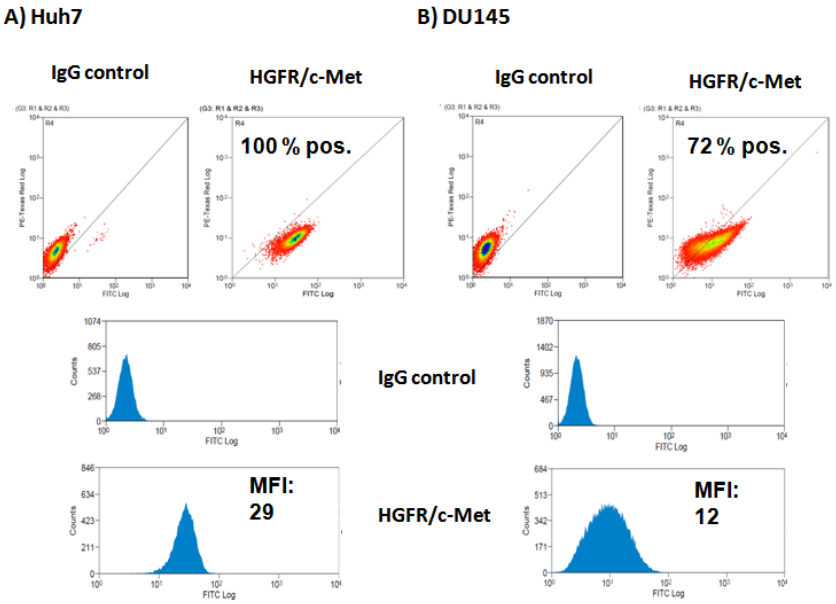

Figure 35. HGFR/c-Met receptor levels on A) Huh7 and B) DU145 cell line showing the results obtained with the monoclonal mouse anti-human HGFR/c-Met antibody and IgG control. Alexa 488-labeled goat anti-mouse secondary antibody was used for the detection of receptor expression by flow cytometry. MFI stands for mean fluorescence intensity.

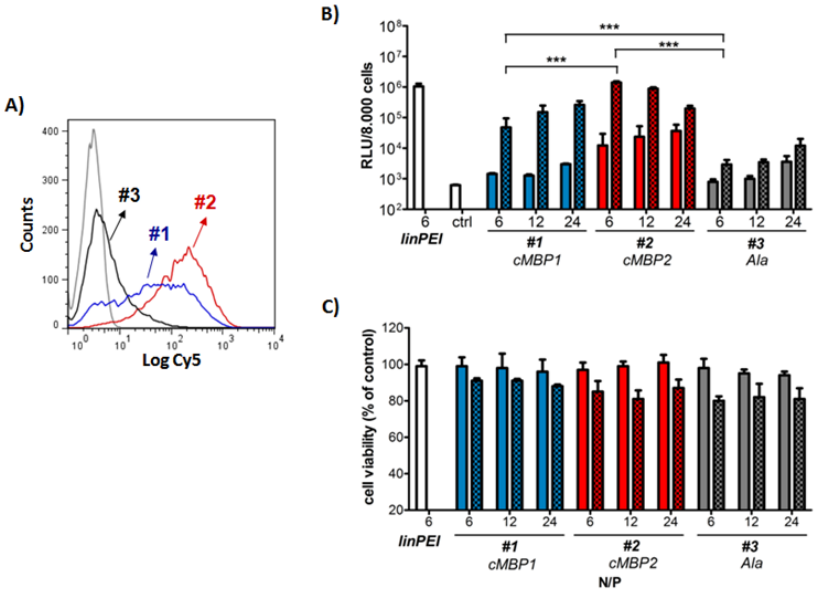

Figure 36. A) DU145 prostate carcinoma cell binding of cMBP1- and cMBP2-targeted Cy5-pDNA polyplexes after 30 min incubation at 4°C, as compared to alanine control polyplexes. B) Luciferase reporter gene expression of cMBP1- and cMBP2-targeted and alanine control polyplexes on DU145 cells with (pattern) or without (no pattern) the addition of chloroquine. C) Cell viability assay performed in parallel. Data are presented as mean value (±SD) out of a quintuplicate.

Following the cellular binding studies, the internalized cMBP1- (**#1**), cMBP2- (**#2**) and non-targeted (**#3**) polyplexes were imaged using the fluorescence microscopy (Figure 34C). The images revealed an intracellular uptake of the labeled nucleic acid in the case of the cMBP2-containing polyplexes, somewhat less for cMBP1-targeted polyplexes, and its absence with the control polyplexes. The c-Met-targeting effect was finally confirmed also by pDNA transfections. As the endosomal escape represents one of the greatest drawbacks in gene delivery, an endosomolytic agent chloroquine [170, 178] was added to the cell culture medium after transfections. In line with the cell binding and uptake studies, with only a short 45 min polyplex incubation on Huh7 cells, and upon addition of chloroquine (presented in pattern bars), the highest luciferase gene expression was obtained with the cMBP2-decorated polyplexes, exceeding the linear PEI polyplexes (linPEI) with 4 h incubation on cells for almost 1 log unit (Figure 34B). Also for the cMBP1 ligand a high reporter gene expression and significant targeting effect over alanine control polyplexes was observed, though more than one log unit lower as compared to cMBP2. In the absence of chloroquine, an only moderate or practically no gene transfer was seen for the cMBP2 or cMBP1 ligand, respectively. The significant activity of cMBP2 polyplexes may partially be attributed to the presence of several endosomal escape facilitating histidines (see chapter 3.4.2 below) in the cMBP2 ligand itself. Cytotoxicity studies performed alongside showed no negative effects of applied polyplexes on the cell viability, apart from a minor cytotoxicity caused by the chloroquine incubation (Figure 34E). Analogous gene transfer (Figure 36B) and cell viability studies (Figure 36C) on DU145 cells led to similar results. Luciferase expression was roughly one log unit lower which is in line with lower c-Met expression in the prostate cancer cell line (Figure 35).

The cMBP2 ligand showed a better delivery effect on two different cell lines than cMBP1. Therefore, the specificity of this more potent ligand was analyzed in more detail prior to successive carrier optimization. For this reason, four scrambled sequences chosen by random computer-supported permutation (cMBP2sc1 (**#4**): LHHHDRKSSIHH, cMBP2sc2 (**#5**): KSHHRDHIHLHS, cMBP2sc3 (**#6**): HHSIHRLHHKSD and cMBP2sc4 (**#7**): RKIHHHLHSHSD) were synthesized and conjugated to the same initial oligomer structure as above (Scheme 4-I**,** Table 10). These control oligomers displayed the expected complete pDNA binding (Figure 37A). In the cell association studies the four scrambled sequence-decorated polyplex

types hardly bound to the cell surface of the Huh7 (Figure 37B) and DU145 (Figure 37C) cells, *i.e.* in a similar extent as the alanine control polyplexes, confirming the target specificity of the cMBP2 ligand.

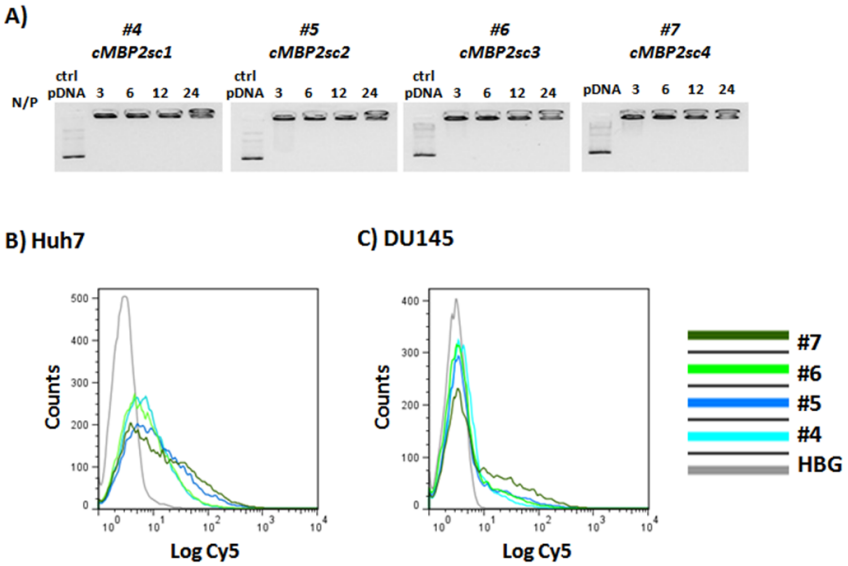

Figure 37. A) pDNA binding assay by electrophoresis. Gel retardation of the scrambled peptide-equipped polyplexes at increasing N/P ratios was compared to the shift of free pDNA. B, C) Cellular association of polyplexes formed with Cy5-labeled pDNA and conjugates with the conjugated scrambled sequences on B) DU145 and C) Huh7 cells after 30 min incubation at 4 °C as determined by flow cytometry.

3.5.2 cMBP-containing polyplexes do not activate c-Met tyrosine kinase signaling

In the next step the possible HGFR/c-Met receptor activation after polyplex administration was investigated. As the binding of its natural ligand hepatocyte growth factor (HGF) causes the c-Met phosphorylation and downstream signaling, the direct receptor phosphorylation was investigated by Western blot using phospho-Met antibody against the phosphorylated receptor form. Only when applying HGF as a positive control, clear receptor activation could be observed. None of the polyplexes regardless of the ligand mediated any receptor phosphorylation (Figure 38A). The similar results were obtained when investigating the activation of the c-Met downstream protein Akt. As expected, the downstream signaling and Akt phosphorylation was observed only when plain HGF was applied (Figure 38B).

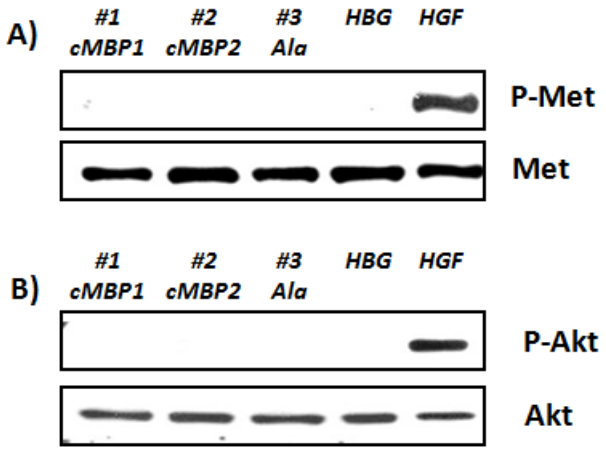

Figure 38. Lack of c-Met receptor activation. Huh7 cells were treated either with cMBP1-targeted (lane 1), cMBP2-containing (lane 2) or alanine control (lane 3) polyplexes at N/P 12. HBG buffer (lane 4) was used as a negative control and natural ligand hepatocyte growth factor (HGF) (lane 5) as a positive control. After 1 h incubation, total cell lysates were subjected to Western blot analysis and incubated with A) p-Met and Met and B) P-Akt and Akt antibodies.

3.5.3 Carrier optimization: Implementation of histidines and extension of polyethylene glycol chain

The high transfection efficiency of the initial oligomers (Scheme 4-I) was dependent on the presence of chloroquine. Therefore endosomal escape facilitating histidines [100, 101] were further implemented into the oligomer backbone before each (oligoethanamino)amide building block of the polycationic arms as well as prior to the lysine branching point, bringing forth the cMBP2-containing oligomer #**8** and its non-targeted alanine counterpart #**9** (Scheme 4-II and Table 10). Apart from modifications of the polycationic part, the PEG chain offers another option to alter the properties of the targeted polyplexes. For this purpose, cMBP2-containing (#**10**) and alanine control (#**11**) oligomers having an additional second PEG moiety of 24 oxyethylene units as well as histidines in the polycationic backbone were synthesized (Scheme 4-III, Table 10). Another control oligomer contains alanines replacing the backbone histidines (#**12**, Scheme 4-IV).

First, pDNA compaction ability of the cMBP2-containing initial oligomer (#**2**), histidines-enriched oligomer with one PEG_{24} chain (#**8**) and more highly shielded two PEG_{24} chains comprising oligomers (#**10** and #**11**) was compared by ethidium bromide exclusion assay (Figure 39A). The nonPEGylated linPEI was used as positive control, leading to a greatest decrease in the intercalator fluorescence and

therewith the highest cargo compaction capacity. The original PEG_{24} (~ 1000 Da) cMBP2-containing oligomer **#2** (Scheme 4-I) without histidines in the carrier backbone also displayed a high compaction ability. The histidine implementation (**#8**) led to a slightly diminished pDNA compaction. The targeted oligomers with two PEG_{24} (~ 2000 Da) chains (**#10**, **#11**) displayed similar pDNA compaction.

Next, the biological efficiency of these modified oligomers was investigated. In cellular internalization experiments (Figure 39) the histidines-enriched polyplexes (**#8**, **#9**; Scheme 4-II) were first compared to the polyplexes formed with the initial oligomers without the histidines (**#2**, **#3**; Scheme 4-I). A pronounced targeting effect was observed for both cMBP2-containing polyplexes **#8** and **#2**. The histidines implementation, as expected, caused no significant change in the cellular uptake. Hardly any difference could be observed between the cMBP2-decorated oligomers plus/minus histidines. Both types of alanine control polyplexes (**#3** and **#9**) displayed practically no cellular uptake, with the histidines modification causing a slightly increased cellular internalization (Figure 39B). Furthermore, the cellular uptake of the polyplexes formed with the oligomers having two PEG_{24} chains was analyzed (Figure 39C). Both cMBP2-containing PEG_{48} oligomers (**#10** and **#11**) showed high cellular internalization, comparable to the targeted PEG_{24} polyplexes before in Figure 39B. No difference between the oligomers with the histidine (**#10**) or alanine (**#11**) spacers in the polycationic part was observed (Figure 39C). The non-targeted oligomer (**#12**) once more displayed very low cellular internalization. In contrast to the cell uptake studies, the luciferase gene transfer studies revealed an immense influence of histidines on pDNA transfection efficiency. In the absence of the endosomolytic chloroquine (no pattern), the histidines-modified cMBP2-containing oligomer **#8** displayed a greatly enhanced gene transfer (100-fold) as compared to the original structure without the histidines (**#2**); pointing out to markedly improved endosomal buffering and endosomal escape of the targeted polyplexes (Figure 39D).

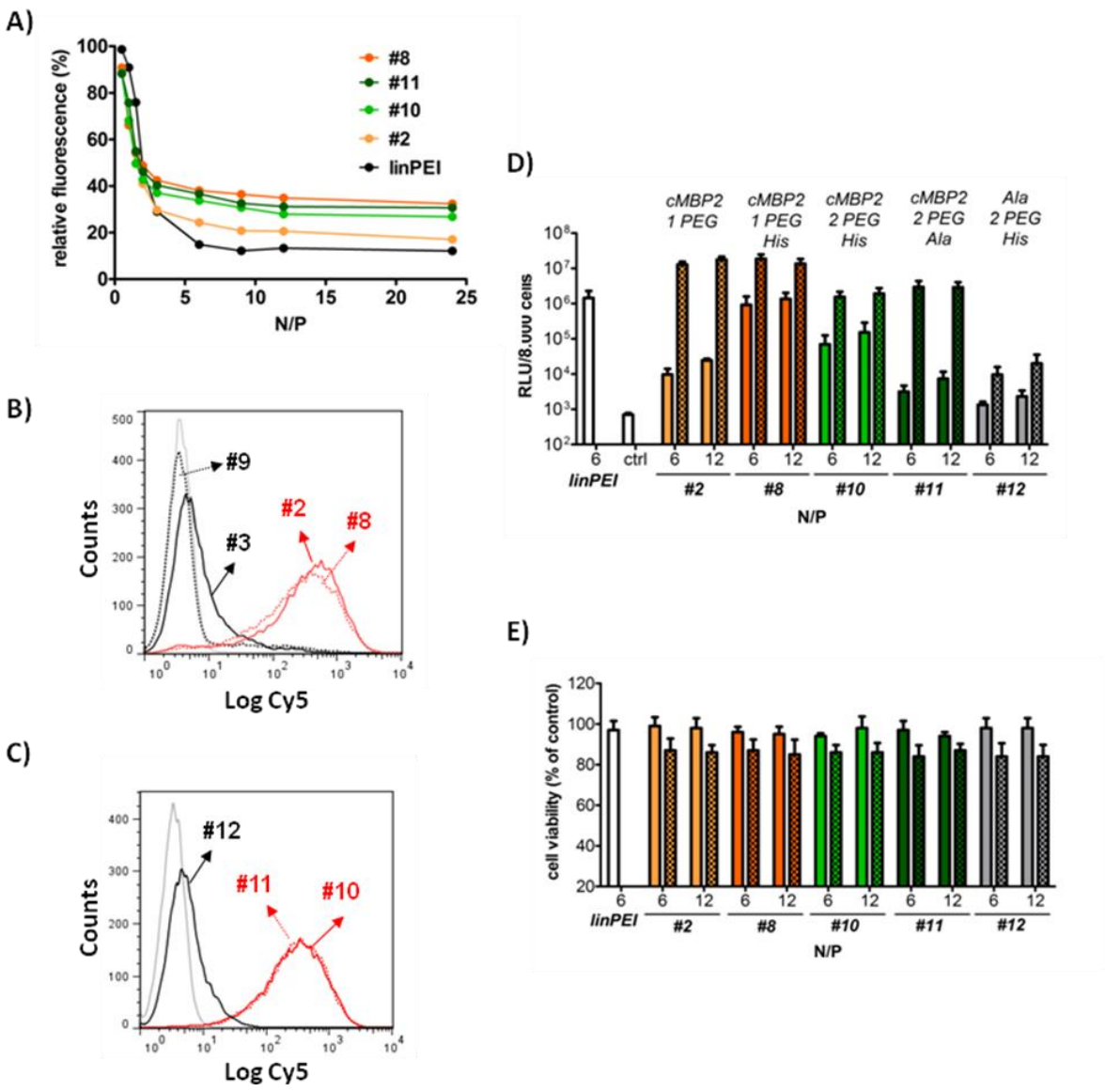

Figure 39. Influence of histidines addition and enhanced PEG shielding. A) pDNA compaction ability determined by EtBr exclusion assay. Oligomer solution was added at increasing N/P ratios to 10 µg pDNA containing 0.4 µg EtBr. Reduction in EtBr fluorescence was determined as percentage of maximal fluorescence of EtBr containing pDNA solution. B) Cellular internalization of the Cy5-pDNA polyplexes (N/P 12) of the oligomers with one PEG24 chain analyzed by flow cytometry after 45 min incubation at 37 °C followed by removal of extracellularly bound polyplexes; cMBP2-containing polyplexes are presented in red (#2 and #8), alanine controls in black (#3 and #9). Initial oligomer structures are displayed with a solid line, histidine modified oligomers with a dotted line. HBG treated cells are presented in grey. C) Cellular internalization of the polyplexes (N/P 12) formed with oligomers comprising two PEG24 chains; cMBP2-containing polyplexes are presented in red (dotted line for the oligomer with the histidine (#10) spacers and solid line for the oligomer with the alanine (#11) spacers), alanine control (#12) polyplexes in black. D) Luciferase reporter gene expression in Huh7 cell line with (pattern) or without (no pattern) chloroquine and E) cell viability assay performed in parallel. linPEI was used a positive control, HBG treated cells served as background. Cell viability was calculated as percentage to cells treated with HBG. Data are presented as mean value (±SD) out of quintuplicate.

In the presence of chloroquine (patterned bar) the transfection efficiency remained unchanged. The cMBP2- and histidine- containing oligomer with a second PEG_{24} chain **#10** led to reduced transfection efficiency as compared to the less shielded **#8** polyplexes. Replacing the histidines in the backbone with the alanine spacers **#11** led to comparably efficient gene transfer with the chloroquine incubation, whereas in the absence of chloroquine vastly diminished transfection efficiency was obtained due to reduced endosomal escape. The alanine control with two PEG_{24} units **#12** mediated only a minor luciferase expression. The MTT assay (Figure 39E) showed no reduction in cell viability for all applied polyplexes. Only in the presence of chloroquine a minor cytotoxicity was observed. Similar effects of histidines and additional PEG units were observed also with the DU145 cell line (Figure 40A-C) confirming the generality of effects of the applied modifications.

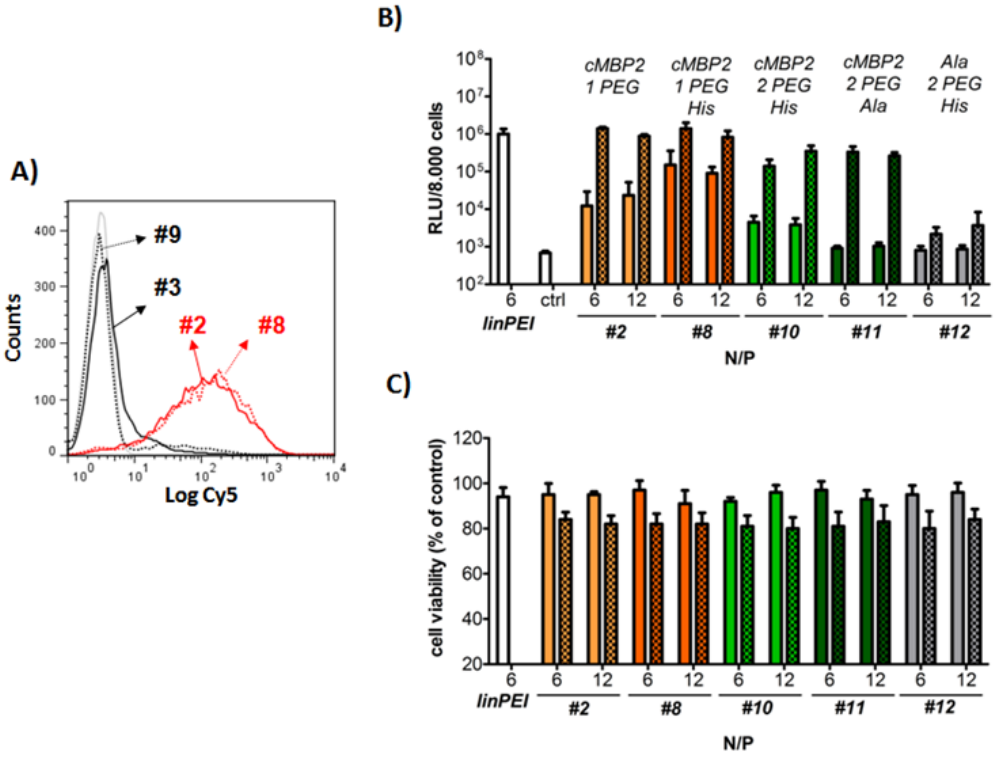

Figure 40. A) Internalization of Cy5-pDNA polyplexes (N/P 12) into DU145 cells analyzed by flow cytometry; cMBP2-targeted polyplexes are presented in red, alanine controls in black. Initial oligomeric structures are displayed with a solid line, histidine modified oligomers with a dotted line. HBG treated cells are presented in grey. "Count" represents cumulative counts of cells with indicated Cy5 fluorescence after appropriate gating by forward/sideward scatter and pulse width. B) Luciferase gene transfer with histidines and additional PEG_{24} chain modified oligomers on DU145 cells with (pattern) or without (no pattern) the addition of chloroquine. C) Corresponding cell viabilities (MTT assay).

Furthermore, Western blotting was performed with the histidines-enriched PEG24 oligomers. As before with their non-histidine analogs, no c-Met receptor activation of Huh7 cells was found (Figure 41).

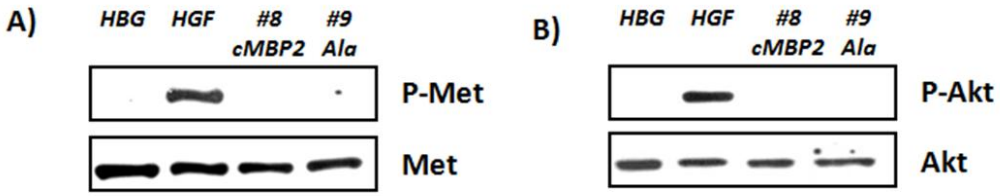

Figure 41. Lack of HGFR/c-Met receptor activation with histidines-enriched polyplexes. Huh7 cells were treated either with HBG buffer (lane 1) or hepatocyte growth factor (HGF) (lane 2), cMBP2-targeted (lane 3) or alanine control (lane 3) polyplexes (N/P 12). After 1 h incubation, total cell lysates were subjected to Western blot analysis and incubated with A) p-Met and Met and B) P-Akt and Akt antibodies.

3.5.4 Carrier optimization: Implementation of additional polycationic arms

As the next step in optimization, further modifications of the polycationic part of the carrier were made. A cMBP2- and histidine-containing oligomer was synthesized having in the carrier backbone four instead of two polycationic arms, and designated as oligomer **#13** and its alanine counterpart as **#14** (Scheme 4-V). Moreover, in these two new highly branched oligomers, the Stp building block was replaced by the Sph building block with one additional diaminoethane repeat (Scheme 4). The EtBr exclusion assay indeed displayed a slightly improved pDNA compaction of the histidines containing 4-arm oligomer **#13** in comparison to 2-arm oligomer **#8** (Figure 42A). The cellular internalization studies of the cMBP2-containing polyplexes formed with this oligomer displayed a clear targeting effect over its alanine control **#14**, though surprisingly a less pronounced cellular uptake than with its 2-arm analog **#8** (Figure 42B). Also in the luciferase gene transfer studies, a significant targeting effect was observed with cMBP2-containing 4-arm oligomers **#13** as compared to its alanine control analog (Figure 42C). However, in line with the cellular uptake studies, approximately one log unit lower gene transfer was achieved with the 4-arm oligomer polyplexes as compared to the 2-arm oligomer **#8** polyplexes (Figure 42D). Once more, none of the polyplexes caused any significant cytotoxicity (Figure 42D). To sum up, increment in the number of polycationic arms did not provide any benefit in the case of cMBP2-containing polyplexes *in vitro*.

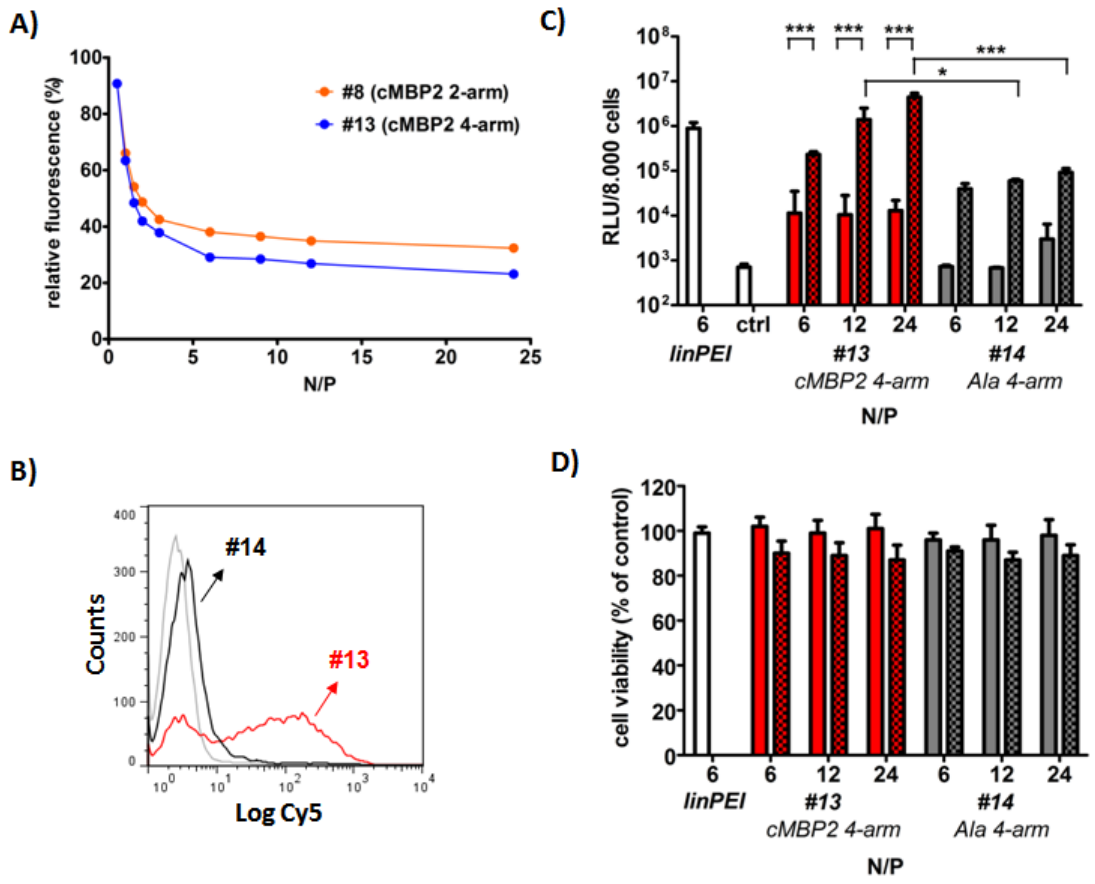

Figure 42. Influence of additional polycationic arms. A) pDNA compaction ability determined by EtBr exclusion assay comparing cMBP2-containing 2-arm (**#8**) and 4-arm (**#13**) oligomers. Reduction in EtBr fluorescence was determined as percentage of maximal fluorescence of EtBr containing pDNA solution. B) Cellular internalization of the polyplexes (N/P 12) of the cMBP2-containing (**#13**) and alanine control (**#14**) 4-arm oligomers analyzed with flow cytometry using Cy5-labeled pDNA. C) pDNA transfection efficiencies of 4-arm structures with (pattern) or without chloroquine (no pattern) and D) corresponding cell viabilities. Data are presented as mean value (±SD) out of a quintuplicate.

3.5.5 Confirmation of cMBP2-mediated targeting in vivo

Due to the fact that the histidines-enriched 2-arm oligomer **#8** with one PEG_{24} unit yielded the most promising cellular uptake and gene transfer *in vitro*, this oligomer was then selected for first *in vivo* studies. An additional PEG_{24} chain had not shown any favorable effects *in vitro*, yet it might be beneficial *in vivo* influencing the polyplex biodistribution and the ligand accessibility. For this purpose, also the histidines-enriched oligomer with two PEG_{24} units **#10** was chosen for further experiments and compared to its less shielded analog **#8**. Prior to *in vivo* experiments the polyplex stability in serum was evaluated *ex vivo*. The pDNA polyplexes were incubated in fetal bovine serum (FCS) for 1, 10, 30 or 90 min and subsequently subjected to gel

electrophoresis. All polyplexes, regardless of the ligand or extent of shielding, displayed a complete stability in 90% FCS and remained stable also after addition of a highly negatively charged heparin (Figure 43A).

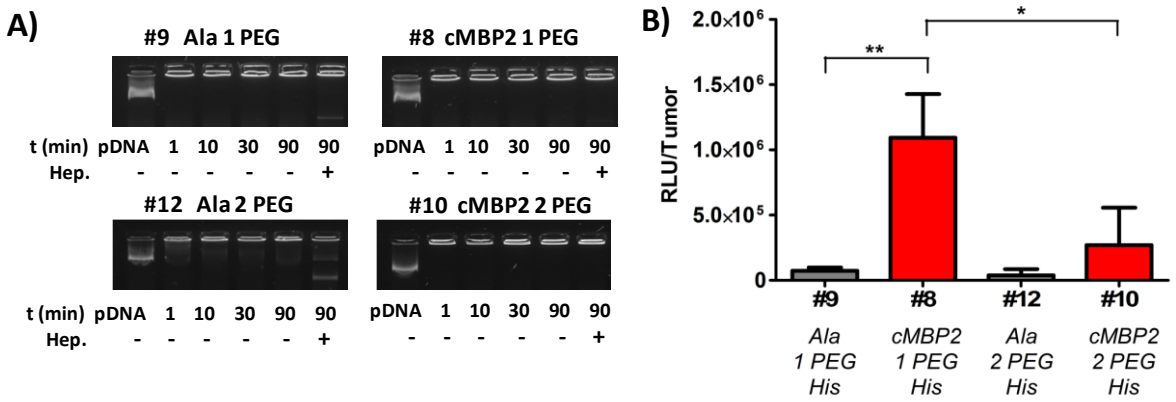

Figure 43. *In vivo* confirmation of the cMBP2 targeting effect. A) Stability of polyplexes in serum. pDNA binding of oligomers **#9**, **#8**, **#12** and **#10** in the presence of 90% fetal bovine serum (FCS) analyzed by means of an agarose gel shift assay. Polyplexes at N/P 12 were incubated at room temperature for 30 min in order to allow polyplex formation. Next, FCS was added and polyplexes were further incubated for 90, 30, 10 or 1 min. As indicated (last lane), heparin was added to the polyplexes after incubation in serum for 90 min. B) Luciferase gene expression 24 h after intratumoral administration of pCMVL polyplexes at N/P 12 into Huh7 tumor bearing mice. Luciferase gene expression is presented as relative light units per tumor (RLU/tumor; N=5, mean±SEM)). Lysis buffer RLU values were subtracted. The Huh7 tumor weights were 387±146 mg. The animal experiments were performed together with Annika Herrmann (veterinary MD study, LMU).

Subsequent *in vivo* experiments were conducted in subcutaneous Huh7 tumor-bearing mice. Polyplexes (50 µg pDNA in 60 µL) were injected intratumorally. The results of luciferase gene transfer (Figure 43B) were in accordance with *in vitro* studies, revealing a significant cMBP2 targeting effect in the case of **#8** polyplexes, with a 15-fold higher gene expression than the alanine **#9** control polyplexes. The oligomer **#10** with higher PEG content displayed a less pronounced gene expression, but a targeting effect compared with its alanine control **#12** (7-fold lower expression). Alongside, as another confirmation of a cMBP2 targeting effect *in vivo*, quantitative polymerase chain reaction was performed for the absolute quantification of the plasmid amount retained in tumors after local application of polyplexes. In line with *in vivo* luciferase gene transfer studies, the highest amount of the plasmid in tumor was obtained with the cMBP2-containing one PEG_{24} chain containing oligomer (**#8**), being significantly (almost 10-fold) higher as compared to its non-targeted analog **#9** and (>3-fold) to the cMBP2-PEG_{48} containing polyplexes **#10** (Figure 44).

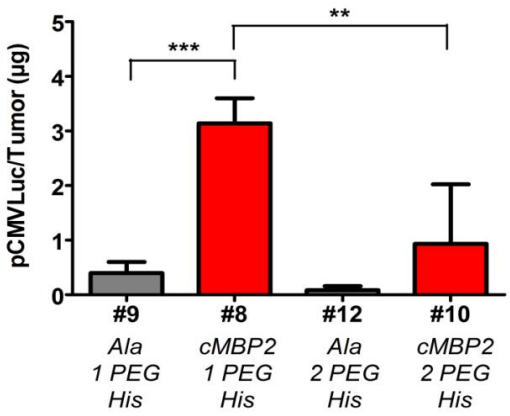

Figure 44. Quantification of pCMVLuc detected in tumors at 24 h after intratumoral injection of cMBP2-targeted and alanine control polyplexes (N/P 12) with either one or two PEG_{24} chains as determined with qPCR (N=4, mean±SEM). The animal experiments were performed together with Annika Herrmann (veterinary MD study, LMU).

3.5.6 Intravenous application of c-Met-directed polypexes

As the intratumoral studies using cMBP2- and histidine-containing oligomer #**8** displayed promising results, this oligomer was consequently chosen for further *in vivo* studies. This time the polyplexes (80 µg pDNA in 200 µL) were injected intravenously and the mice were sacrificed two days after #**8** and control #**9** polyplex administrations. The subsequent analysis of luciferase expression in tumors of the mice treated with the cMBP2-decorated polyplexes (#**8**) showed moderate expression levels in various organs and did not reveal any significant targeting effect over the non-targeted polyplexes (Figure 45A). As shown above *in vitro* and upon intratumoral administration, the increase to an even 2-fold higher PEG content was found as unfavorable.

Therefore for further optimization, the opposite direction was taken towards enhanced dimension of the polycationic oligomer part. Thus, the polyplexes formed with the PEGylated 4-arm oligomers #**13** and #**14** (Scheme 4-V) although they showed no improvement *in vitro* (Figure 42C), were subjected to the intravenous administration studies.

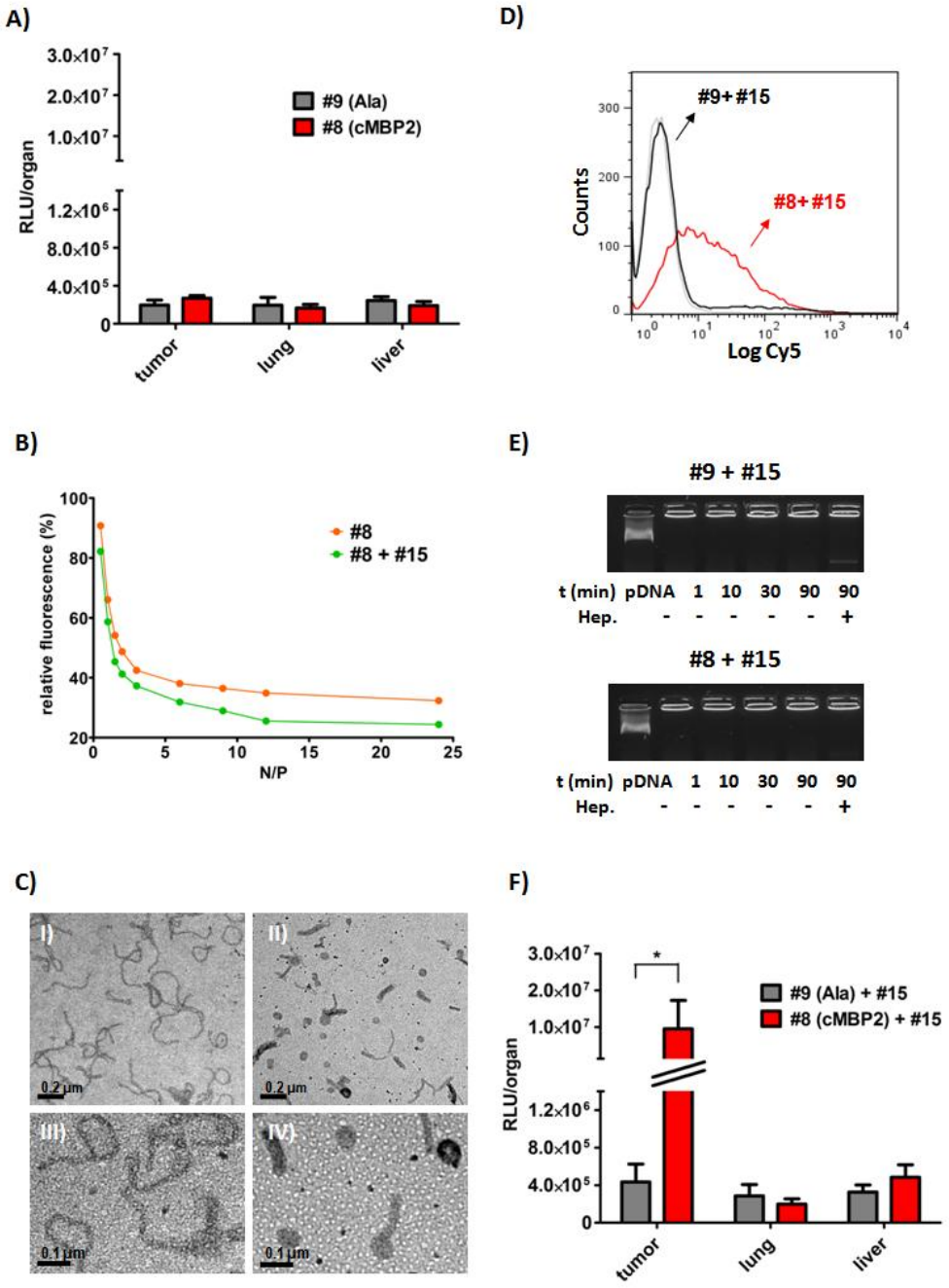

Figure 45. Improving gene transfer after intravenous administration by combination of 2-arm PEGylated cMBP2-containing oligomer #**8** or alanine control oligomer #**9** with non-PEGylated 3-arm oligomer #**15**. A) *In vivo* gene expression 48 h after i.v. administration of #**8** and #**9** polyplexes at N/P 12 into Huh7 tumor bearing mice (N=5, mean±SEM) in tumor, lung and liver. B) EtBr exclusion assay comparing single oligomer polyplexes of #**8** and combination polyplexes of #**8** plus #**15** at the adequate ratio (oligomer #**8** at 70% and oligomer #**15** at 30% of the total N/P). C) Transmission electron microscopy images (Markus Döblinger, Department of Chemistry, LMU) of polyplexes (N/P 12) formed (I and III) with single oligomer #**8** and (II and IV) with the combination of oligomers #**8** and #**15**. D) Cellular internalization comparing the cellular uptake of the Cy5-labeled pDNA polyplexes formed with the cMBP2-containing (#**8** + #**15**) and alanine control (#**9** + #**15**) polyplexes. E) Serum stability of combination polyplexes (total N/P 12) formed with cMBP2 or alanine control oligomers analyzed at different serum incubation times by an agarose gel shift assay. Where indicated, heparin was added to polyplexes after incubation in serum for 90 min. F) *In vivo* gene expression in tumor, lung and liver at 48 h after i.v. administration

of the combination polyplexes at N/P 12 into Huh7 tumor bearing mice (N=5, mean±SEM). Luciferase gene expression is presented as relative light units per organ or tumor (RLU/organ). Lysis buffer RLU values were subtracted. Liver weight was around 1.6 g, lung weight around 230 mg and Huh7 tumor weight 452±189 mg. The animal experiments were performed together with Annika Herrmann (veterinary MD study, LMU).

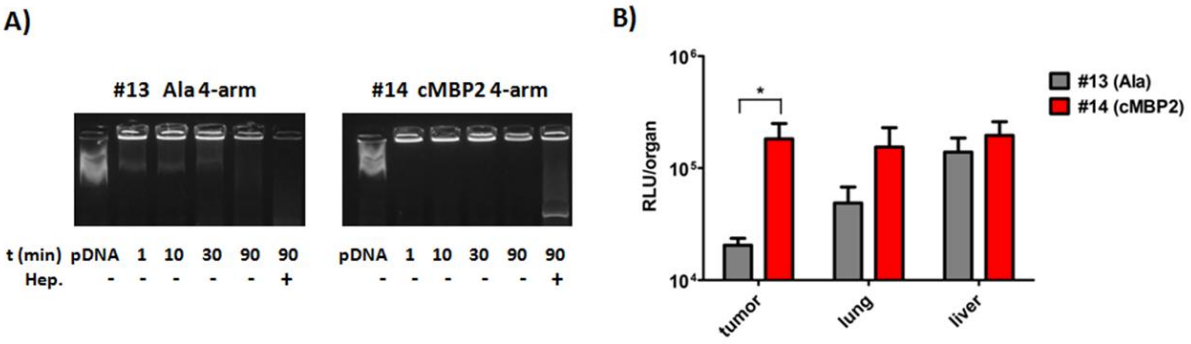

Figure 46. A) Serum stability of the polyplexes (N/P 12) formed with 4-arm PEGylated cMBP2-targeted (**#14**) or non-targeted control (**#13**) oligomers analyzed at different serum incubation times by an agarose gel shift assay. Where indicated, heparin was added to the polyplexes after incubation in serum for 90 min. B) *In vivo* gene expression at 48 h after i.v. administration of pCMVLuc polyplexes formed with the cMBP2-targeted (**#13**) and alanine control (**#14**) 4-arm PEG_{24} oligomers at N/P 12 into Huh7 tumor bearing mice (N=5, mean±SEM) in tumor, lung and liver. Luciferase gene expression is presented as relative light units per organ or tumor (RLU/organ). Lysis buffer RLU values were subtracted. Liver weight was around 1.5 g, lung weight around 210 mg and Huh7 tumor weight 282±197 mg. The animal experiments were performed together with Annika Herrmann (veterinary MD study, LMU).

Encouragingly, these more polycationic oligomers indeed triggered a significant cMBP2 targeting-dependent gene expression in the distant tumor (Figure 46), though expression levels were moderate and similar as in other organs (liver and lung).

In order to further improve cMBP2 targeting also upon intravenous administration, an alternative approach was considered in optimizing the nanoparticles. For this purpose, a novel compacting 3-arm oligomer **#15** (Scheme 4-VI) was synthesized being devoid PEG but having three oligocationic arms of the repeating Stp units with alternating histidines and terminal cysteines that are supposed to disulfide-crosslink with the terminal cysteines of the targeted PEGylated oligomer. This new compacting oligomer **#15** was mixed with the PEGylated cMBP2-containing 2-arm oligomer **#8** at an optimized 30:70 cationic ratio to reach the total N/P ratio of 12 (oligomer **#15** at N/P 3.6 and oligomer **#8** at N/P 8.4) prior to polyplex formation with the pDNA. The resulting combination polyplexes were first evaluated for their pDNA compaction ability and compared to polyplexes formed with only oligomer **#8**. The decreased

fluorescence in the EtBr exclusion assay confirmed an increased pDNA compaction (Figure 45B). Transmission electron microscopy images revealed profound change in nanoparticles shape when the oligomer **#8** was mixed with the non-PEGylated oligomers **#15**. The single oligomer **#8** polyplexes (Figure 45C, I and III) formed rather longer spaghetti-like structures of several hundred nanometers, whereas the novel combination polyplexes (Figure 45C, II and IV) led to preferred formation of either approx. 50 nm round-shaped toroidal nanoparticles or 100-150 nm short nanorods. Next, the preservation of the cMBP2 target-specificity for such bi-oligomeric polyplexes needed to be analyzed, as the co-addition of the 30% positively charged non-shielded oligomer might reduce the effects of the surface shielding and targeting. The cellular internalization studies using Cy5-labeled pDNA revealed a far higher cellular uptake of the cMBP2-containing combination polyplexes (**#8** + **#15**) as compared to their alanine control analogs (**#9** + **#15**) (Figure 45D), although the uptake was somewhat lower as compared to the cellular internalization of the single oligomer **#8** polyplexes tested before (Figure 45B). Nevertheless, the receptor-specificity was well maintained and the alanine control combination polyplexes exhibited practically no cellular uptake (Figure 45D). Prior to *in vivo* experiments, the stability of combination polyplexes in serum was evaluated. The *ex vivo* pDNA compaction studies in 90% FCS confirmed their intactness in serum (Figure 45E). Finally, the compacted polyplexes were injected intravenously in the subcutaneous Huh7 tumor-bearing mice. Remarkably and in sharp contrast to **#8** polyplexes (Figure 45A), with the cMBP2-containing (**#8** + **#15**) polyplexes a greatly increased luciferase expression was achieved in the tumor (Figure 45F) exceeding the signal of the non-targeted compacted control (**#9** + **#15**) polyplexes by 22-fold and, excitingly, of the cMBP2-equipped mono-oligomer (**#8**) polyplexes by 35-fold (Figure 45A). Remarkably, the luciferase expression in the tumor was up to 50-fold higher than in the lung or liver (Figure 45F).

To investigate whether this co-addition effect is specific for the added compacting oligomer **#15** or it can be achieved also by the addition of another non-shielded oligomer a different oligomer combination was evaluated in polyplex formation. Instead of 3-arm oligomer **#15**, a 4-arm polycationic oligomer comprising Sph building blocks (Scheme 4-VII) was combined with the PEGylated targeting oligomer **#8** to the total N/P ratio of 12 as above. This combination resulted in only minor additional decrease in EtBr fluorescence as compared to the single oligomer **#8**

(Figure 47A) and slightly lower cellular uptake of the cMBP2-containing polyplexes (Figure 47B) as compared to the 3-arm oligomer combination (Figure 45D). The stability in serum was again confirmed (Figure 47C). The intravenous application of these combination polyplexes again led to a significant cMBP2 targeting effect (Figure 47D), though with a lower luciferase expression in tumor and, interestingly, increased gene transfer in the lung.

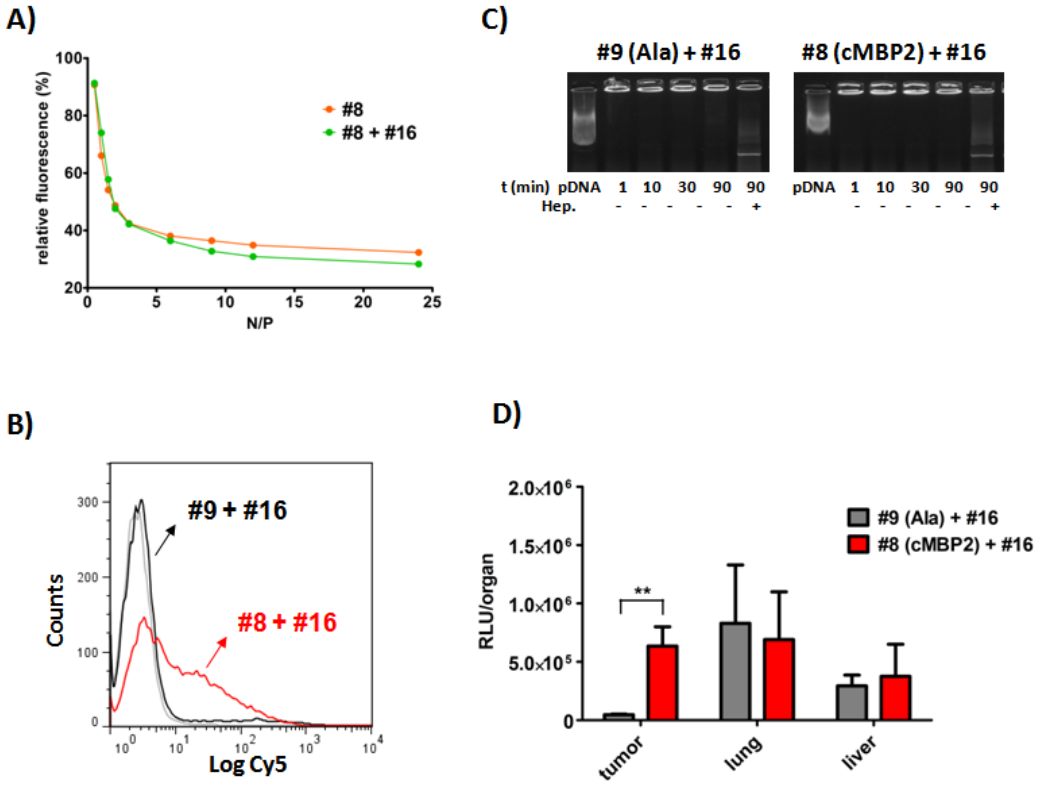

Figure 47. A) pDNA compaction ability of combination polyplexes of 2-arm PEGylated oligomer (#8) and 4-arm compacting oligomer (#16) compared to single oligomer polyplexes formed only with the oligomer (#8) as determined by EtBr exclusion assay. Oligomer solution was added at increasing N/P ratios to 10 µg pDNA containing 0.4 µg EtBr. Reduction in EtBr fluorescence was determined as percentage of maximal fluorescence of EtBr containing pDNA solution. B) Cellular uptake of combination polyplexes (total N/P 12) comparing the cMBP2-targeted (red line) and alanine control (black line) nanoparticles by Huh7 cells after 45 min at 37°C and removal of cell surface-bound polyplexes. "Count" represents cumulative counts of cells with indicated Cy5 fluorescence after appropriate gating by forward/sideward scatter and pulse width. Dead cells (DAPI positive, less than 2%) were excluded from analysis. C) Serum stability analyzed by gel-shift assay. Polyplexes (N/P 12) were incubated for 30 min with subsequent incubation in 90% serum for 1, 10, 30 or 90 min. Where indicated, heparin was added to the polyplexes to evaluate the influence of this highly polyanionic molecule on polyplex stability. D) In vivo gene expression 48 h after i.v. administration of cMBP2-targeted (#8 + #16) and alanine control (#9 + #16) combination polyplexes at total N/P 12 (oligomer #8 or #9 at 70% and oligomer #16 at 30% of the total N/P) into Huh7 tumor bearing mice (N=5, mean±SEM) in tumor, lung and liver. Luciferase gene expression is presented as relative light units per organ or tumor (RLU/organ). Lysis buffer RLU values were subtracted. Liver weight was around 1.5 g, lung weight around 210 mg and Huh7 tumor weight 438±152 mg. The animal experiments were performed together with Annika Herrmann (veterinary MD study, LMU).

4 DISCUSSION

4.1 Evaluation of polypropylenimine dendrimers bioreducibly tailored with sequence-defined oligo(ethanamino)amides as gene delivery systems

Synthetic nucleic acid carrier systems gained increasing attention during the last decades as they offer the opportunity to overcome drawbacks associated with the viral vectors. High Mw of cationic polymers can be on the one hand associated with good transfection efficacy, on the other hand also with increased cytotoxicity [127]. Gene carriers with environment-triggered biodegradation characteristics have the potential to overcome this dilemma [179-181]. Encouraging proof of concept studies have been made using oligomers cross-linked *via* degradable ester and disulfide bonds; however these carriers often lack precision with respect to coupling sites and product molecular weight [137, 182]. The symmetrical dendrimer structure presents a known effective strategy to increase the Mw of polymers while maintaining a defined structure [111, 183]. In our current concept we tested small, linear, sequence-defined oligomers based on the unnatural oligoamino acid succinoyl-tetraethylene pentamine (Stp) [119] coupled to the symmetrical polypropylenimine dendrimer G2 core. This protonatable Stp repeat unit is responsible for the favorable transfection properties, mediating electrostatic binding with pDNA and additional buffering capacity upon cell entry into endolysosomal compartments [184]. Biodegradability was achieved by modification of the eight primary amines on the PPI G2 surface with activated cysteines, making them feasible for reaction with free thiols. Linear oligomers, consisting of increasing number (1-5 units) of the cationic building block Stp and a C-terminal cysteine in free thiol form, were coupled to this activated core to create reducible disulfide linkages. Thus, five compounds with increasing Mw were assembled (PPI-Stp1, PPI-Stp2, PPI-Stp3, PPI-Stp4, PPI-Stp5) and compared to unmodified PPI G2 regarding their biophysical and biological properties necessary to overcome the drawbacks of different delivery steps. As initial requirement, a sufficient nucleic acid binding is necessary for stable dendriplex formation of adequate sizes. Higher-generation dendrimers are usually required for satisfactory binding of

especially smaller siRNA molecules, whereas lower-generation dendrimers lacking the multivalency may enable sufficient interactions with larger RNA molecules or DNA molecules [116, 185]. Interactions between our Stp modified PPI dendrimers and pDNA were evaluated from the ability of dendrimers to displace the intercalating dye and pDNA binding assay. The binding affinity mainly increased with the oligomer chain length, whereas only the conjugate with the highest number of Stp units efficiently bound pDNA at all N/P ratios. The unmodified PPI G2 as well showed effective DNA complexation, similar as reported by Choi *et al*., where native PAMAM interestingly displayed more efficient pDNA complex formation than arginine or lysine surface modified PAMAM. The latter was explained with higher pKa values of primary dendrimer amines as compared with the α-amines of lysines or arginines included in charge ratio calculations [112].

Although unmodified PPI G2 displayed good pDNA binding by EtBr exclusion assay and agarose gel shift, it formed very large aggregates with pDNA (> 1µm). In line with this, Tang *et al.* demonstrated that the unmodified dendrimers usually appear as clusters in electron micrographs with their diameters above 1000 nm; else typically formed toroidal complexes aggregate in solution [186]. In contrast to unmodified PPI the Stp-modified conjugates formed nanoparticles of adequate sizes (150-400 nm). Subsequent cellular internalization studies also demonstrated the necessity for surface modification. Stp modification led to substantially improved cellular uptake of pDNA polyplexes. Apart from pDNA binding and cellular uptake, the endosomal escape presents a critical requirement for efficient gene delivery. For PEI and related carriers, protonation capacity of polymer within the endolysosomal pH range has been found associated with improved vesicular escape to the cytosol (so-called ‘proton-sponge effect’) [22, 187, 188]. Mostly histidine surface modifications of dendrimers have shown to increase the buffer capacity within the endolysosomal pH range, especially in the lowest pH ranges [112]. Acidimetric titrations of conjugates PPI-Stp4 and PPI-Stp5 also revealed an improved total buffering capacity in the endolysosomal pH range as compared to PPI G2. The best buffering capacity of the two Stp modified conjugates was observed at the pH range between 6 and 7.4, providing high buffering capacity already in an early endosome phase. Consistent with endosomal escape, an increase in nuclear association of Cy5 labeled pDNA was observed for PPI-Stp2 to PPI-Stp5 (but not PPI-Stp1 or unmodified PPI). Highest luciferase gene transfer levels, exceeding those of unmodified PPI, were observed

for PPI-Stp3 to PPI-Stp5 (Figure 3). Extending the Stp oligomers sequence from three to five Stp units apparently did not significantly further enhance gene transfer (at least *in vitro*), despite favorable stability data (Figure 1). Cytotoxicity of dendrimers and other gene delivery carriers is a major issue in successful gene therapy. A microarray analysis revealed many of the intrinsically altered genes after treatment with PPI G2 and G3 dendriplexes on two human cell lines [189]. Several surface modifications have been exploited in order to reduce the cytotoxicity [114, 115, 190]. Due to the dissociation of our Stp modified conjugates in the reducing cytosol environment, in spite of a high MW, a reduced cytotoxicity based on dissociation in the cytosol should be achieved. Under pDNA transfection conditions no cytotoxicity of polyplexes was visible (MTT assay). A metabolic activity ATP assay with N2a cells treated with PPI conjugates at higher concentrations disclosed a far higher cytotoxicity for the unmodified PPI G2 (at concentrations above 0.2 mg/mL) as compared to the Stp conjugates. Compaction of the dendrimers with pDNA generally reduces toxicity [139], and one has to keep in mind that for the metabolic ATP activity assay high concentrations of cationic carriers were used (the lowest 0.01 mg/mL conjugate concentration would correspond to approximately N/P 30 for PPI G2 and N/P 8 for Stp modified conjugates).

Based on promising *in vitro* data the PPI conjugate with the longest Stp chains, PPI-Stp5, was further investigated *in vivo* and examined in comparison with PPI G2. Transgene expression for both polyplex types was predominantly found in tumor, lung and liver (Figure 8). PPI G2 polyplexes resulted in a significantly higher reporter gene expression in the lungs and liver as compared to PPI-Stp5. The lung expression might in part be due to the large size and aggregate formation of the PPI G2 polyplexes that could lead to the entrapment of the polyplexes in the pulmonary vasculature [191, 192]. In contrast gene reporter expression in tumors was significantly higher for the smaller PPI-Stp5 conjugate. Although the exact reason is not proven, this finding is compatible with a better systemic distribution and accumulation of these polyplexes in tumor tissues due to tumor-selective enhanced permeability and retention (EPR) effect [193]. In brief, first *in vivo* studies confirm the possible relevance of precise conjugates by bioreducible attachment of oligo (ethane amino) amides to the octavalent PPI G2 dendritic core. Of all evaluated structures, PPI-Stp5 seems to be the most promising candidate for pDNA delivery, exhibiting good nucleic acid binding, medium-low particle size, the highest cellular uptake, low

cytotoxicity and the most efficient gene transfer. The data demonstrate that the simple unmodified linear Stp_x oligomer series, which because the small size *per se* is ineffective [141], by precise attachment to PPI can be converted into effective gene carriers. This proof of concept obviously may be extended to attachment of more potent, better stabilizing [120, 121] and functional, targeted and shielded [57], sequence-defined oligomers.

4.2 Evaluation of sequence-defined linear oligo (ethane amino) amides of increasing length in gene delivery

Increasing repeat units of artificial amino acid succinoyl-tetraethylene pentamine (Stp) [119] containing the diaminoethane motif like the transfection agent PEI [194, 195] were applied for the assembly of well-defined linear peptide-like carriers without any dendritic core or other functional groups. The gold standard LPEI, containing approximately 500(±200) protonatable nitrogens [137], obviously has a far larger average polymer size than previously synthesized Stp oligomers; a linear oligomer of 5 Stp units did not facilitate pDNA delivery [120]. In addition, Stp and oligomers differ from LPEI by an amide-bonded succinic acid linker every fifth or sixth ethanamino unit.

To address the question whether longer linear Stp oligomers can mimic LPEI in gene transfer efficacy, the influence of increasing the Mw of linear oligo (ethane amino) amides on pDNA mediated gene transfer and cytotoxicity was investigated. We demonstrated that - beyond a critical oligomer size - indeed the diaminoethane motif containing building blocks enable efficient gene transfer without the need for further functional modifications. In agreement with the previous studies [141], initial pDNA complexation studies with agarose gel shift assay and EtBr exclusion assay showed almost no pDNA binding with the shortest 5 Stp oligomer. With increasing number of Stp units, improved binding characteristics were observed. Such polyplex stabilization can be attributed to multivalent electrostatic interactions between the pDNA and oligomers carrying more positive charges per molecule. The subsequent cellular internalization studies were in accordance with the pDNA binding studies demonstrating very low cellular uptake of the Stp5-W oligomer that greatly increased

with increased carrier length reaching maximum already with 15 Stp units. Similarly, the gene transfer experiments exhibited a clear increase in transfection efficiency with increasing Mw. Interestingly; Stp15-W with an Mw of around 4.3 kDa exceeded the LPEI transfection level but only at the highest tested N/P ratio of 24. Stp30-W, containing 91 protonatable nitrogens, displayed a greater gene transfer than LPEI already at N/P ratio 3, indicating the excellent capability of these carrier systems for pDNA delivery. As Stp40-W achieved similar pDNA transfection levels but did not exceed the performance of Stp30-W, we assume that an optimum length was reached at around 30 units and further elongation does not result in a greater benefit. The cytotoxicity of the cationic polymer PEI represents one of the major concerns in gene delivery. It causes toxic effects by versatile mechanisms such as cytosolic and mitochondrial membrane damage as well as necrotic-like and apoptotic changes [127, 128, 196, 197]. Thus, the comparison between LPEI and the synthesized Stp oligomers of increasing Mw is particularly relevant. As above in the case of PPI dendrimers bioreducibly modified with sequence-defined oligo (ethane amino) amides, MTT assay performed in parallel with the pDNA transfection experiments revealed no reduction in cell viability after treatment of cells with the pDNA polyplexes. On the other hand, applying the oligomers only, the CellTiter-Glo® cytotoxicity assay revealed at least 10-fold reduction of toxicity of the Stp-based oligomers in comparison to the commonly used LPEI, whereby the cytotoxicity clearly correlated with Mw. Not only the lower Mw of Stp30-W, but also the succinate spacer between the oligoamine units may contribute to the favorable biocompatibility of the Stp oligomers over standard PEIs. In fact, previous work demonstrated about 10-fold reduced toxicity of randomly branched PEI 25 kDa upon partial amidation with propionic or succinic acid [31].

4.3 Evaluation of native chemical ligation as a screening tool for easy conversion of sequence-defined oligomers into targeted pDNA carriers

Previously, a polymer library of >600 diaminoethane motif containing sequence-defined oligomers has been reported [120, 141]. Various functional domains have been identified as crucial for promoting gene transfer, e.g. terminal cysteines for polyplex stabilization *via* disulfide bridging, tyrosine trimers incorporation for

additional polyplex stabilization via *π*-*π* interactions [121]. Histidines were included for an improved endosomal escape based on their buffering capacity in the endosomal pH-range [101, 122]. Also different topologies and increasing number of polycationic arms were demonstrated to have a crucial role in the oligomer transfection efficiency. However, all these oligomers were untargeted and would *in vivo* lead to unspecific tissue accumulation and unwanted side-effects. By conjugating targeting moieties, *e.g.* ligands, to a polymeric carrier the expression in specific tissues can be enhanced and adverse effects minimized. Thus, the idea was to employ a novel strategy to easily convert the existing non-targeted oligomers from our library into ligand-modified oligomers. The folic acid, targeting the human folic acid receptor, which is over-expressed on the surface of several tumor cells, was chosen as a targeting ligand. Furthermore, carrier PEGylation and attachment of the targeting ligands to the distal end of the PEG chain improves its ligand accessibility and at the same time masks the positive surface charge of the polyplexes and prolongs the blood circulation half-life [198]. Therefore, NCL was here employed and demonstrated as powerful method to convert a small library of sequence-defined transfection oligomers with N-terminal cysteines of different topological structures into receptor-targeted and PEG-shielded carriers. Analyzing triplets (A-PEG or folate-PEG ligated, or unligated) of six different carrier types (2-arm oligomers with central or peripheral tyrosine trimers, 3-arms without or with tyrosine trimers, 4-arm oligomers with histidines) for polyplex formation and pDNA gene transfer provided the following predictable and unpredictable results. All NCL-modified oligomers displayed good cargo binding (Figure 15) in an agarose gel shift assay and formed particles below 350 nm (Table 6) stable in serum (Figure 17) and hence suitable for potential *in vivo* experiments. As expected, polyplexes of oligomers with folate-PEG have strongly reduced zeta potential (Figure 16) and still higher cell binding (Figure 19) and cellular uptake (Figure 18) than unmodified oligomers or A-PEG negative controls. Consistent with folate-receptor-specific cell binding, pDNA polyplexes of the targeted oligomers mediate much higher gene transfer than the negative controls. Not predictable was the advantage of peripheral over the central tyrosine trimer modification for 2-arm structures (Figure 21). This highlights the importance of sequence-defined positioning into specific topologies. The incorporation of stabilizing tyrosine trimers in the 3-arm structure led to an improved transfection efficiency of the unmodified oligomers in KB cells (Figure 21). Similar was observed before with N2a

cells [121]. The positive effect of tyrosines after NCL ligation was maintained leading to a significantly improved cellular uptake of tyrosine trimer-enriched FolA-modified structures (Figure 18) and greatly enhanced reporter gene expression (Figure 21). The replacement of the Stp building block by the Sph building block in the 3-arm oligomers did not have any favorable effects (Figure 21). Obviously, the number of polycationic arms and inclusion of endosomal escape promoting histidines also played an important role. Comparing the FolA-equipped 3-arm oligomer with Sph building blocks and the 4-arm histidines-enriched Sph oligomer, an up to 3-log units higher luciferase gene transfer was obtained with the more highly polycationic structure, although the unmodified oligomers did not differ much in the transfection efficiency. Thus, most important and critical for further carrier optimization is the observation that the ranking in efficiency of non-PEGylated oligomers strongly differs from PEG-ligated oligomers. In other words, screening libraries of unshielded oligomers is not reliable for subsequent optimization of targeted shielded analogs. To solve this dilemma, native chemical ligation is a most convenient tool for easily converting untargeted into targeted oligomers libraries making a search for an optimal carrier *in vivo* less time- and cost-consuming. Here, folate was applied as a targeting ligand, but NCL can be utilized to various different ligands. Encouraging lead structures obtained by NCL ligation may then be optimized by all-in-one solid phase synthesis for *in vivo* application [52, 122].

4.4 Dual-targeted polyplexes based on sequence-defined peptide-PEG-oligoaminoamides

For active cell targeting, viruses frequently capitalize on dual-receptor binding. With the intention to mimic this natural process and thus enhance the transfection efficiency of targeted carriers, a dual peptide-based approach for targeting cancer cells was evaluated. Different combinations of the following targeting ligands were investigated; integrin receptor targeting cyclic RGD ligand, transferrin receptor (TfR) targeting B6 peptide and epidermal growth factor receptor (EGFR) targeting GE11. The latter was for the first time conjugated to a sequence-defined nucleic acid carrier. Integrins are playing a key role in the adhesion, migration, invasion and proliferation of tumor cells and are usually expressed at low levels in normal tissues, but can be

highly upregulated in tumor tissues [59]. EGFR has a crucial role in tumorigenesis and various therapeutics targeting these receptors have been developed for cancer treatment [60, 61]. The TfR which triggers the main uptake for protein iron is over-expressed on malignant cells related to the tumor stage [46, 199]. The advantages of dual-targeted over single-targeted formulations were already demonstrated in combinations with RGD-containing peptides [162, 200, 201]. In particular simultaneous targeting of integrin and TfR has shown encouraging results. Tf and RGD peptide were conjugated to a thermosensitive nanogel carrying doxorubicin and exhibited an improved targeting and anti-tumor effect [202]. This was demonstrated also by the conjugation of Tf and cRGDfk to a hyperbranched copolymer yielding paclitaxel-loaded nanoparticles with enhanced intracellular uptake [203]. Tf-modified cRGDfk-paclitaxel micelles significantly prolonged retention in glioma tumor and peritumoral tissue [204]. Also in our previous work using PEI-based polyplexes [162] the advantage of the combination of TfR targeting short peptide B6 and integrin binding RGD was demonstrated. Few other studies have reported the benefits of growth factor receptor ligands in dual-targeting systems [205]. PEI polyplexes containing a combination of fibroblast growth factor receptor targeting peptide and integrin targeting peptide were tested [69]. Moreover, PEI polyplexes containing Tf and the EGFR binding transforming growth factor alpha displayed intensified receptor-mediated endocytosis [206].

Herein, the synthesized shielded targeting oligomers (RGD-PEG-STP, B6-PEG-STP and GE11-PEG-STP) were first investigated in single-targeted polyplexes formed with pDNA at two different N/P ratios, 6 and 12. All three oligomers showed good cargo binding and polyplex formation of adequate sizes (Figure 24, Table 8). Successful targeting with these peptide ligand-equipped single-oligomer polyplexes as compared to their alanine control was confirmed by means of DU145 prostate cancer cell binding (Figure 25A, B), cellular internalization (Figure 27) and pDNA transfection (Figure 25C, D). pDNA transfections were performed in the presence of the endosomolytic agent chloroquine [170] in order to reduce the endosomal escape bottleneck as limiting barrier in the delivery process and focus on the ligand effect. When formulated at the N/P ratio of 6, pDNA complexation is already complete. All three dual targeting polyplex combinations of RGD-PEG-STP and B6-PEG-STP (Figure 28), RGD-PEG-STP and GE11-PEG-STP (Figure 30), and GE11-STP and B6-STP (Figure 32) showed strongly enhanced cell binding and transfection activity

compared with single targeting polyplexes. Transfection activity correlated well with cell association. The GE11/B6 combination showed the highest efficiency. Not only the combination of peptide ligands, but also the ratio between the targeting ligands played a key role. GE11/B6 (oligomer molar ratio of 4:2) > RGD/B6 (4:2) > RGD/GE11 (5:1) were the optimum combinations. With regard to the RGD/B6 targeting, our previous data in the PEI polyplex system suggest that RGD (integrin binding) had a major contribution in cell binding, whereas B6 enhanced the cellular uptake [162]. The current studies well confirm an enhanced cell binding by combining B6 with RGD, and cellular uptake studies demonstrate B6 as responsible for a pronounced uptake (Figure 29).

Interestingly, in contrast to cRGD and B6 which both displayed rather homogenous monomodal cell association, peptide GE11 polyplexes displayed bimodal cell binding: a large proportion of cells displayed no polyplex binding, whereas a low percentage of cells showed very high cell association. In dual targeting, incorporation of GE11 increased the unimodal association of RGD (Figure 30) and B6 (Figure 32). The reasons remain to be clarified. The GE11 peptide had been previously demonstrated to bind the EGFR with 20-fold lower affinity than the native ligand EGF. Native GE11 peptide itself did not display satisfactory EGFR binding as opposed to a GE11-PEG-PEI conjugate [167]. High receptor densities and other help in cell binding, likewise ligand multivalency and positive polyplex charges are needed for cell association. This hypothetical model is further supported by the fact that GE11 polyplex binding is strongly influenced by enhancing the N/P ratio towards positive polyplex charge. When single and dual targeted polyplexes were formulated at a higher N/P ratio of 12, both cell binding and transfection levels further increased, especially for GE11 polyplexes. The further enhancements have to be regarded as indirect effects such as increased unspecific cell binding by positive oligomer charges as well as contribution of free, uncomplexed oligomers as previously observed for PEI polyplexes [22]. Thus not surprisingly, at the higher N/P 12 ratio, due to the high cell bindings and transfections already of single targeting polyplexes, dual combination effects were less pronounced or absent.

4.5 Evaluation of targeted c-Met receptor-directed oligo (ethane amino) amides for efficient gene transfer *in vitro* and *in vivo*

As c-Met presents an encouraging target receptor in cancer therapy, we applied two phage display library derived c-Met binding peptides (cMBP 1 and 2) and evaluated their suitability as targeting ligands in gene delivery. The first peptide herein designated as cMBP1 with the amino acid sequence YLFSVHWPPLKA was previously proven to specifically bind to c-Met, thereby competing with its natural ligand hepatocyte growth factor in a dose dependent manner and inhibiting tumor cell proliferation *in vitro*. The nuclear imaging experiments with the radioiodinated cMBP1 verified its potential as a diagnostic agent for tumor imaging [207]. Kim *et al.* utilized another c-Met binding ligand here called cMBP2 having the amino acid sequence KSLSRHDHIHHH. They reported ^{125}I-radiolabeled cMBP2 targeting *in vitro* and *in vivo* [208] as well as demonstrated the possibility to apply this ligand for specific optical imaging by employing the cyanine dye 5.5 (Cy5)-conjugated Gly-Gly-Gly (GGG)- or 8-aminooctanoic acid (AOC)- linker modified cMBP2 [209].

Both c-Met binding peptides were for the first time applied as a targeting ligand for receptor-mediated gene transfer. The cMBP2 ligand showed superiority over another c-Met binding peptide ligand denoted as cMBP1. The cMBP2 ligand was conjugated to monodisperse sequence-defined oligomers, comprising polyethylene glycol (PEG) units for shielding and 1,2-diaminoethane motif containing artificial amino acids for alleviation of crucial steps in gene delivery. Terminal cysteines were provided for disulfide-based increased pDNA polyplex stability and redox-sensitive cargo release within the cells [210]. The novel cMBP2-decorated polyplexes synthesized as all-in-one solid-phase synthesis resulted in noteworthy target-specific gene transfer efficiency *in vitro,* though only upon addition of an endosomolytic agent chloroquine (Figure 34). Chloroquine accumulates in endosomes by protonation, triggers osmotic swelling and thereby promotes release of the entrapped nanoparticles. Thus, additional histidines were implemented in the oligomeric structure for improved endosomal escape. The buffering capacity of the histidines, based on their imidazole ring with the pKa around 6 that can be protonated in slightly acidic pH of the endosomes, can greatly ameliorate the endosomal release of the polyplexes [122, 211, 212]. The histidines-enriched polyplexes indeed led to a significantly improved

gene transfer already in the absence of chloroquine (Figure 39). A slightly reduced cargo binding was observed upon incorporation of histidines. This effect was previously observed also for the non-PEGylated Stp oligomers and explained in relation to the influence of unprotonated histidines on the relative oligomer cationization [122]. Moreover, hydrophilic polymers such as PEG have been verified as indispensable for nanoparticle surface shielding against unintended interactions with biological surfaces, inhibition of activation of the complement system and prolongation of the circulation half-life. The length of the PEG spacer not only influences the accessibility of the targeting ligand to the tumor tissue, but can also alter the polyplex biodistribution. Several studies have reported favorable effects with an increasing PEG length, whereas other studies have favored shorter PEG chains and emphasized that the shielding needs to be adjusted individually to the carrier and peptidic ligand [198, 213-217]. Incorporation of additional PEG_{24} chain led to somewhat reduced gene transfer of cMBP2-containing polyplexes *in vitro* (Figure 39). Apart from implementation of the functional moieties within each polycationic arm, addition of extra polycationic arms and design of more highly branched oligomers has previously been proven as favorable for different steps of gene delivery process of non-targeted conjugates [120, 152]. Thus, more highly branched cMBP2-decorated 4-arm conjugates were synthesized. The Stp building block was furthermore substituted with a Sph building block. This replacement was based on our recent reports on non-targeted structures showing an improved nucleic acid compaction and gene transfer with the novel Sph building block [122, 152]. However, doubling the number of polycationic arms in the cMBP2-containing polyplexes did not lead to any additional favorable effect on the gene expression *in vitro* (Figure 42). As c-Met activation causes an increased cell proliferation and invasion [218] and could therewith lead to unwanted side effects of the cMBP-mediated gene delivery, it was essential to analyze it. The western blots demonstrated that the novel cMBP-equipped polyplexes do not induce c-Met receptor phosphorylation and its downstream signaling (Figure 38, Figure 41). Following the encouraging experiments *in vitro*, first *in vivo* studies with local injection of histidines-enriched polyplexes were conducted. Importantly, regardless of the extent of shielding, the cMBP2-equipped polyplexes showed much higher reporter gene expression in tumor than their control polyplexes. The *in vivo* results were in accordance with *in vitro* studies favoring less shielded polyplexes formed with oligomers having only one PEG_{24} chain (Figure 43,

Figure 44). However, when intravenously administering these, upon local injection more potent, less shielded polyplexes, disappointingly, no cMBP2-targeting effect was obtained at first (Figure 45). These disappointing results pointed out to additional requirements of the systemic delivery in comparison to cell culture or regional intratumoral delivery. The evaluated oligomers contain a very high content of PEG (same number of ethyleneglycol units as protonatable Stp nitrogens already in the case of PEG_{24} oligomers) which had revealed imperfect pDNA compaction in a previous *in vitro* study [57]. Thus, in spite of no beneficial effects of augmented polycation part *in vitro*, polyplexes formed with the targeted four-arm oligomers were injected intravenously resulting in only fairly increased c-Met targeting effect (Figure 46).

Hence, instead of directly tuning the chemical oligomer structure, the desired two nanoparticle functions, pDNA compaction on the one hand, targeting and surface shielding on the other hand, were distributed between two different sequence-defined oligomers with or without PEG-content. As shown before [57], the PEG chains presumably not only shield the surface of the nanoparticles, but also interfere with the condensation process between the pDNA double strands. PEG-free analogs however were shown to mediate effective compaction of pDNA into rod- or toriod-like structures [57]. Here, the cMBP-equipped PEGylated polyplexes formed rather long spaghetti-like structures, whereas the co-addition of only 30 % (of the total N/P ratio) of the non-shielded oligomer led to a greatly improved particle formation in rod- and round-shaped nanoparticles and remarkably, a significantly improved gene transfer in tumor (Figure 45, 47). Apparently, the co-formulation of non-shielded compacting oligomers can significantly alter the nanoparticle compaction and shape. Interestingly, only intravenous *in vivo* studies and not *in vitro* transfections were able to disclose the advantage of polyplex compaction; this appears as important requirement to improve targeted gene transfer *in vivo*.

5 SUMMARY

Nucleic acids delivery manifests the future of medicines though the limitations of the currently available carriers are impeding its breakthrough. From the outset of the cationic polymers as nucleic acids delivery agents onwards, LPEI has arisen as most ubiquitously used transfection agent. Myriad of modifications of LPEI improved its efficacy and diminished its cytotoxicity. Still, its high molecular weight and polydispersity remain critical issues setting back the related clinical studies and potential use in medicine. A development of monodisperse precise polymeric carriers mimicking LPEI in its potency but with diminished toxic effects might be a key to the solution. Thus, by exploiting solid-phase synthesis, diaminoethane motif containing building blocks (*e.g.* Stp, Sph) were developed allowing an assembly of user-defined monodisperse and biocompatible oligomers and their easy and site-specific modification.

The extensively investigated low generation dendrimers like PPI have previously demonstrated tolerable toxicity, though also the necessity of surface modification to enhance their gene transfer capacity. Hence, in this thesis disulfide-based conjugates of sequence-defined oligo (ethane amino) amide oligomers of different lengths possessing one to five Stp units with the PPI dendritic core were used. In this manner both defined and biodegradable Stp modified gene carriers were available avoiding polydispersity and cytotoxicity related to higher molecular weight but displaying encouraging properties for pDNA delivery *in vitro.* With increasing Stp chain an increased cargo binding, cellular internalization and gene transfer were obtained. The most promising conjugate with the highest number of Stp units per branch furthermore displayed promising results *in vivo* after intravenous injection.

As the next step, a gradual elongation of the Stp chain and increase of Mw was again correlated with the relevant biophysical and biological properties for polymer-based gene transfer. In this case, however, an optimal carrier containing only the diaminoethane motifs without a dendritic core or any other functional domains was pursued. The carrier with a length of 30 Stp units was demonstrated as an ideal LPEI mimic with a six-fold higher transfection efficiency and ten-fold lower cytotoxicity.

Moreover, the study provided fundamental insights in the pertinence of sequence-defined oligo (ethane amino) amide oligomers as gene delivery systems.

Non-targeted carriers are usually related to unspecific tissue accumulation and undesired adverse effects. Efficient targeting to cancerous tissues still represents a major challenge in gene delivery. Thus, a novel method, NCL, was applied allowing easy and fast modification of non-targeted into targeted polymeric nucleic acid carriers. Folic acid targeting the over-expressed folic acid receptor was employed as a ligand. The resulting gene transfer studies using the assembled FolA-equipped conjugates showed high cellular uptake, association and gene transfer in contrast to non-targeted control confirming the suitability of the method. NCL allowed high-throughput modification and screening of different terminal cysteines-containing untargeted oligomers simplifying and facilitating the search for an optimal targeted carrier that could be a potential potent delivery agent *in vivo*.

Not only naturally occurring small molecules like FolA, but also various short peptides have shown vast potential as targeting ligands due to their reduced risk of unforeseen side-reactions. Moreover, for enhanced receptor-specific gene transfer, the dual-ligand targeting approach has been exploited. Such dual-targeting concept has thus been applied to pDNA polyplexes of recently developed sequence-defined succinoyl-tetraethylenepentamine (Stp)-PEG based oligomers. The dual-peptide equipped nanocarriers simultaneously recognizing either integrin and TfR, integrin and EGFR, or EGFR and TfR led to significantly enhanced cell binding and transfection efficiency in prostate cancer cells expressing all three receptors. The extent of dual targeting was demonstrated as strongly dependent on the ratio between the two ligand-targeted oligomers and had to be carefully investigated for each pair of the targeting peptides. Concurrent addressing of TfR and the epidermal growth factor receptor turned out to be the most effective strategy for the investigated polyplexes.

Furthermore, for the first time the proto-oncogene c-Met / hepatocyte growth factor which is over-expressed in many solid tumors was applied for non-viral tumor-targeted gene delivery. The selected c-Met-binding peptide called cMBP2 was confirmed as a potent and very promising targeting ligand. Incorporating this peptide, novel c-Met directed nanocarriers were developed for efficient gene delivery *in vitro* and, notably, successful c-Met targeted systemic gene transfer *in vivo*. A recent

combination of solid-phase supported peptide and polymer synthesis enabled easy modifications and implementation of various peptidic and artificial functional groups. This provides an optimal tool for determination of structure-activity relationships and optimization of gene carriers. The carriers were thus readily functionalized with c-Met targeting peptides, PEG for shielding against unintended interactions with biological surfaces, and cysteines for additional polyplex stabilization *via* bioreversible disulfide bond formation. Further optimization with the endosomal escape promoting histidines yielded an oligomer which displayed high luciferase expression in tumor upon locoregional administration. For intravenous administration, a new form of pDNA polyplexes, containing both a pDNA compacting oligomer and a surface-shielding cMBP2-PEG-oligomer, had to be formulated for successful systemic and receptor-mediated gene transfer into distant tumors. The designed c-Met directed polyplexes emphasize the importance of each functional moiety and the proper relation of the polycationic part in relation to the shielding part within the nanoparticle. Moreover, the clear-cut functional findings with precise oligomers present a very useful springboard for further chemical evolution of biocompatible receptor-targeted nucleic acid carriers.

6 APPENDIX

6.1 Abbreviations

ADA	Adenosine deaminase
AIDS	Acquired immunodeficiency syndrome
AOC	8-aminooctanoic acid
ASO	Allele-specific oligonucleotide
ATP	Adenosine triphosphate
BCA	Bicinchoninic acid
cMBP	c-Met binding peptide
CMV	Cytomegalovirus
Cy5	Cyanine 5
DAPI	4',6-diamidino-2-phenylindole
DLS	Dynamic light scattering
DMEM	Dulbecco´s modified eagle´s medium
DMSI	Dimethylsuberimidate
DMSO	Dimethyl sulfoxide
DNA	Deoxyribonucleic acid
DOPE	Dioleoylphosphatidylethanolamine
DOTAP	N-[1-(2,3-dioleoyloxy)propyl]-N,N,N-trimethylammoniumethyl sulfate
DOTMA	N-[1-(2,3-dioleyloxy)propyl]-N,N,N-trimethylammonium chloride
DTT	Dithiothreitol
EDTA	Ethylenediaminetetraacetic acid
EGF	Epidermal growth factor
EGFR	Epidermal growth factor receptor
EPR	Enhanced permeability and retention effect
EtBr	Ethidium bromide

FCS	Fetal calf serum
FDA	Food and drug administration
Fmoc	9-Fluorenylmethyloxycarbonyl
FolA	Folate
GelRed	Intercalating nucleic acid stain
HBG	HEPES buffered glucose
HD	Hexanedioldiacrylate
HEPES	N-(2-hydroxyethyl)piperazine-N´-(2-ethanesulfonic acid)
HES	Hydroxyethyl starch
HGF	Hepatocyte growth factor
HGFR	Hepatocyte growth factor receptor
HPMA	N-(2-hydroxypropyl)methacrylamide
LHRH	Luteinizing-hormone-releasing hormone
LNA	Locked nucleic acid
LPEI	Linear polyethylenimine
MMP	Matrix metalloproteinase
mRNA	Messenger RNA
MTT	3-(4,5-dimethylthiazol-2-yl)-2,5-diphenyltetrazolium bromide
Mw	Molecular weight
Nbz	*N*-acyl-benzimidazolinone
NCL	Native chemical ligation
OEI	Oligoethylenimine
PAA	Poly(amidoamine)
PAMAM	Polyamidoamine
PBS	Phosphate buffered saline
pCMVLuc	Plasmid encoding firefly luciferase under the control of CMV promotor
pDNA	Plasmid DNA
PEG	Polyethylene glycol
PEG24	Polyethylene glycol with 24 ethylene glycol units
PEI	Polyethylenimine

PLL	Polylysine
PPI	Polypropylenimine
PTA	Phosphotungstic acid solution
RAC	Recombinant Advisory Committee
RES	Reticuloendothelial system
RGD	Arginylglycylaspartic acid
RISC	RNA-induced silencing complex
RNA	Ribonucleic acid
RPMI	Roswell Park Memorial Institute medium
RT-PCR	Reverse transcription polymerase chain reaction
SCID	Severe combined immune deficiency
SDS-PAGE	Sodium dodecyl sulfate polyacrylamide gel electrophoresis
siRNA	Small interfering RNA
Sph	Succinoyl-pentaethylenhexamine
SPPS	Solid-phase peptide synthesis
Stp	Succinoyl-tetraethylenpentamine
TBE	Tris/Borate/EDTA buffer solution
TfR	Transferrin receptor
Tris	Tris(hydroxymethyl)aminomethane)
VEGF	Vascular endothelial growth factor

6.2 Publications

6.2.1 Original articles

Kos P*, Lächelt U*, Herrmann A, Döblinger M, He D, Wagner E. *cMet-directed compacted polyplexes for tumor-targeted gene transfer in vivo*. Submitted

Kos P, Lächelt U, He D, Nie Y, Gu Z, Wagner E. *Dual-targeted polyplexes based on sequence-defined peptide-PEG-oligoaminoamides*. Prepared for submission

Jorge AF, Röder R, **Kos P**, Dias SR, Wagner E, Pais AA. *Combining polyethylenimine and Fe(III) for mediating pDNA transfection*. Submitted

Lächelt U, Wittmann V, Müller K, Edinger D, **Kos P**, Hoehn M, Wagner E. *Synthetic polyglutamylation of dual-functional MTX Ligands for enhanced combined cytotoxicity of poly(I:C) nanoplexes*. Mol Pharm. 2014 May 2. doi: 10.1021/mp500017u. [Epub ahead of print]

Zhang CY*, **Kos P***, Müller K, Schrimpf W, Troiber C, Lächelt U, Scholz C, Lamb DC, Wagner E. *Native chemical ligation for conversion of sequence-defined oligomers into targeted pDNA and siRNA carriers*. J Control Release. 2014 Feb 22; 180:42-50. doi: 10.1016/j.jconrel.2014.02.015.

Murayama S, **Kos P**, Miyata K, Kataoka K, Wagner E, Kato M. *Gene regulation by intracellular delivery and photodegradation of nanoparticles containing small interfering RNA*. Macromol Biosci. 2014 Feb 7; 14(5):626-31. doi: 10.1002/mabi.201300393.

Scholz C, **Kos P**, Leclercq L, Jin X, Cottet H, Wagner E. *Correlation of length of linear oligo(ethanamino) amides with gene transfer and cytotoxicity*. ChemMedChem. 2014 Feb 6. doi: 10.1002/cmdc.201300483. [Epub ahead of print]

Scholz C, **Kos P**, Wagner E. *Comb-like oligoaminoethane carriers: change in topology improves pDNA Delivery*. Bioconjug Chem. 2014 Feb 19; 25(2):251-61. doi: 10.1021/bc400392y.

Kos P, Scholz C, Salcher EE, Herrmann A, Wagner E. *Gene Transfer with Sequence-Defined Oligo(ethanamino)amides Bioreducibly Attached to a Propylenimine Dendrimer Core*. Pharmaceutical Nanotechnology. 2013 Nov; 1(4):269-281. doi: 10.2174/ 22117385113019990006.

Lächelt U, **Kos P**, Mickler FM, Herrmann A, Salcher EE, Rödl W, Badgujar N, Bräuchle C, Wagner E. *Fine-tuning of proton sponges by precise diaminoethanes and histidines in pDNA polyplexes*. Nanomedicine. 2014 Jan; 10(1):35-44. doi: 10.1016/j.nano.2013.07.008.

Troiber C, Edinger D, **Kos P**, Schreiner L, Kläger R, Herrmann A, Wagner E. *Stabilizing effect of tyrosine trimers on pDNA and siRNA polyplexes*. Biomaterials. 2013 Feb; 34(5):1624-33. doi: 10.1016/j.biomaterials.2012.11.021.

Salcher EE, **Kos P**, Fröhlich T, Badgujar N, Scheible M, Wagner E. *Sequence-defined four-arm oligo(ethanamino)amides for pDNA and siRNA delivery: Impact of building blocks on efficacy*. J Control Release. 2012 Dec 28; 164(3):380-6. doi: 10.1016/j.jconrel.2012.06.023.

Martin I, Dohmen C, Mas-Moruno C, Troiber C, **Kos P**, Schaffert D, Lächelt U, Teixidó M, Günther M, Kessler H, Giralt E, Wagner E. *Solid-phase-assisted synthesis of targeting peptide-PEG-oligo(ethane amino)amides for receptor-mediated gene delivery*. Org Biomol Chem. 2012 Apr 28; 10(16):3258-68. doi: 10.1039/c2ob06907e.

Pavli M, Baumgartner S, **Kos P**, Kogej K. *Doxazosin-carrageenan interactions: a novel approach for studying drug-polymer interactions and relation to controlled drug release*. Int J Pharm. 2011 Dec 12; 421(1):110-9. doi: 10.1016/j.ijpharm.2011.09.019.

6.2.2 Review

Kos P, Wagner E. *Polymers for siRNA Delivery: Combining precision with multifunctionality*. Chimica Oggi-Chemistry Today. 2013 Mar; 31(2): 6-11.

6.2.3 Meeting abstracts

Kos P, Lächelt U, Herrmann A, He Dongsheng, Wagner E. *Sequence-defined nanocarriers for c-Met receptor-directed gene transfer in vitro and in vivo.* 17th Annual Meeting of the American Society of Gene & Cell Therapy, Washington, USA (May 2014).

Kos P, Lächelt U, Mickler FM, Herrmann A, Wagner E. Aiming at the bullseye: *Pursuing the tumor-addressed gene delivery with sequence-defined nanocarriers comprising novel protein and peptidic targeting ligands*. XIX. Annual Meeting of German Society for Gene Therapy, Ulm, Germany (March 2014).

Murayama S, **Kos P**, Miyata K, Kataoka K, Wagner E, Kato M. *Gene regulation by intracellular delivery and photodegradation of nanoparticles containing small interfering RNA*. IUMRS-ICA 2014, Fukuoka, Japan (August 2014).

Kos P, Müller K, Zhang CY, Troiber C, Lächelt U, Scholz C, Wagner E. *Native chemical ligation for conversion of sequence-defined oligomers of different topologies into targeted pDNA and siRNA Carriers*. Young Ideas in Nanoscience, NIM Workshop, Munich, Germany (November 2013).

Niño A, Scholz C, **Kos P**, Wagner E, Vicent MJ. *Novel zwitterionic systems for cytosolic delivery*. X. Spanish-Portuguese Conference on Controlled Drug Delivery, Valencia, Spain (November 2013).

Kos P, Müller K, Zhang CY, Troiber C, Lächelt U, Scholz C, Wagner E. *Targeted sequence-defined oligomers of different topologies for pDNA and siRNA delivery synthesized via native chemical ligation*. Nanosciences: Great Adventures on Small Scales, CeNS Workshop, Venice, Italy (September 2013).

Lächelt U, **Kos P**, Hermann A, Wagner E. *Proton sponge mechanism revisited and revised: Precise polymer DNA complexes for tumor-directed gene transfer*. XIX. Annual Meeting of German Society for Gene Therapy, Hamburg, Germany (February/March 2013).

Troiber C, Froehlich T, Edinger D, Klaeger R, **Kos P**, Lächelt U, Schaffert D, Wagner E. *Nucleic acid carriers for in vitro and in vivo delivery based on sequence-defined T-Shape Polymers*. 15th Annual Meeting of the ASGCT, Philadelphia, USA (May 2012).

Scholz C, Salcher EE, Troiber C, Fröhlich T, **Kos P**, Wagner E. *Artificial Fmoc/Boc protected amino acids for the solid-phase-assisted synthesis of defined polyaminoamides for pDNA and siRNA delivery*. 9th international symposium on polymer therapeutics, Valencia, Spain (May 2012).

Lächelt U, Dohmen C, **Kos P**, Martín I, Edinger D, Fröhlich T, Wagner E. *Step by step into the cell: A precise nucleic acid carrier incorporating distinct modules for complexation, shielding, targeting and endosomal escape*. 9th international symposium on polymer therapeutics, Valencia, Spain (May 2012).

Salcher EE, Schaffert D, Fröhlich T, **Kos P**, Wagner E. *Solid-phase supported synthesis of precise branched polymers for gene delivery*. Nanosciences: From Molecular Systems to Functional Materials, CeNS Workshop, Venice, Italy (2011).

Lächelt U, Dohmen C, Martín I, **Kos P**, Edinger D, Fröhlich T, Wagner E. *Facing barriers: a precise modular nucleic acid carrier to investigate shielding, targeting and endosomolytic performance*. Nanosciences: From Molecular Systems to Functional Materials, CeNS Workshop, Venice, Italy (2011).

7 REFERENCES

1. Labbadia, J. and R.I. Morimoto, *Huntington's disease: underlying molecular mechanisms and emerging concepts.* Trends Biochem Sci, 2013. **38**(8): p. 378-85.
2. Rosenecker, J., S. Huth, and C. Rudolph, *Gene therapy for cystic fibrosis lung disease: current status and future perspectives.* Curr.Opin.Mol Ther, 2006. **8**(5): p. 439-445.
3. Scott, D.W. and J.N. Lozier, *Gene therapy for haemophilia: prospects and challenges to prevent or reverse inhibitor formation.* Br J Haematol, 2012. **156**(3): p. 295-302.
4. Wirth, T., N. Parker, and S. Yla-Herttuala, *History of gene therapy.* Gene, 2013. **525**(2): p. 162-9.
5. Blaese, R.M., et al., *T lymphocyte-directed gene therapy for ADA- SCID: initial trial results after 4 years.* Science, 1995. **270**(5235): p. 475-480.
6. Aiuti, A., et al., *Progress and prospects: gene therapy clinical trials (part 2).* Gene Ther, 2007. **14**(22): p. 1555-63.
7. Deng, Y., et al., *Therapeutic potentials of gene silencing by RNA interference: principles, challenges, and new strategies.* Gene, 2014. **538**(2): p. 217-27.
8. Braasch, D.A., et al., *RNA interference in mammalian cells by chemically-modified RNA.* Biochemistry, 2003. **42**(26): p. 7967-75.
9. Watts, J.K. and D.R. Corey, *Silencing disease genes in the laboratory and the clinic.* J Pathol, 2012. **226**(2): p. 365-79.
10. Allerson, C.R., et al., *Fully 2'-modified oligonucleotide duplexes with improved in vitro potency and stability compared to unmodified small interfering RNA.* Journal of medicinal chemistry, 2005. **48**(4): p. 901-4.
11. Jabs, D.A. and P.D. Griffiths, *Fomivirsen for the treatment of cytomegalovirus retinitis.* Am.J.Ophthalmol., 2002. **133**(4): p. 552-556.
12. Ng, E.W., et al., *Pegaptanib, a targeted anti-VEGF aptamer for ocular vascular disease.* Nat Rev Drug Discov, 2006. **5**(2): p. 123-32.
13. Resnier, P., et al., *A review of the current status of siRNA nanomedicines in the treatment of cancer.* Biomaterials, 2013. **34**(27): p. 6429-43.
14. Houk, B.E., G. Hochhaus, and J.A. Hughes, *Kinetic modeling of plasmid DNA degradation in rat plasma.* AAPS.PharmSci., 1999. **1**(3): p. E9.
15. Xiang, S., et al., *Uptake mechanisms of non-viral gene delivery.* J Control Release, 2012. **158**(3): p. 371-8.
16. Nguyen, J. and F.C. Szoka, *Nucleic acid delivery: the missing pieces of the puzzle?* Acc Chem Res, 2012. **45**(7): p. 1153-62.
17. Boussif, O., et al., *A versatile vector for gene and oligonucleotide transfer into cells in culture and in vivo: polyethylenimine.* Proc.Natl.Acad.Sci.U.S.A, 1995. **92**(16): p. 7297-7301.
18. Dauty, E. and A.S. Verkman, *Actin cytoskeleton as the principal determinant of size-dependent DNA mobility in cytoplasm: a new barrier for non-viral gene delivery.* J.Biol Chem, 2005. **280**(9): p. 7823-7828.
19. Melchior, F. and L. Gerace, *Mechanisms of nuclear protein import.* Curr Opin.Cell Biol, 1995. **7**(3): p. 310-318.
20. Brunner, S., et al., *Cell cycle dependence of gene transfer by lipoplex, polyplex and recombinant adenovirus.* Gene Ther, 2000. **7**(5): p. 401-407.
21. Gagnon, K.T., et al., *RNAi factors are present and active in human cell nuclei.* Cell Rep, 2014. **6**(1): p. 211-21.
22. Wagner, E., *Polymers for siRNA Delivery: Inspired by Viruses to be Targeted, Dynamic, and Precise.* Acc Chem Res, 2012. **45**(7): p. 1005-13.
23. Felgner, P.L., et al., *Nomenclature for synthetic gene delivery systems.* Hum Gene Ther, 1997. **8**(5): p. 511-2.
24. Felgner, P.L., et al., *Lipofection: A highly efficient, lipid mediated DNA-transfection procedure.* Proc Natl Acad Sci U S A, 1987. **84**: p. 7413-7417.
25. Zhang, S., et al., *Cationic compounds used in lipoplexes and polyplexes for gene delivery.* J Control Release, 2004. **100**(2): p. 165-180.
26. Hui, S.W., et al., *The role of helper lipids in cationic liposmes as a vector for gene transfer 303.*

27. Erbacher, P., et al., *Chitosan-based vector/DNA complexes for gene delivery: biophysical characteristics and transfection ability 826.* Pharm.Res., 1998. **15**(9): p. 1332-1339.
28. Dufes, C., I.F. Uchegbu, and A.G. Schatzlein, *Dendrimers in gene delivery.* Adv Drug Deliv.Rev., 2005. **57**(15): p. 2177-2202.
29. Wagner, E., M. Ogris, and W. Zauner, *Polylysine-based transfection systems utilizing receptor-mediated delivery.* Adv.Drug Deliv.Rev., 1998. **30**(1-3): p. 97-113.
30. Baker, A., et al., *Polyethylenimine (PEI) is a simple, inexpensive and effective reagent for condensing and linking plasmid DNA to adenovirus for gene delivery.* Gene Ther., 1997. **4**(8): p. 773-782.
31. Zintchenko, A., et al., *Simple Modifications of Branched PEI Lead to Highly Efficient siRNA Carriers with Low Toxicity.* Bioconjug Chem, 2008. **19**(7): p. 1448-1455.
32. Prevette, L.E., et al., *Deciphering the role of hydrogen bonding in enhancing pDNA-polycation interactions.* Langmuir, 2007. **23**(19): p. 9773-9784.
33. Zheng, M., et al., *Lipoic acid modified low molecular weight polyethylenimine mediates nontoxic and highly potent in vitro gene transfection.* Mol Pharm, 2011. **8**(6): p. 2434-43.
34. Oskuee, R.K., et al., *Alkylcarboxylate grafting to polyethylenimine: a simple approach to producing a DNA nanocarrier with low toxicity.* J Gene Med, 2009. **11**(10): p. 921-32.
35. Sochanik, A., et al., *In vivo gene transfer using cetylated polyethylenimine.* Acta Biochim.Pol., 2004. **51**(3): p. 693-702.
36. Creusat, G. and G. Zuber, *Self-assembling polyethylenimine derivatives mediate efficient siRNA delivery in mammalian cells.* Chembiochem, 2008. **9**(17): p. 2787-9.
37. Zaupa, A., et al., *Influence of tyrosine-derived moieties and drying conditions on the formation of helices in gelatin.* Biomacromolecules, 2011. **12**(1): p. 75-81.
38. Hunter, C.A. and J.K.M. Sanders, *The nature of .pi.-.pi. interactions.* J. Am. Chem. Soc., 1990. **112**(14): p. 5525–5534.
39. Creusat, G., et al., *Pyridylthiourea-grafted polyethylenimine offers an effective assistance to siRNA-mediated gene silencing in vitro and in vivo.* J Control Release, 2012. **157**(3): p. 418-26.
40. Wu, G.Y. and C.H. Wu, *Receptor-mediated in vitro gene transformation by a soluble DNA carrier system.* J Biol Chem, 1987. **262**: p. 4429-4432.
41. Wu, G.Y. and C.H. Wu, *Receptor-mediated gene delivery and expression in vivo.* J Biol Chem, 1988. **262**: p. 14621-14624.
42. Wagner, E., et al., *Transferrin-polycation-DNA complexes: the effect of polycations on the structure of the complex and DNA delivery to cells.* Proc.Natl.Acad.Sci.U.S.A, 1991. **88**(10): p. 4255-4259.
43. Huang, R.Q., et al., *Efficient gene delivery targeted to the brain using a transferrin-conjugated polyethyleneglycol-modified polyamidoamine dendrimer.* FASEB J, 2007. **21**(4): p. 1117-25.
44. Chan, C.K. and D.A. Jans, *Enhancement of polylysine-mediated transferrinfection by nuclear localization sequences: polylysine does not function as a nuclear localization sequence 804.* Hum.Gene Ther., 1999. **10**(10): p. 1695-1702.
45. Liang, K.W., E.P. Hoffman, and L. Huang, *Targeted delivery of plasmid DNA to myogenic cells via transferrin-conjugated peptide nucleic acid.* Mol Ther, 2000. **1**(3): p. 236-43.
46. Daniels, T.R., et al., *The transferrin receptor and the targeted delivery of therapeutic agents against cancer.* Biochim Biophys Acta, 2012. **1820**(3): p. 291-317.
47. Wang, L., et al., *CD44 antibody-targeted liposomal nanoparticles for molecular imaging and therapy of hepatocellular carcinoma.* Biomaterials, 2012. **33**(20): p. 5107-14.
48. Merdan, T., et al., *Pegylated polyethylenimine-fab' antibody fragment conjugates for targeted gene delivery to human ovarian carcinoma cells.* Bioconjug.Chem., 2003. **14**(5): p. 989-996.
49. Cheng, J., et al., *Formulation of functionalized PLGA-PEG nanoparticles for in vivo targeted drug delivery.* Biomaterials, 2007. **28**(5): p. 869-76.
50. Kim, E.M., et al., *Asialoglycoprotein receptor targeted gene delivery using galactosylated polyethylenimine-graft-poly(ethylene glycol): in vitro and in vivo studies.* J Control Release, 2005. **108**(2-3): p. 557-567.
51. Kim, K.S., et al., *Bifunctional compounds for targeted hepatic gene delivery.* Gene Ther, 2007. **14**(8): p. 704-708.
52. Dohmen, C., et al., *Nanosized multifunctional polyplexes for receptor-mediated siRNA delivery.* ACS nano, 2012. **6**(6): p. 5198-208.
53. Weissleder, R., et al., *Cell-specific targeting of nanoparticles by multivalent attachment of small molecules.* Nat Biotechnol, 2005. **23**(11): p. 1418-23.

54. Ping, Y., et al., *FGFR-targeted gene delivery mediated by supramolecular assembly between beta-cyclodextrin-crosslinked PEI and redox-sensitive PEG.* Biomaterials, 2013. **34**(27): p. 6482-94.
55. Harbottle, R.P., et al., *An RGD-oligolysine peptide: a prototype construct for integrin-mediated gene delivery.* Hum.Gene Ther, 1998. **9**(7): p. 1037-1047.
56. Lee, T.Y., et al., *Peptide-mediated targeting to tumor blood vessels of lung cancer for drug delivery.* Cancer Res, 2007. **67**(22): p. 10958-65.
57. Martin, I., et al., *Solid-phase-assisted synthesis of targeting peptide-PEG-oligo(ethane amino)amides for receptor-mediated gene delivery.* Org Biomol Chem, 2012. **10**(16): p. 3258-68.
58. Molek, P., B. Strukelj, and T. Bratkovic, *Peptide phage display as a tool for drug discovery: targeting membrane receptors.* Molecules, 2011. **16**(1): p. 857-87.
59. Desgrosellier, J.S. and D.A. Cheresh, *Integrins in cancer: biological implications and therapeutic opportunities.* Nat Rev Cancer, 2010. **10**(1): p. 9-22.
60. Levitzki, A., *EGF receptor as a therapeutic target.* Lung Cancer, 2003. **41 Suppl 1**: p. S9-14.
61. West, C.M., L. Joseph, and S. Bhana, *Epidermal growth factor receptor-targeted therapy.* Br J Radiol, 2008. **81 Spec No 1**: p. S36-44.
62. Wolschek, M.F., et al., *Specific systemic nonviral gene delivery to human hepatocellular carcinoma xenografts in SCID mice.* Hepatology, 2002. **36**(5): p. 1106-1114.
63. Mickler, F.M., et al., *Tuning nanoparticle uptake: live-cell imaging reveals two distinct endocytosis mechanisms mediated by natural and artificial EGFR targeting ligand.* Nano Lett, 2012. **12**(7): p. 3417-23.
64. Koepsel, J.T., E.H. Nguyen, and W.L. Murphy, *Differential effects of a soluble or immobilized VEGFR-binding peptide.* Integr Biol (Camb), 2012. **4**(8): p. 914-24.
65. Blessing, T., et al., *Different strategies for formation of pegylated EGF-conjugated PEI/DNA complexes for targeted gene delivery.* Bioconjug Chem, 2001. **12**(4): p. 529-537.
66. Li, Z., et al., *Identification and characterization of a novel peptide ligand of epidermal growth factor receptor for targeted delivery of therapeutics.* Faseb J, 2005. **19**(14): p. 1978-1985.
67. Bergelson, J.M., et al., *Isolation of a common receptor for Coxsackie B viruses and adenoviruses 2 and 5.* Science, 1997. **275**(5304): p. 1320-3.
68. Wickham, T.J., et al., *Integrins alpha v beta 3 and alpha v beta 5 promote adenovirus internalization but not virus attachment.* Cell, 1993. **73**(2): p. 309-319.
69. Li, D., et al., *Dual-targeting non-viral vector based on polyethylenimine improves gene transfer efficiency.* J Biomater Sci Polym Ed, 2007. **18**(5): p. 545-60.
70. Owens, D.E., 3rd and N.A. Peppas, *Opsonization, biodistribution, and pharmacokinetics of polymeric nanoparticles.* Int J Pharm, 2006. **307**(1): p. 93-102.
71. Kircheis, R., et al., *Polycation-based DNA complexes for tumor-targeted gene delivery in vivo.* J Gene Med, 1999. **1**(2): p. 111-120.
72. Burke, R.S. and S.H. Pun, *Extracellular Barriers to in Vivo PEI and PEGylated PEI Polyplex-Mediated Gene Delivery to the Liver.* Bioconjug Chem, 2008. **19**(3): p. 693-704.
73. Pirotton, S., et al., *Enhancement of transfection efficiency through rapid and noncovalent post-PEGylation of poly(dimethylaminoethyl methacrylate)/DNA complexes.* Pharm.Res., 2004. **21**(8): p. 1471-1479.
74. Verbaan, F.J., et al., *Steric stabilization of poly(2-(dimethylamino)ethyl methacrylate)-based polyplexes mediates prolonged circulation and tumor targeting in mice.* J.Gene Med., 2004. **6**(1): p. 64-75.
75. Carlisle, R.C., et al., *Polymer-coated polyethylenimine/DNA complexes designed for triggered activation by intracellular reduction.* J Gene Med, 2004. **6**(3): p. 337-344.
76. Oupicky, D., A.L. Parker, and L.W. Seymour, *Laterally stabilized complexes of DNA with linear reducible polycations: strategy for triggered intracellular activation of DNA delivery vectors.* J.Am.Chem.Soc., 2002. **124**(1): p. 8-9.
77. Toncheva, V., et al., *Novel vectors for gene delivery formed by self-assembly of DNA with poly(L-lysine) grafted with hydrophilic polymers.* Biochim Biophys Acta, 1998. **1380**: p. 354-368.
78. Tseng, W.C. and C.M. Jong, *Improved stability of polycationic vector by dextran-grafted branched polyethylenimine.* Biomacromolecules., 2003. **4**(5): p. 1277-1284.
79. Hornof, M., et al., *Low molecular weight hyaluronan shielding of DNA/PEI polyplexes facilitates CD44 receptor mediated uptake in human corneal epithelial cells.* J Gene Med., 2008. **10**(1): p. 70-80.
80. Noga, M., et al., *Controlled shielding and deshielding of gene delivery polyplexes using hydroxyethyl starch (HES) and alpha-amylase.* J Control Release, 2012. **159**(1): p. 92-103.

81. Kakizawa, Y., A. Harada, and K. Kataoka, *Glutathione-sensitive stabilization of block copolymer micelles composed of antisense DNA and thiolated poly(ethylene glycol)-block-poly(L-lysine): a potential carrier for systemic delivery of antisense DNA.* Biomacromolecules., 2001. **2**(2): p. 491-497.
82. Takae, S., et al., *PEG-detachable polyplex micelles based on disulfide-linked block catiomers as bioresponsive nonviral gene vectors.* J Am Chem Soc, 2008. **130**(18): p. 6001-6009.
83. Hatakeyama, H., et al., *Development of a novel systemic gene delivery system for cancer therapy with a tumor-specific cleavable PEG-lipid.* Gene Ther, 2007. **14**(1): p. 68-77.
84. Lin, S., et al., *An acid-labile block copolymer of PDMAEMA and PEG as potential carrier for intelligent gene delivery systems.* Biomacromolecules., 2008. **9**(1): p. 109-115.
85. Guo, X. and F.C. Szoka, Jr., *Steric stabilization of fusogenic liposomes by a low-pH sensitive PEG--diortho ester--lipid conjugate.* Bioconjug.Chem., 2001. **12**(2): p. 291-300.
86. Lai, T.C., et al., *pH-sensitive multi-PEGylated block copolymer as a bioresponsive pDNA delivery vector.* Pharmaceutical research, 2010. **27**(11): p. 2260-73.
87. Murthy, N., et al., *Design and synthesis of pH-responsive polymeric carriers that target uptake and enhance the intracellular delivery of oligonucleotides.* J.Control Release, 2003. **89**(3): p. 365-374.
88. Knorr, V., et al., *An acetal-based PEGylation reagent for pH-sensitive shielding of DNA polyplexes.* Bioconjug Chem, 2007. **18**(4): p. 1218-1225.
89. Wang, C.Y. and L. Huang, *pH-sensitive immunoliposomes mediate target-cell-specific delivery and controlled expression of a foreign gene in mouse 86.* Proc.Natl.Acad.Sci.U.S.A., 1987. **84**(0027-8424): p. 7851-7855.
90. Damen, M., et al., *Delivery of DNA and siRNA by novel gemini-like amphiphilic peptides.* J Control Release, 2010. **145**(1): p. 33-9.
91. Tonges, L., et al., *Stearylated octaarginine and artificial virus-like particles for transfection of siRNA into primary rat neurons.* RNA, 2006. **12**(7): p. 1431-8.
92. Lehto, T., et al., *Delivery of nucleic acids with a stearylated (RxR)4 peptide using a non-covalent co-incubation strategy.* J Control Release, 2010. **141**(1): p. 42-51.
93. Kuo, W.T., H.Y. Huang, and Y.Y. Huang, *Polymeric micelles comprising stearic acid-grafted polyethyleneimine as nonviral gene carriers.* J Nanosci Nanotechnol, 2010. **10**(9): p. 5540-7.
94. Wang, D.A., et al., *Novel branched poly(ethylenimine)-cholesterol water-soluble lipopolymers for gene delivery.* Biomacromolecules., 2002. **3**(6): p. 1197-1207.
95. Oba, M., et al., *Polyplex micelles prepared from omega-cholesteryl PEG-polycation block copolymers for systemic gene delivery.* Biomaterials, 2011. **32**(2): p. 652-63.
96. Doms, R.W., A. Helenius, and J. White, *Membrane fusion activity of the influenza virus hemagglutinin. The low pH-induced conformational change.* The Journal of biological chemistry, 1985. **260**(5): p. 2973-81.
97. Raghuraman, H. and A. Chattopadhyay, *Melittin: a membrane-active peptide with diverse functions.* Biosci Rep, 2007. **27**(4-5): p. 189-223.
98. Boeckle, S., et al., *Melittin analogs with high lytic activity at endosomal pH enhance transfection with purified targeted PEI polyplexes.* J.Control Release, 2006. **112**(2): p. 240-248.
99. Stevenson, M., et al., *Delivery of siRNA mediated by histidine-containing reducible polycations.* J Control Release, 2008. **130**(1): p. 46-56.
100. Cho, Y.W., J.D. Kim, and K. Park, *Polycation gene delivery systems: escape from endosomes to cytosol.* J Pharm.Pharmacol., 2003. **55**(6): p. 721-734.
101. Chang, K.L., et al., *Efficient gene transfection by histidine-modified chitosan through enhancement of endosomal escape.* Bioconjug Chem, 2010. **21**(6): p. 1087-95.
102. Dufès, C., I.F. Uchegbu, and A.G. Schätzlein, *Dendrimers in gene delivery.* Advanced Drug Delivery Reviews, 2005. **57**(15): p. 2177-2202.
103. Sideratou, Z., et al., *Synthesis of a folate functionalized PEGylated poly(propylene imine) dendrimer as prospective targeted drug delivery system.* Bioorg Med Chem Lett, 2010. **20**(22): p. 6513-7.
104. Koppu, S., et al., *Tumor regression after systemic administration of a novel tumor-targeted gene delivery system carrying a therapeutic plasmid DNA.* J Control Release, 2010. **143**(2): p. 215-21.
105. Yu, H., et al., *Epidermal growth factor-PEG functionalized PAMAM-pentaethylenehexamine dendron for targeted gene delivery produced by click chemistry.* Biomacromolecules, 2011. **12**(6): p. 2039-47.
106. Taratula, O., et al., *Surface-engineered targeted PPI dendrimer for efficient intracellular and intratumoral siRNA delivery.* J Control Release, 2009. **140**(3): p. 284-93.

107. Jiang, L.Y., B. Lv, and Y. Luo, *The effects of an RGD-PAMAM dendrimer conjugate in 3D spheroid culture on cell proliferation, expression and aggregation.* Biomaterials, 2013. **34**(11): p. 2665-73.
108. Santos, J.L., et al., *Functionalization of poly(amidoamine) dendrimers with hydrophobic chains for improved gene delivery in mesenchymal stem cells.* J Control Release, 2010. **144**(1): p. 55-64.
109. Jevprasesphant, R., et al., *Engineering of dendrimer surfaces to enhance transepithelial transport and reduce cytotoxicity.* Pharm Res, 2003. **20**(10): p. 1543-50.
110. Wang, X., et al., *Synthesis and Evaluation of Phenylalanine-Modified Hyperbranched Poly(amido amine)s as Promising Gene Carriers.* Biomacromolecules, 2010. **11**(1): p. 245-251.
111. Kim, T.I., et al., *Arginine-conjugated polypropylenimine dendrimer as a non-toxic and efficient gene delivery carrier.* Biomaterials, 2007. **28**(11): p. 2061-7.
112. Choi, J.S., et al., *Enhanced transfection efficiency of PAMAM dendrimer by surface modification with l-arginine.* J Control Release, 2004. **99**(3): p. 445-456.
113. Yu, G.S., et al., *Synthesis of PAMAM dendrimer derivatives with enhanced buffering capacity and remarkable gene transfection efficiency.* Bioconjug Chem, 2011. **22**(6): p. 1046-55.
114. Kolhatkar, R.B., et al., *Surface acetylation of polyamidoamine (PAMAM) dendrimers decreases cytotoxicity while maintaining membrane permeability.* Bioconjug Chem, 2007. **18**(6): p. 2054-60.
115. Li, X., et al., *PAMAM dendrimers with an oxyethylene unit-enriched surface as biocompatible temperature-sensitive dendrimers.* Bioconjug Chem, 2013. **24**(2): p. 282-90.
116. Chen, A.M., et al., *Labile catalytic packaging of DNA/siRNA: control of gold nanoparticles "out" of DNA/siRNA complexes.* ACS Nano, 2010. **4**(7): p. 3679-88.
117. Merrifield, R.B., *Solid Phase Peptide Synthesis. I. The Synthesis of a Tetrapeptide.* Journal of the American Chemical Society, 1963. **85**(14): p. 2149-2154.
118. Hartmann, L., et al., *Solid-phase supported polymer synthesis of sequence-defined, multifunctional poly(amidoamines).* Biomacromolecules., 2006. **7**(4): p. 1239-1244.
119. Schaffert, D., N. Badgujar, and E. Wagner, *Novel Fmoc-polyamino acids for solid-phase synthesis of defined polyamidoamines.* Org Lett, 2011. **13**(7): p. 1586-9.
120. Schaffert, D., et al., *Solid-phase synthesis of sequence-defined T-, i-, and U-shape polymers for pDNA and siRNA delivery.* Angew Chem Int Ed Engl, 2011. **50**(38): p. 8986-9.
121. Troiber, C., et al., *Stabilizing effect of tyrosine trimers on pDNA and siRNA polyplexes.* Biomaterials, 2013. **34**(5): p. 1624-33.
122. Lachelt, U., et al., *Fine-tuning of proton sponges by precise diaminoethanes and histidines in pDNA polyplexes.* Nanomedicine, 2014. **10**(1): p. 35-44.
123. Frohlich, T., et al., *Structure-activity relationships of siRNA carriers based on sequence-defined oligo (ethane amino) amides.* J Control Release, 2012. **160**(3): p. 532-41.
124. Scholz, C., P. Kos, and E. Wagner, *Comb-like oligoaminoethane carriers: change in topology improves pDNA delivery.* Bioconjug Chem, 2014. **25**(2): p. 251-61.
125. Schaffert, D., et al., *Poly(I:C)-mediated tumor growth suppression in EGF-receptor overexpressing tumors using EGF-polyethylene glycol-linear polyethylenimine as carrier.* Pharm Res, 2011. **28**(4): p. 731-41.
126. Grandinetti, G. and T.M. Reineke, *Exploring the mechanism of plasmid DNA nuclear internalization with polymer-based vehicles.* Mol Pharm, 2012. **9**(8): p. 2256-67.
127. Moghimi, S.M., et al., *A two-stage poly(ethylenimine)-mediated cytotoxicity: implications for gene transfer/therapy.* Mol Ther, 2005. **11**(6): p. 990-995.
128. Grandinetti, G., A.E. Smith, and T.M. Reineke, *Membrane and nuclear permeabilization by polymeric pDNA vehicles: efficient method for gene delivery or mechanism of cytotoxicity?* Mol Pharm, 2012. **9**(3): p. 523-38.
129. Ward, C.M., M.L. Read, and L.W. Seymour, *Systemic circulation of poly(L-lysine)/DNA vectors is influenced by polycation molecular weight and type of DNA: differential circulation in mice and rats and the implications for human gene therapy.* Blood, 2001. **97**(8): p. 2221-9.
130. Gosselin, M.A., W. Guo, and R.J. Lee, *Efficient gene transfer using reversibly cross-linked low molecular weight polyethylenimine.* Bioconjug Chem, 2001. **12**(6): p. 989-994.
131. Ahn, C.H., et al., *Biodegradable poly(ethylenimine) for plasmid DNA delivery.* J Control Release, 2002. **80**(1-3): p. 273-82.
132. Anderson, D.G., D.M. Lynn, and R. Langer, *Semi-automated synthesis and screening of a large library of degradable cationic polymers for gene delivery.* Angew Chem Int Ed Engl, 2003. **42**(27): p. 3153-8.

133. Zhang, H. and S.V. Vinogradov, *Short biodegradable polyamines for gene delivery and transfection of brain capillary endothelial cells.* J Control Release, 2010. **143**(3): p. 359-66.
134. Eltoukhy, A.A., et al., *Effect of molecular weight of amine end-modified poly(beta-amino ester)s on gene delivery efficiency and toxicity.* Biomaterials, 2012. **33**(13): p. 3594-603.
135. Forrest, M.L., J.T. Koerber, and D.W. Pack, *A degradable polyethylenimine derivative with low toxicity for highly efficient gene delivery.* Bioconjug Chem, 2003. **14**(5): p. 934-40.
136. Breunig, M., et al., *Breaking up the correlation between efficacy and toxicity for nonviral gene delivery.* Proc Natl Acad Sci U S A, 2007. **104**(36): p. 14454-9.
137. Russ, V., et al., *Novel degradable oligoethylenimine acrylate ester-based pseudodendrimers for in vitro and in vivo gene transfer.* Gene Ther, 2008. **15**(1): p. 18-29.
138. Russ, V., et al., *Oligoethylenimine-grafted polypropylenimine dendrimers as degradable and biocompatible synthetic vectors for gene delivery.* J Control Release, 2008. **132**(2): p. 131-40.
139. Dufes, C., I.F. Uchegbu, and A.G. Schatzlein, *Dendrimers in gene delivery.* Adv Drug Deliv Rev, 2005. **57**(15): p. 2177-202.
140. Schatzlein, A.G., et al., *Preferential liver gene expression with polypropylenimine dendrimers.* J Control Release, 2005. **101**(1-3): p. 247-258.
141. Schaffert, D., C. Troiber, and E. Wagner, *New Sequence-Defined Polyaminoamides with Tailored Endosomolytic Properties for Plasmid DNA Delivery.* Bioconjug Chem, 2012. **23**(6): p. 1157-1165.
142. Kos, P., et al., *Gene Transfer with Sequence-Defined Oligo(ethanamino)amides Bioreducibly Attached to a Propylenimine Dendrimer Core.* Pharmaceutical Nanotechnology, 2013. **1**(4): p. 269-281.
143. Zinselmeyer, B.H., et al., *The lower-generation polypropylenimine dendrimers are effective gene-transfer agents.* Pharm Res, 2002. **19**(7): p. 960-7.
144. Heidel, J.D. and M.E. Davis, *Clinical developments in nanotechnology for cancer therapy.* Pharm Res, 2011. **28**(2): p. 187-99.
145. Kunath, K., et al., *The structure of PEG-modified poly(ethylene imines) influences biodistribution and pharmacokinetics of their complexes with NF-kappaB decoy in mice 1.* Pharm.Res., 2002. **19**(6): p. 810-817.
146. Fischer, D., et al., *A novel non-viral vector for DNA delivery based on low molecular weight, branched polyethylenimine: effect of molecular weight on transfection efficiency and cytotoxicity.* Pharm Res, 1999. **16**(8): p. 1273-1279.
147. Werth, S., et al., *A low molecular weight fraction of polyethylenimine (PEI) displays increased transfection efficiency of DNA and siRNA in fresh or lyophilized complexes.* J.Control Release, 2006. **112**(2): p. 257-270.
148. Gosselin, M.A., W. Guo, and R.J. Lee, *Incorporation of reversibly cross-linked polyplexes into LPDII vectors for gene delivery 1.* Bioconjug.Chem., 2002. **13**(5): p. 1044-1053.
149. Forrest, M.L., J.T. Koerber, and D.W. Pack, *A degradable polyethylenimine derivative with low toxicity for highly efficient gene delivery.* Bioconjug.Chem., 2003. **14**(5): p. 934-940.
150. Wen, Y., et al., *A biodegradable low molecular weight polyethylenimine derivative as low toxicity and efficient gene vector.* Bioconjug Chem, 2009. **20**(2): p. 322-32.
151. Hashemi, M., et al., *Modified polyethyleneimine with histidine-lysine short peptides as gene carrier.* Cancer Gene Ther, 2011. **18**(1): p. 12-9.
152. Salcher, E.E., et al., *Sequence-defined four-arm oligo(ethanamino)amides for pDNA and siRNA delivery: Impact of building blocks on efficacy.* J Control Release, 2012. **164**(3): p. 380-6.
153. Scholz, C., et al., *Correlation of length of linear oligo(ethanamino) amides with gene transfer and cytotoxicity.* ChemMedChem. doi:10.1002/cmdc.201300483: in press, 2014.
154. Dawson, P., et al., *Synthesis of proteins by native chemical ligation.* Science, 1994. **266**(5186): p. 776-779.
155. Byun, E., et al., *Surface PEGylation via Native Chemical Ligation.* Bioconjugate Chemistry, 2010. **22**(1): p. 4-8.
156. Blanco-Canosa, J.B. and P.E. Dawson, *An efficient Fmoc-SPPS approach for the generation of thioester peptide precursors for use in native chemical ligation.* Angew Chem Int Ed Engl, 2008. **47**(36): p. 6851-5.
157. Hunter, C.A. and J.K.M. Sanders, *The Nature of π-π Interactions.* J. Am. Chem. Soc., 1990. **112**: p. 5525-5534.
158. Dohmen, C., et al., *Defined Folate-PEG-siRNA Conjugates for Receptor-specific Gene Silencing.* Mol Ther Nucleic Acids, 2012. **1**: p. e7.
159. Kularatne, S.A. and P.S. Low, *Targeting of nanoparticles: folate receptor.* Methods in molecular biology, 2010. **624**: p. 249-65.

160. Zhang, C.Y., et al., *Native chemical ligation for conversion of sequence-defined oligomers into targeted pDNA and siRNA carriers.* J Control Release, 2014. **180**: p. 42-50.
161. Li, Y., et al., *Potent retro-inverso D-peptide for simultaneous targeting of angiogenic blood vasculature and tumor cells.* Bioconjug Chem, 2013. **24**(1): p. 133-43.
162. Nie, Y., et al., *Dual-targeted polyplexes: one step towards a synthetic virus for cancer gene therapy.* J Control Release, 2011. **152**(1): p. 127-34.
163. Schraa, A.J., et al., *Targeting of RGD-modified proteins to tumor vasculature: a pharmacokinetic and cellular distribution study.* Int J Cancer, 2002. **102**(5): p. 469-75.
164. Cressman, S., et al., *Synthesis of a labeled RGD-lipid, its incorporation into liposomal nanoparticles, and their trafficking in cultured endothelial cells.* Bioconjug Chem, 2009. **20**(7): p. 1404-11.
165. Li, L., et al., *Pigment epithelium-derived factor gene loaded in cRGD-PEG-PEI suppresses colorectal cancer growth by targeting endothelial cells.* Int J Pharm, 2012. **438**(1-2): p. 1-10.
166. Xia, H., et al., *Recombinant human adenovirus: targeting to the human transferrin receptor improves gene transfer to brain microcapillary endothelium.* J Virol, 2000. **74**(23): p. 11359-66.
167. Abourbeh, G., et al., *PolyIC GE11 polyplex inhibits EGFR-overexpressing tumors.* IUBMB Life, 2012. **64**(4): p. 324-30.
168. Pignon, J.C., et al., *Androgen receptor controls EGFR and ERBB2 gene expression at different levels in prostate cancer cell lines.* Cancer Res, 2009. **69**(7): p. 2941-9.
169. Wagner, E., *Effects of membrane-active agents in gene delivery.* J Control Release, 1998. **53**(1-3): p. 155-158.
170. Zauner, W., et al., *Glycerol and polylysine synergize in their ability to rupture vesicular membranes: a mechanism for increased transferrin-polylysine-mediated gene transfer.* Exp.Cell Res., 1997. **232**(1): p. 137-145.
171. Martin, T.A. and W.G. Jiang, *Hepatocyte growth factor and its receptor signalling complex as targets in cancer therapy.* Anticancer Agents Med Chem, 2010. **10**(1): p. 2-6.
172. Peruzzi, B. and D.P. Bottaro, *Targeting the c-Met signaling pathway in cancer.* Clin Cancer Res, 2006. **12**(12): p. 3657-60.
173. Lu, R.M., et al., *Single chain anti-c-Met antibody conjugated nanoparticles for in vivo tumor-targeted imaging and drug delivery.* Biomaterials, 2011. **32**(12): p. 3265-74.
174. Vosjan, M.J., et al., *Nanobodies targeting the hepatocyte growth factor: potential new drugs for molecular cancer therapy.* Mol Cancer Ther, 2012. **11**(4): p. 1017-25.
175. Mittra, E.S., et al., *Preclinical efficacy of the anti-hepatocyte growth factor antibody ficlatuzumab in a mouse brain orthotopic glioma model evaluated by bioluminescence, PET, and MRI.* Clin Cancer Res, 2013. **19**(20): p. 5711-21.
176. Chen, X., et al., *A human anti-c-Met Fab fragment conjugated with doxorubicin as targeted chemotherapy for hepatocellular carcinoma.* PLoS One, 2013. **8**(5): p. e63093.
177. Nguyen, T.H., et al., *Improved gene transfer selectivity to hepatocarcinoma cells by retrovirus vector displaying single-chain variable fragment antibody against c-Met.* Cancer Gene Ther, 2003. **10**(11): p. 840-9.
178. Cheng, J., et al., *Structure-function correlation of chloroquine and analogues as transgene expression enhancers in nonviral gene delivery.* J.Med.Chem, 2006. **49**(22): p. 6522-6531.
179. Scholz, C. and E. Wagner, *Therapeutic plasmid DNA versus siRNA delivery: Common and different tasks for synthetic carriers.* J Control Release, 2012. **161**(2): p. 554-65.
180. Schatzlein, A.G., *Targeting of Synthetic Gene Delivery Systems.* J Biomed Biotechnol, 2003. **2003**(2): p. 149-158.
181. Wagner, E., *Strategies to improve DNA polyplexes for in vivo gene transfer: will "artificial viruses" be the answer?* Pharm Res, 2004. **21**(1): p. 8-14.
182. Kloeckner, J., et al., *Gene carriers based on hexanediol diacrylate linked oligoethylenimine: effect of chemical structure of polymer on biological properties.* Bioconjug Chem, 2006. **17**(5): p. 1339-1345.
183. Kukowska-Latallo, J.F., et al., *Efficient transfer of genetic material into mammalian cells using Starburst polyamidoamine dendrimers.* Proceedings of the National Academy of Sciences, 1996. **93**(10): p. 4897-4902.
184. Akinc, A., et al., *Exploring polyethylenimine-mediated DNA transfection and the proton sponge hypothesis.* J Gene Med, 2005. **7**(5): p. 657-663.
185. Shen, X.C., et al., *Importance of size-to-charge ratio in construction of stable and uniform nanoscale RNA/dendrimer complexes.* Org Biomol Chem, 2007. **5**(22): p. 3674-81.
186. Tang, M.X. and F.C. Szoka, *The influence of polymer structure on the interactions of cationic polymers with DNA and morphology of the resulting complexes.* Gene Ther, 1997. **4**(8): p. 823-32.

187. Benjaminsen, R.V., et al., *The Possible "Proton Sponge" Effect of Polyethylenimine (PEI) Does Not Include Change in Lysosomal pH.* Mol Ther, 2013. **21**(1): p. 149-157.
188. Sonawane, N.D., F.C. Szoka, Jr., and A.S. Verkman, *Chloride accumulation and swelling in endosomes enhances DNA transfer by polyamine-DNA polyplexes.* J Biol Chem, 2003. **278**(45): p. 44826-31.
189. Omidi, Y., et al., *Polypropylenimine dendrimer-induced gene expression changes: the effect of complexation with DNA, dendrimer generation and cell type.* J Drug Target, 2005. **13**(7): p. 431-43.
190. Taratula, O., et al., *Multifunctional nanomedicine platform for cancer specific delivery of siRNA by superparamagnetic iron oxide nanoparticles-dendrimer complexes.* Curr Drug Deliv, 2011. **8**(1): p. 59-69.
191. Li, S.D. and L. Huang, *Gene therapy progress and prospects: non-viral gene therapy by systemic delivery.* Gene Ther, 2006. **13**(18): p. 1313-1319.
192. Chollet, P., et al., *Side-effects of a systemic injection of linear polyethylenimine-DNA complexes.* J Gene Med, 2002. **4**(1): p. 84-91.
193. Maeda, H., *The enhanced permeability and retention (EPR) effect in tumor vasculature: the key role of tumor-selective macromolecular drug targeting.* Adv Enzyme Regul, 2001. **41**: p. 189-207.
194. Erbacher, P., et al., *Genuine DNA/polyethylenimine (PEI) complexes improve transfection properties and cell survival.* J Drug Target, 2004. **12**(4): p. 223-236.
195. Lungwitz, U., et al., *Polyethylenimine-based non-viral gene delivery systems.* European Journal of Pharmaceutics and Biopharmaceutics, 2005. **60**(2): p. 247-266.
196. Fischer, D., et al., *In vitro cytotoxicity testing of polycations: influence of polymer structure on cell viability and hemolysis.* Biomaterials, 2003. **24**(7): p. 1121-1131.
197. Grandinetti, G., N.P. Ingle, and T.M. Reineke, *Interaction of poly(ethylenimine)-DNA polyplexes with mitochondria: implications for a mechanism of cytotoxicity.* Mol Pharm, 2011. **8**(5): p. 1709-19.
198. Hamidi, M., A. Azadi, and P. Rafiei, *Pharmacokinetic consequences of pegylation.* Drug Deliv., 2006. **13**(6): p. 399-409.
199. Wagner, E., D. Curiel, and M. Cotten, *Delivery of drugs, proteins and genes into cells using transferrin as a ligand for receptor-mediated endocytosis.* Adv Drug Del Rev, 1994. **14**: p. 113-136.
200. Li, Z.B., et al., *18F-labeled BBN-RGD heterodimer for prostate cancer imaging.* J Nucl Med, 2008. **49**(3): p. 453-61.
201. Kluza, E., et al., *Synergistic targeting of alphavbeta3 integrin and galectin-1 with heteromultivalent paramagnetic liposomes for combined MR imaging and treatment of angiogenesis.* Nano Lett, 2010. **10**(1): p. 52-8.
202. Quan, C.Y., et al., *Dual targeting of a thermosensitive nanogel conjugated with transferrin and RGD-containing peptide for effective cell uptake and drug release.* Nanotechnology, 2009. **20**(33): p. 335101.
203. Xu, Q., et al., *Anti-tumor activity of paclitaxel through dual-targeting carrier of cyclic RGD and transferrin conjugated hyperbranched copolymer nanoparticles.* Biomaterials, 2012. **33**(5): p. 1627-39.
204. Zhang, P., et al., *Transferrin-modified c[RGDfK]-paclitaxel loaded hybrid micelle for sequential blood-brain barrier penetration and glioma targeting therapy.* Mol Pharm, 2012. **9**(6): p. 1590-8.
205. Saul, J.M., A.V. Annapragada, and R.V. Bellamkonda, *A dual-ligand approach for enhancing targeting selectivity of therapeutic nanocarriers.* J Control Release, 2006. **114**(3): p. 277-87.
206. Kakimoto, S., et al., *Dual-ligand effect of transferrin and transforming growth factor alpha on polyethyleneimine-mediated gene delivery.* J Control Release, 2007. **120**(3): p. 242-9.
207. Zhao, P., et al., *Identification of a met-binding peptide from a phage display library.* Clin Cancer Res, 2007. **13**(20): p. 6049-55.
208. Kim, E.M., et al., *Characterization, biodistribution and small-animal SPECT of I-125-labeled c-Met binding peptide in mice bearing c-Met receptor tyrosine kinase-positive tumor xenografts.* Nucl Med Biol, 2009. **36**(4): p. 371-8.
209. Kim, E.M., et al., *In vivo imaging of mesenchymal-epithelial transition factor (c-Met) expression using an optical imaging system.* Bioconjug Chem, 2009. **20**(7): p. 1299-306.
210. Klein, P.M. and E. Wagner, *Bioreducible Polycations as Shuttles for Therapeutic Nucleic Acid and Protein Transfection.* Antioxid Redox Signal. doi:10.1089/ars.2013.5714: in press, 2014.

211. Midoux, P., et al., *Chemical vectors for gene delivery: a current review on polymers, peptides and lipids containing histidine or imidazole as nucleic acids carriers.* Br J Pharmacol, 2009. **157**(2): p. 166-78.
212. Chou, S.T., et al., *Surface-modified HK:siRNA nanoplexes with enhanced pharmacokinetics and tumor growth inhibition.* Biomacromolecules, 2013. **14**(3): p. 752-60.
213. Stefanick, J.F., et al., *A systematic analysis of peptide linker length and liposomal polyethylene glycol coating on cellular uptake of peptide-targeted liposomes.* ACS Nano, 2013. **7**(4): p. 2935-47.
214. Khargharia, S., et al., *PEG length and chemical linkage controls polyacridine peptide DNA polyplex pharmacokinetics, biodistribution, metabolic stability and in vivo gene expression.* J Control Release, 2013. **170**(3): p. 325-33.
215. Mishra, S., P. Webster, and M.E. Davis, *PEGylation significantly affects cellular uptake and intracellular trafficking of non-viral gene delivery particles.* Eur.J Cell Biol., 2004. **83**(3): p. 97-111.
216. Nelson, C.E., et al., *Balancing cationic and hydrophobic content of PEGylated siRNA polyplexes enhances endosome escape, stability, blood circulation time, and bioactivity in vivo.* ACS Nano, 2013. **7**(10): p. 8870-80.
217. Synatschke, C.V., et al., *Multicompartment Micelles with Adjustable Poly(ethylene glycol) Shell for Efficient in Vivo Photodynamic Therapy.* ACS Nano, 2014. **8**(2): p. 1161-1172.
218. Appleman, L.J., *MET signaling pathway: a rational target for cancer therapy.* J Clin Oncol, 2011. **29**(36): p. 4837-8.

8 ACKNOWLEDGEMENTS

Coming to an end of this exciting and unforgettable time as a PhD student, there are many people that need to be acknowledged.

First and foremost, I would like to thank my supervisor Prof. Dr. Wagner for giving me an opportunity to do my PhD in his group. I very much appreciate his professional guidance, scientific support, trust and valuable advice.

I am very grateful to all “delivery” group members for a great working atmosphere and collaboration making our work more successful. I would like to thank Uli, Claudia, Edith, Christina, Dongsheng, Irene and Philipp K. for providing the oligomers and Annika for conducting numerous animal experiments with me. Especially, I would like to thank Thomas and Daniel for leading me in the world of cell culture and for becoming great friends along the way. Big thanks go also to all other cell culture room inhabitants, Flo, Miriam, Prajakta, Rebekka, Adam and Christian M. I would like to express my gratitude to Martina and Andi for always having an open ear for us, Martina also for her support in biochemistry lab courses, Wolfgang for accepting my evening and weekend calls when the flow cytometer was down and for solving any imaginable technical issue in the lab, as well as Miriam, Ursula, Anna, Olga and Markus for their help in keeping everything running. I would particularly like to thank the “PhD room” group, Daniel, “Thommislav”, Flo, Andi, Christian D., Rebekka, Alex and Raphaela for the awesome time we spent together that will always be looked back at with nostalgia. Claudia alias “Clau loca” deserves big thanks for our crazy travels and inline skating survival missions and Rebekka and Prajakta for our nice coffee breaks. Thanks also to my “new” lab-mates, Ruth, Katharina and Philipp H. for enriching my last months in the lab and not being that bad at all.

Finally, I would like to express my gratitude to my old friends that due to the circumstances turned into “skype friends" in the last few years and Kopp family for making me feel at home on weekends. Thank you, Flo, just for being you and for all your big support. Last but not least, I owe my gratitude to my family, my parents and sister Nina, for always believing in me and being there for me. Hvala vam!

It was “epic”!